



UNIVERSITY OF IOANNINA
SCHOOLS OF SCIENCES – HEALTH SCIENCES
INTERDEPARTMENTAL POSTGRADUATE
PROGRAM «MEDICINAL CHEMISTRY»
DIPLOMA THESIS
IOANNINA, MAY 2025



Development of a multi-enzyme nanobiocatalytic system for the bioconversion of CO₂

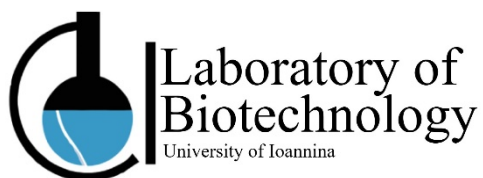
Christos Gakis

R.N.: 307



Diploma Thesis:

Development of a multi-enzyme nanobiocatalytic system for the bioconversion of CO₂



Author

Christos Gakis <chris.gakis1@gmail.com>

Department of Biological Application and Technology

University of Ioannina

Place of Project

Ioannina, Greece

Supervisor and Main Examiner

Prof. Haralambos Stamatis

Department of Biological Application and Technology

University of Ioannina

Examination committee

Prof. Ioannis Pavlidis

Department of Chemistry

University of Crete

Prof. Dimitrios Gournis

School of Chemical Engineering and Environmental Engineering

Technical University of Crete

Acknowledgements

This diploma thesis was conducted at the **Laboratory of Biotechnology** in the **Department of Biological Applications and Technology** at the **University of Ioannina**. The experimental work began shortly before the academic year 2023 and was completed in summer of 2024.

First and foremost, I would like to express my deepest gratitude to my mentor, professor, and head of the laboratory, Professor Haralambos Stamatis, for giving me the opportunity to once again be part of his research team as a master's student. I am truly thankful for his continuous guidance and support throughout this thesis. Most importantly, he was the first to inspire me to cultivate my own enthusiasm for research. His passion and dedication to biotechnology sparked my interest in biocatalysis and laid the foundation for my academic development.

I would like to extend my special thanks to Associate Professor Io Antonopoulou from the Department of Civil, Environmental and Natural Resources Engineering at Luleå University of Technology for kindly providing the heterologously expressed thermophilic enzymes. I am also sincerely grateful to Assistant Professor Konstantinos Spyrou from the Department of Materials Science and Engineering at the University of Ioannina for his contribution in synthesizing the porous nanoparticles used for enzyme immobilization.

My sincere appreciation goes to the members of my thesis examination committee: Assistant Professor Ioannis Pavlidis from the Department of Chemistry at the University of Crete, and Professor Dimitrios Gournis from the School of Chemical and Environmental Engineering at the Technical University of Crete, for their valuable feedback and constructive criticism, which significantly contributed to improving the quality of this work.

I would also like to express my gratitude to my colleagues from the Laboratory of Biotechnology. A special thanks to Postdoctoral Researchers and Friends Michaela Patila and Renia Fotiadou. Michaela, thank you for your invaluable support, insightful criticism, valuable advice, and the time you dedicated to reviewing and correcting this thesis. Renia, I am deeply grateful for the high-level training you provided in analytical chemistry techniques, your generous offer of the hybrid olive extract nanoparticles, and your thoughtful guidance. Beyond your professional support, I also truly appreciated the quality time shared with both of you throughout this experience.

Furthermore, I would like to acknowledge the support and friendship of my fellow lab members, including Postdoctoral Researcher Georgios Bakratsas and PhD students Panagiotis Athanasiou, Angelos Papanikolaou, Christina Alatzoglou, Matina Spyrou, Myrto Bellou, and Anastasia Skonta. Working with all of you over the years has been a truly enriching experience. I admire your

dedication and expertise, and our interactions have continually inspired me to strive for excellence.

I am also grateful to have shared my master's courses and laboratory work with Andreas Vasios, Stefania Zampara, Katerina Karaiskou, and Theodora Bobotsiari. Lastly, I extend my thanks to the undergraduate students in the lab for helping make my time there both productive and enjoyable.

A heartfelt thank you to my closest friends, Marios Epirotis, Taxiarchis Danelis, Stefanos Koilakos, Theodoros Spiliopoulos, Nikolaos Kastellos, Kyriakos Leonidakis, Kleanthis Kipouros, Georgia Louskou, and Christina Mitzelou, for all the unforgettable moments we shared throughout our student years in Ioannina. I am grateful that our friendships have grown and evolved over the years.

This work is especially dedicated to my family for their invaluable emotional and financial support throughout my years as a student in Ioannina. I hope to always make them proud.

Christos Gakis

May, 2025

Abstract

This thesis focuses on the characterization and laboratory-scale application of enzymatic biocatalytic systems for carbon dioxide (CO₂). With the ultimate goal of developing nanobiocatalytic systems, the study is divided into two sections, each centered on the application of two different enzymes: Carbonic Anhydrase (CA) and Formate Dehydrogenase (FDH).

The primary objective of immobilization concerns the immobilization of CA and FDH into hierarchically porous carbons nanoparticles (HPCs), which exhibit CO₂ adsorption properties. Additionally, another category of nanomaterials is utilized, the zinc oxide-iron oxide nanoparticles derived from aqueous olive leaf extract (ZnOFe(OLE)).

In the first section of this thesis, the biochemical characterization of the activity of five different overexpressed thermophilic CAs and commercially available CA from bovine erythrocytes was conducted. The characterization of CAs hydratase activity was performed using CO₂ gas as a substrate through three different methods based on the pH drop of the reaction medium. Additionally, the thermostability and esterase activity of CAs were assessed via the hydrolysis of p-nitrophenyl ester. The immobilization of CAs onto HPCs and ZnOFe was also studied, and the activity of the nanobiocatalysts was evaluated based on the esterase activity of CAs. Furthermore, the application of CAs in a CO₂ gas capture system was examined using two CO₂ mineralization protocols for gaseous CO₂ sequestration into calcium carbonate (CaCO₃).

Regarding the second part of this thesis, the enzymatic catalysis of CO₂ for formic acid production was investigated. The commercially available enzyme *Candida boidinii* FDH was selected as the CO₂ biocatalyst. The study focused on optimizing conditions that favor the reversibility of FDH's natural reaction, shifting from formate oxidation to CO₂ reduction, by increasing the reductive equivalents of the system. Additionally, an attempt was made to incorporate a cofactor regeneration system into the setup by introducing the commercial enzyme glutamate dehydrogenase. Lastly, FDH was also immobilized onto HPCs and ZnOFe, and the resulting nanobiocatalysts were characterized in both the natural and reversible reactions of the enzyme.

Περίληψη

Η παρούσα διπλωματική εργασία εστιάζεται στον χαρακτηρισμό και στην εφαρμογή ενζυμικών βιοκαταλυτικών συστημάτων του διοξειδίου του άνθρακα (CO₂) σε εργαστηριακή κλίμακα. Με απώτερο στόχο την ανάπτυξη νανοβιοκαταλυτικών συστημάτων, η διπλωματική μπορεί να χωριστεί σε δύο ενότητες, οι οποίες επικεντρώνονται στην εφαρμογή δύο διαφορετικών ενζύμων, της καρβονικής ανυδράσης (CA) και της αφυδρογονάσης του φορμικού (FDH).

Κύριος στόχος της ιδέας της ακινητοποίησης αφορά την ακινητοποίηση σε νανοϋλικά Ιεραρχημένου πορώδους άνθρακα (HPCs), τα οποία χαρακτηρίζονται από προσροφητικές ικανότητες ως προς το αέριο CO₂. Παράλληλα, στα πλαίσια αυτής της διπλωματικής αξιοποιείται ακόμη μία κατηγορία νανοϋλικών, τα νανοϋλικά οξειδίων ψευδαργύρου-οξειδίων σιδήρου που προέρχονται από υδατικό εκχύλισμα φύλλου ελιάς (ZnOFe (OLE)).

Στην πρώτη ενότητα της διπλωματικής πραγματοποιήθηκε ο βιοχημικός χαρακτηρισμός της δραστικότητας πέντε διαφορετικών υπερεκφρασμένων θερμοφίλων CAs και της εμπορικά διαθέσιμης CA από ερυθροκύτταρα βοοειδών. Ο χαρακτηρισμός της ιδιότητα της υδρατάσης, πραγματοποιήθηκε με αέριο CO₂ ως υπόστρωμα μέσω τριών διαφορετικών μεθόδων, οι οποίες βασίζονται στην μεταβολή του pH του μέσου αντίδρασης. Παράλληλα, πραγματοποιήθηκε χαρακτηρισμός της θερμοδραστικότητας της ιδιότητας εστεράσης CAs μέσω υδρόλυσης του π-νιτροφαινυλεστέρα. Μελετήθηκε εξίσου η ακινητοποίηση των CAs στα HPCs και στα ZnOFe και αξιολογήθηκε η δραστικότητα των νανοβιοκαταλυτικών μέσω της ιδιότητας της εστεράσης των CAs. Επιπλέον, μελετήθηκε η εφαρμογή των CAs σε σύστημα δέσμευσης αερίου CO₂, μέσω της χρήσης σε δύο πρωτόκολλων κατακρήμνισης του CO₂ σε ανθρακικό ασβέστιο.

Στο δεύτερο μέρος της διπλωματικής, μελετήθηκε η δυνατότητα ενζυμικής κατάλυσης του CO₂ για την παραγωγή φορμικού οξέος. Ως βιοκαταλύτης του CO₂ επιλέχθηκε το εμπορικά διαθέσιμο ένζυμο *Candida boidinii* FDH. Πραγματοποιήθηκε η μελέτη των συνθηκών που ωφελούν την αναστρεψιμότητα της φυσικής αντίδρασης της FDH, από την οξειδωση του φορμικού στην αναγωγή του CO₂, μέσω περίσσειας της αναγωγικής ισχύος του συστήματος. Παράλληλα, έγινε προσπάθεια ένταξης ενός συστήματος αναγέννησης συμπαραγόντα στο σύστημα, μέσω εισαγωγής του εμπορικού ενζύμου αφυδρογονάση του γλουταμικού. Παράλληλα, η FDH ακινητοποιήθηκε εξίσου στα νανοϋλικά HPCs και ZnOFe και πραγματοποιήθηκε ο χαρακτηρισμός των νανοβιοκαταλυτών τόσο στην φυσική όσο και στην αναστρέψιμη αντίδραση του ενζύμου.

Table of Contents

Chapter One: Introduction and Research Context	15
1. Introduction to Carbon Dioxide.....	15
1.1 Climate Change and Carbon Dioxide.....	15
1.2 Carbon Capture, Storage and Utilization Technologies	16
1.3 Carbon Dioxide Chemistry	18
1.3.1 Distribution of Carbonate Species in Aqueous Solutions.....	19
1.3.2 Parameters affecting CO ₂ solubility.....	20
1.4 Enzyme-mediated CO ₂ reactions.....	23
1.5 Formic acid	25
2. Enzymes.....	27
2.1 Carbonic Anhydrase	27
2.1.1 Mechanism.....	28
2.1.2 Harnessing CAs for Efficient and Thermostable Carbon Capture and Storage	30
2.1.3 Activity assays of CAs.....	31
2.1.3.1 Electrometric or Wilbur-Anderson-related Assays	32
2.1.3.2 Nitrophenyl acetate assay.....	33
2.2 Formate Dehydrogenases	34
2.2.1 <i>Candida boidinii</i> Formate Dehydrogenase	35
2.2.2 Mechanism	36
2.2.2.1 Formate catalysis mechanism of metal-independent FDH .	36
2.2.2.2 CO ₂ catalysis mechanism of metal-independent FDH.....	37
3. Chemistry of CO ₂ Catalysis	38
3.1 Thermodynamic Challenges in CO ₂ Utilization	38
3.2 Enzymatic Utilization of CO ₂ into methanol.....	39
3.2 Challenges and Prospective Solutions	41
3.2.1 Enzyme-Related Limitations Enzymatic Performance	41
3.2.2 Substrate Related Limitations	42
3.2.3 Cofactor Related Limitations.....	43
4 Enzyme Immobilization	45
Chapter Two: Materials and Methods	49
5. Materials	49

5.1 Commercial Enzymes.....	49
5.2 Heterologous expressed Enzymes (<i>E.coli</i>).....	49
5.3 Nanoparticles	49
5.4 Reagents.....	49
6. Methods.....	51
6.1 Carbonic Anhydrase Assays.....	51
6.1.1 Preparation of CO ₂ saturated H ₂ O	51
6.1.2 Electrometric Wilbur Anderson Assay	51
6.1.3 Colorimetric Wilbur Anderson Assay.....	52
6.1.4 Electrometric Assay pH-Stat.....	53
6.1.4.1 pH-stat Apparatus Setup.....	53
6.1.4.2 Experimental Results Evaluation	54
6.1.5 Esterase activity.....	55
6.1.5.1 Thermoactivity.....	55
6.1.6 CA-mediated CO ₂ Mineralization Experiments.....	55
6.1.6.1 One-step CaCO ₃ precipitation.....	55
6.1.6.2 Two-step CaCO ₃ precipitation	56
7.1 Dehydrogenase Assays	56
7.1.1 FDH Activity Assay and Kinetics	56
7.1.2 FDH Thermoactivity and pH-activity	57
7.1.3 FDH thermal stability.....	57
7.1.4 Glutamate Dehydrogenase pH-activity	57
8 Enzyme Immobilization.....	58
8.1 Non-Covalent Immobilization of CA/FDH onto Hierarchical Porous Carbon Nanoparticles (HPCs)	58
8.2 Hybrid zinc oxide–iron oxide ZnOFe(OLE) magnetic nanoparticles	58
8.2.1 Synthesis Of Hybrid Zinc oxide–Iron oxide magnetic nanoparticles.....	58
8.2.2 Immobilization of FDH onto ZnOFe (OLE) Nanoparticles	59
8.2.2.1 Non-Covalent Immobilization	59
8.2.2.2 Covalent Immobilization	59
8.3 Immobilization Efficiency of FDH Immobilization	60
8.4 Activity Assays of Immobilized Enzymes	61
8.4.1 FDH@ZnOFe Activity Assay	61
8.4.2 FDH@ZnOFe Reusability	61

8.4.3 FDH@ZnOFe Thermoactivity and pH-activity	62
8.4.4 FDH@ZnOFe Thermal stability.....	62
8.5 Fourier-transform infrared spectroscopy (FTIR)	62
9 Enzymatic reduction of CO ₂ to formic acid	63
9.1 pH stability of NADH Cofactor.....	63
9.2 FDH-mediated CO ₂ Reduction to Formic Acid.....	63
10 Analytical Methods	65
10.1 Formic Acid Quantification	65
10.1.1 Formic Acid Derivatization with 2,3,4,5,6-Pentafluorobenzyl bromide (PFBBr).....	65
10.1.2 GC-MS analysis of PFBBr-formic acid ester	66
Chapter Three: Results and Discussion	68
1 Carbonic Anhydrase Assays	68
1.1 Hydratase Activity of CAs.....	68
1.2 Esterase Activity of CAs	70
1.3 CA-mediated CO ₂ Mineralization.....	71
1.3.1 One-step CO ₂ mineralization	72
1.3.2 Two-step CO ₂ mineralization	74
Outline for Carbonic Anhydrase assays.....	77
2 Enzyme Immobilization.....	79
2.1 Selection of Nanoparticles.....	79
2.2 Thermophilic CAs Immobilization onto HPCs.....	80
2.3 Thermophilic CAs immobilization onto ZnOFe	81
2.4 FDH Immobilization.....	83
2.4.1 FDH@HPCs nanobiocatalyst.....	83
2.4.2 FDH@ZnOFe nanobiocatalyst	85
2.4.3 Activity of FDH@ZnOFe Nanobiocatalysts.....	86
2.4.4 Kinetic comparison of Free and Immobilized FDH (FDH@ZnOFe) .	87
2.4.5 FDH@ZnOFe Reusability	89
2.4.6 pH Activity and Thermoactivity of Covalently Immobilized FDH@ZnOFe.....	90
2.4.7 Thermal Stability of FDH@ZnOFe at 60 °C	91
2.4.8 FTIR of Free and Immobilized FDH	92
Outline for Enzyme Immobilization.....	94

3 CO ₂ reduction to formic acid	95
3.1 pH activity of FDH AND GDH.....	95
3.2 Investigation of NADH stability	96
3.3 FDH-mediated reduction of CO ₂ to formic acid	98
3.4 Cofactor Regeneration in the presence of Glutamate Dehydrogenase	101
3.5 Comparison between bubbled CO ₂ or NaHCO ₃	103
3.6 CO ₂ reduction with Immobilized FDH	104
Outline for FDH-mediated CO ₂ reduction	107
Supplementary	108
Enzyme Protein Content	108
Dehydrogenases	108
Carbonic Anhydrases	108
Thermoactivity of CAs.....	109
Non-CA-mediated CaCO ₃ precipitation	109
Free FDH Michaelis Menten Kinetics	110
Covalently immobilized FDH@ZnOFe Michaelis Menten Kinetics.....	110
GDH pH Activity Profile	111
Derivatized PFBBr-Formic Acid Ester Calibration Line (GC-MS)	111
GC-MS Chromatograph of derivatized Formic Acid-PFBBr Ester.....	111
Total Ion Chromatogram of Formic Acid-PFBBr Ester	112
Bibliography.....	113

Chapter One: Introduction and Research Context

1. Introduction to Carbon Dioxide

1.1 Climate Change and Carbon Dioxide

Carbon Dioxide (CO₂) has always been present in the atmosphere, playing the most important role in regulating the Earth's climate through the greenhouse effect (Cassia et al., 2018). Unlike the other atmosphere gasses, nitrogen and oxygen, the presence of CO₂ is crucial for trapping heat and re-emitting it, either back toward the Earth's surface or out to space. This heat-trapping process helps maintain surface temperatures above freezing. Fluctuations in CO₂ levels have influenced climate patterns, contributing to both warming and cooling periods throughout Earth's history (Lindsey R., 2024). However, to this day, the rapid increase in CO₂ concentrations due to human activities is disrupting this natural balance, leading to unprecedented changes in global temperatures and climate stability (Jones et al., 2023). The primary cause of the rise in human-caused emissions is the significant use of fossil fuels, including lignite, coal, oil, and natural gas, particularly in the energy sector.

The increasing accumulation of CO₂ in the atmosphere has become one of the most pressing environmental challenges humanity faces. By 2023, CO₂ levels reached an unprecedented concentration of 419.3 parts per million, representing a significant 50% increase compared to pre-industrial levels (Fig. 1). As a major contributor to global warming, CO₂ was a key factor in making 2023 the warmest year on record since global temperature measurements began in 1850, with an average temperature of 1.18 °C above the 20th-century average. Furthermore, in 2023, global energy-related CO₂ emissions rose by 1.1%, increasing by 410 million tonnes to a new all-time high of 37.4 billion tonnes (NOOA, 2024). Nearly 65% of this increase in emissions came from coal. Between 2019 and 2023, energy-related emissions rose by approximately 900 million tonnes (IEA, 2024). Without the significant deployment of five major clean energy technologies, solar photovoltaic, wind, nuclear, heat pumps, and electric vehicles, emissions would have tripled during this period.

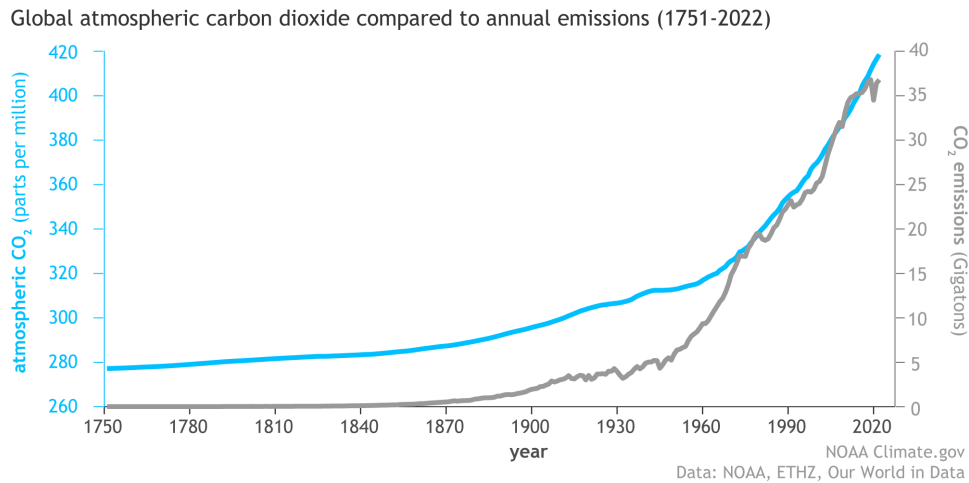


Figure 1 Representation of the increase of the amount of CO₂ in the atmosphere (blue line) compared with human emissions (gray line) since the start of the Industrial Revolution in 1750. Emissions rose slowly to about 5 gigatons—one gigaton is a billion metric tons—per year in the mid-20th century before skyrocketing to more than 35 billion tons per year by the end of the century. NOAA Climate.gov graph, adapted from original by Dr. Howard Diamond (NOAA ARL). Atmospheric CO₂ data from NOAA and ETHZ. CO₂ emissions data from Our World in Data and the Global Carbon Project (Lindsey R., 2024).

Given the anticipated rise in global energy demand, primarily fueled by developing economies, atmospheric CO₂ levels are expected to increase substantially over the coming decades. According to the Intergovernmental Panel on Climate Change (2023) achieving net-zero CO₂ emissions and rapidly adapting to renewable energy resources are essential for limiting human-induced global warming (Lee et al., 2023). The total cumulative carbon emissions up to the point of reaching net-zero CO₂, along with the level of greenhouse gas emission reductions implemented during this decade, play a critical role in determining whether a global temperature rise can be confined to 1.5 or 2 °C. This transition is crucial not only to mitigate the severe impacts of climate change, but also to enhance energy security and foster sustainable economic growth. Furthermore, global cooperation and policy frameworks that incentivize investment in renewable energy and establish clear emissions reduction targets will be imperative for driving the necessary changes in both public and private sectors.

1.2 Carbon Capture, Storage and Utilization Technologies

Among the potential solutions to reduce CO₂ emissions, Carbon Capture, Utilization, and Storage (CCUS) technologies represent a vital and promising approach for decarbonizing global industrial sectors (Kang et al., 2020; Talekar et

al., 2022). A common requirement for both Carbon Capture and Storage (CCS) and Carbon Capture and Utilization (CCU) is the effective transfer of CO₂ from the gas to the aqueous phase. However, it is essential to distinguish between CCS and CCU, as they serve different purposes while collaboratively contributing to reducing CO₂ emissions.

CCS refers to technologies designed to extract and isolate CO₂ from flue gas, either before combustion (pre-combustion) or after combustion (post-combustion) of carbon-containing fuels. After separation, the CO₂ is compressed and transported via pipeline infrastructure to designated storage sites, such as saline aquifers beneath the Earth's surface (Mortezaei et al., 2021). CCS technologies commonly employ wet absorption processes using amine-based or carbonate-based solvents to capture CO₂ from emission sources. This is followed by the desorption process, which produces a purified form of CO₂ for compression and storage.

CCU, on the other hand, involves using CO₂ as a feedstock to produce carbon-based valuable products (Hepburn et al., 2019). CCU can be categorized into inorganic and organic utilization. Inorganic utilization typically results in the formation of carbonate-based materials, such as metal carbonates, which find applications in construction and manufacturing. Organic utilization expands the range of potential products by converting CO₂ into chemicals, fuels, and polymers. This approach can lead to more cost-effective and environmentally friendly production methods, especially compared to traditional fossil hydrocarbon-based processes (De Luna et al., 2019).

Focusing on organic-derived products, CCU employs various conversion methods, which are typically classified as chemical, electrochemical, photochemical, thermochemical, and biocatalytic approaches. All these methods require significant energy input to activate and convert the chemically stable CO₂ molecule, making energy efficiency a key consideration in the development and implementation of these technologies.

1.3 Carbon Dioxide Chemistry

CO₂ (Fig. 2) is a colorless, odorless, relatively non-toxic, and incombustible gas that plays a crucial role in various biological and chemical processes. This inorganic molecule has a molecular weight of 44.01 g/mol and is nonpolar, existing as a gas under standard temperature and pressure conditions due to weak intermolecular interactions (van der Waals forces) (Haynes, 2014). These weak forces are insufficient to maintain CO₂ in a liquid state under normal conditions. Despite its simple molecular structure, CO₂ exhibits a remarkable range of complex behaviors across diverse chemical and biological systems.

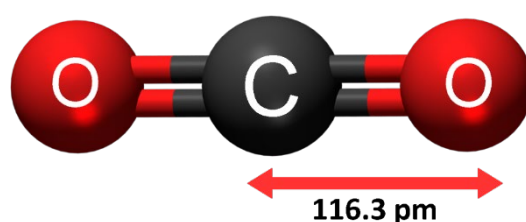


Figure 2 Representation of the carbon dioxide (CO₂) molecule and its structural characteristics (Commons, 2024).

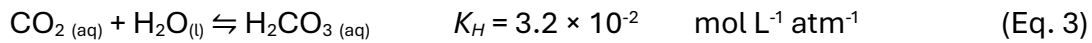
The solubility of gaseous CO₂ (CO_{2(g)}) in water is governed by its partial pressure and the chemical interactions between dissolved CO₂ (CO_{2(aq)}) and other solutes in the aqueous phase (Butler, 2019). Under standard conditions, CO_{2(g)} is considered a moderately soluble gas in water. In acidic solutions (pH < 5), the concentration of CO₂ can be described by Henry's Law (Eq. 1), where Henry's constant K_H quantifies the solubility of CO₂ in water at a given partial pressure. At a partial pressure of 1 atm, the maximum concentration of CO_{2(aq)} in water is approximately 0.034 mol L⁻¹ (25 °C).

$$[\text{CO}_{2(\text{aq})}] = K_H P_{\text{CO}_2} \quad (\text{Eq. 1})$$

Equation 1 Henry's Gas Law: the concentration of a gas dissolved in a liquid is directly proportional to its partial pressure in the gas phase above the liquid. In this formula, $[\text{CO}_{2(\text{aq})}]$ represents the concentration of dissolved CO₂ (mol L⁻¹), K_H is Henry's constant for CO₂ solubility in water (mol L⁻¹ atm⁻¹), and P_{CO_2} denotes the partial pressure of CO₂ (atm).

Beyond its solubility, CO₂'s interaction with water initiates a cascade of chemical transformations (Knoche, 1980; Villa et al., 2023). Initially, CO_{2(g)} dissolves into water to form aqueous carbon dioxide CO_{2(aq)}, where the hydrated CO₂ molecules are dispersed but not chemically bonded to the water molecules (Eq. 2). Subsequently, dissolved CO_{2(aq)} partially reacts with water to form carbonic

acid (H_2CO_3) in a slow equilibrium process (Eq. 3). Notably, the hydration constant (K_H) indicates that only a small fraction of $\text{CO}_{2(\text{aq})}$ is converted to H_2CO_3 . As a result, most of the dissolved CO_2 remains in the form of $\text{CO}_{2(\text{aq})}$, rather than being hydrated into H_2CO_3 (Schulz et al., 2006). As a diprotic acid, H_2CO_3 dissociates twice in water: first into bicarbonate ions (HCO_3^-) and then into carbonate ions (CO_3^{2-}), with the concurrent production of protons (H^+), described in Eq. 4 and Eq. 5, respectively. In both cases, the production of H^+ during the dissociation of carbonate species contributes to the acidification of the aqueous solution. Additionally, the dissociation constants K_{a1} and K_{a2} of the carbonate species reflect their weak Brønsted acid nature, with K_{a1} typically being larger than K_{a2} .



Equations 2-4. Acid–base equilibria for CO_2 water-soluble species. Henry's constant (hydration constant) is represented as K_H , and K_{a1} , K_{a2} denote the dissociation constants of $\text{H}_2\text{CO}_{3(\text{aq})}$ and $\text{HCO}_3^-_{(\text{aq})}$, respectively.

As previously mentioned, in aqueous solutions, CO_2 primarily exists in four forms: $\text{CO}_{2(\text{aq})}$, $\text{H}_2\text{CO}_{3(\text{aq})}$, $\text{HCO}_3^-_{(\text{aq})}$, and $\text{CO}_3^{2-}_{(\text{aq})}$. The total CO_2 content in an aqueous system extends beyond just the physically dissolved ($\text{CO}_{2(\text{aq})}$) and integrates the entire dissolved inorganic carbon (DIC) pool as observed at Eq. 6. Usually, when considering the DIC, H_2CO_3 can be omitted since it stably comprises less than 0.01% of the DIC or 0.1% of $\text{CO}_{2(\text{aq})}$ and thus is considered to be merged with $\text{CO}_{2(\text{aq})}$ (Konig et al., 2019; Schulz et al., 2006). In the subsequent sections, the notation "_(aq)" will be omitted from $\text{HCO}_3^-_{(\text{aq})}$ and $\text{CO}_3^{2-}_{(\text{aq})}$, as the discussion will exclusively refer to the dissolved forms of carbonate species.

$$\text{DIC} = [\text{CO}_{2(\text{aq})}] + [\text{H}_2\text{CO}_{3(\text{aq})}] + [\text{HCO}_3^-_{(\text{aq})}] + [\text{CO}_3^{2-}_{(\text{aq})}] \quad (\text{Eq. 6})$$

1.3.1 Distribution of Carbonate Species in Aqueous Solutions

The relationship between pH and the distribution of carbonate species is fundamental to understanding carbonate chemistry in water (Fig. 3). This relationship is governed by acid-base equilibrium constants, enabling the

calculation of the relative concentrations of all carbon species as a function of pH in a hypothetical closed system (constant partial pressure of CO_2) illustrates the fractional distributions of dissolved CO_2 species ($\text{CO}_{2(\text{aq})}$ and HCO_3^- , CO_3^{2-}), which can be derived using the Henderson-Hasselbalch equation (Butler, 2019). Therefore, under acidic conditions (pH values < 4.0), $\text{CO}_{2(\text{aq})}$ and H_2CO_3 predominate. As the pH increases, HCO_3^- ions become the dominant species in the slightly acidic to slightly basic range ($6.35 < \text{pH} < 10.33$). Lastly, at higher alkaline pH values, CO_3^{2-} ions are the most prevalent carbon-containing species.

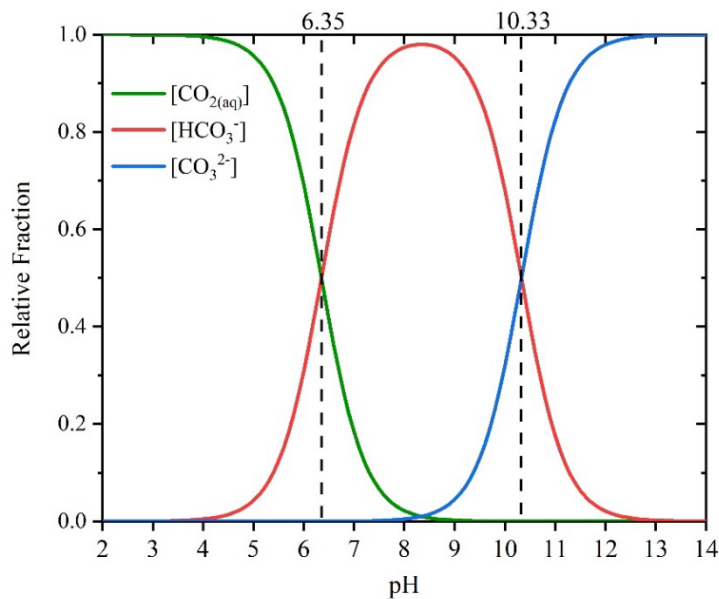


Figure 3 Relative fractions of dissolved carbon dioxide species ($[\text{CO}_{2(\text{aq})}]$, $[\text{HCO}_3^-]$, and $[\text{CO}_3^{2-}]$) as a function of pH. The graph depicts the equilibrium distribution of carbonate species in aqueous solution. The dashed lines correspond to the first ($\text{p}K_{a1} \approx 6.35$) and second ($\text{p}K_{a2} \approx 10.33$) acid dissociation constants of carbonic acid, marking the transitions between dominant species.

1.3.2 Parameters affecting CO_2 solubility

This subsection will be focused on the key factors influencing CO_2 solubility in aqueous solutions, including temperature, pressure, and the presence of other solutes. (e.g., salts or organic molecules) (Mao et al., 2013; Steel et al., 2016).

Temperature plays a crucial role in CO_2 solubility, as an increase in temperature leads to a rise in the kinetic energy of molecules, including CO_2 . This increased energy enables CO_2 molecules to more easily overcome the attractive forces of the liquid phase and escape, resulting in reduced solubility. This decrease in solubility at higher temperatures is reflected in Henry's law constant

K_H , which significantly decreases compared to standard temperatures. As illustrated at Fig. 4 an increase in temperature has an inverse effect on CO_2 solubility.

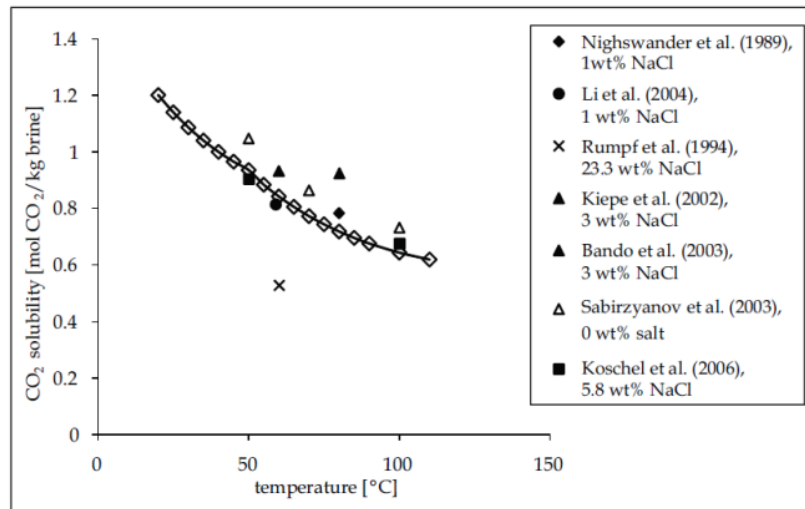


Figure 4 Comparison of modeled and experimental data on temperature-dependent CO_2 solubility at 10 MPa and 1 mol NaCl kg^{-1} brine (Steel et al., 2016).

Conversely, CO_2 solubility increases with rising pressure, as explained by Henry's Law, which states that the solubility of a gas in a liquid is directly proportional to its partial pressure above the liquid surface. Higher pressure forces CO_2 molecules to be more solvated and remain in the liquid phase. Fig. 5 illustrates how an increase in pressure enhances CO_2 solubility.

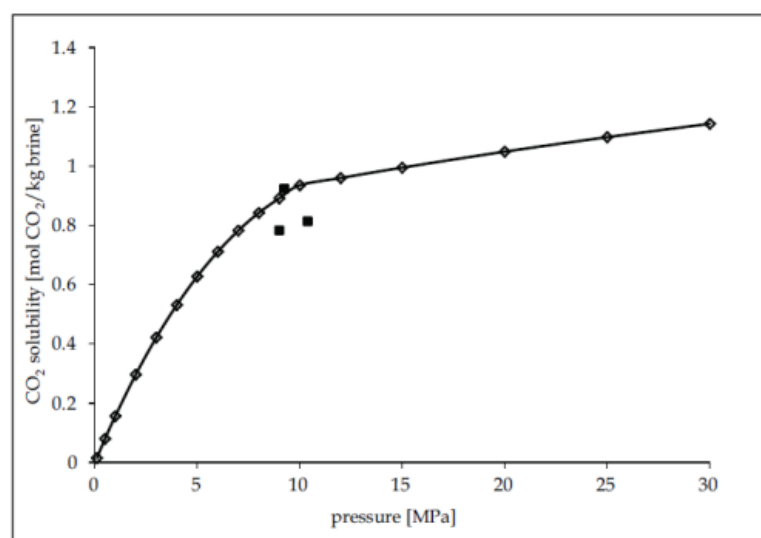


Figure 5 Comparison of modeled and experimental data on the relationship between CO_2 solubility and pressure at 323 K in 1 mol NaCl kg^{-1} brine (Steel et al., 2016).

The presence of other solutes in an aqueous solution can influence CO₂ solubility, as they alter the physical and chemical properties of the medium. Salts (e.g., salinity) act as regulators of CO₂ solubility, leading to the 'salting-out' effect, where CO₂ solubility decreases as the salt concentration in the solution increases. The addition of salts like sodium chloride (NaCl) increases the ionic strength of the solution. This higher ionic strength reduces CO₂ solubility because the dissolved ions compete with CO₂ for water molecules, thereby reducing the number of water molecules available to solvate CO₂ (Fig. 6). Furthermore, the increased ionic strength enhances electrostatic interactions between the ions and water molecules, which can slightly increase the solution's viscosity. As viscosity increases, the rate of CO₂ diffusion decreases, since a more viscous solution presents greater resistance to the movement of CO₂ molecules, resulting in fewer interactions between CO₂ and water.

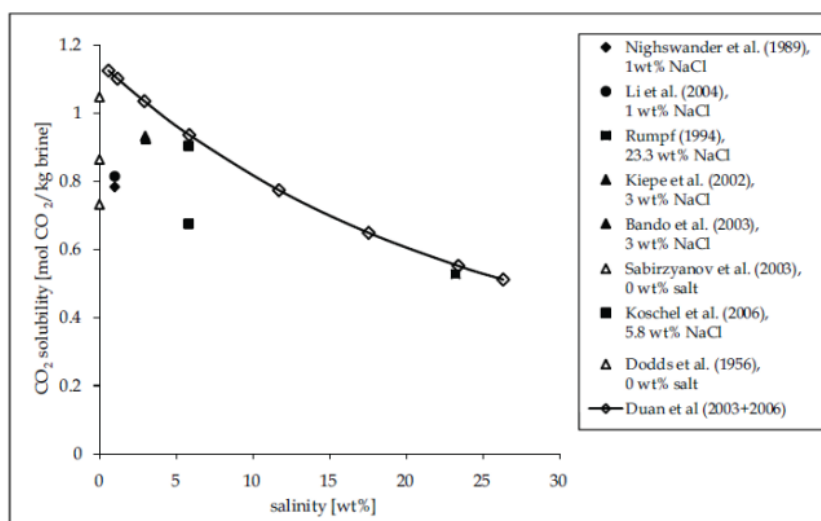


Figure 6 Comparison of modeled and experimental data on Salinity-dependent CO₂ solubility at 323K and 10MPa (Steel et al., 2016).

Similarly to salinity, some organic compounds generally decrease CO₂ solubility, although the specific effects depend on their chemical structure and concentration. However, certain specially tailored organic compounds, particularly those with branched structures, can increase CO₂ solubility thus presenting new opportunities (Kobayashi & Firoozabadi, 2023). Furthermore, mentionable and promising mediums like Deep Eutectic Solvents (DES) and Ionic Liquids (ILs) exhibit remarkable properties of enhancing CO₂ solubility compared

to water due to their unique chemical structures, which facilitate stronger interactions with CO₂ molecules for CCU technologies (Marcus, 2018; Zhang et al., 2016). Although this thesis focuses only on aqueous solutions, further discussion of these mediums is beyond the scope of this work.

1.4 Enzyme-mediated CO₂ reactions

Enzyme-mediated CO₂ reactions are fundamental biochemical processes occurring on a massive scale in nature, facilitating essential carbon transformations that support life and influence planetary systems. According to the BRENDA database, CO₂ plays multiple roles as a ligand in various enzymatic processes (Chang et al., 2021; Jeske et al., 2019). More than 5,130 reactions have been reported where CO₂ functions as a ligand, substrate, product, activator, or inhibitor. In the context of CO₂ as a substrate in enzyme-mediated reactions, 239 unique reactions have been documented. Fig. 7 provides an overview of the 59 distinct EC numbers associated with these 239 reactions, along with the diversity of the classes and subclasses of enzymes or enzymatic systems involved in CO₂-substrate mediated reactions.

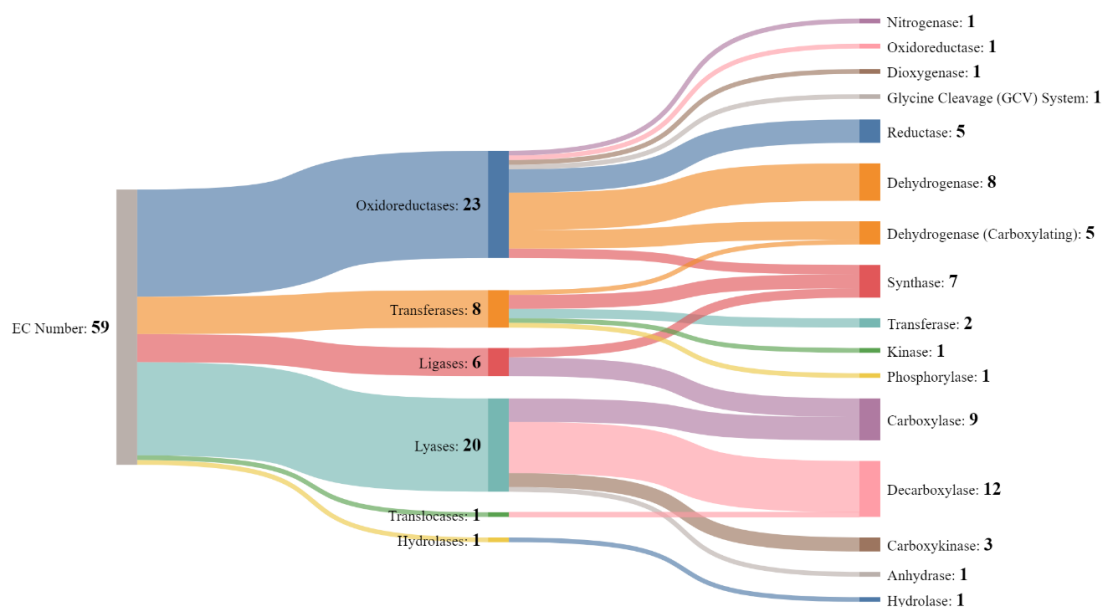


Figure 7 Sankey Diagram of 59 EC Numbers involved at 239 enzyme-mediated reactions, where the CO₂ molecule serves as substrate. Data was collected from BRENDA database, accessed at December 2024.

CO₂ serves as a substrate in six out of the seven major enzymatic classes. Oxidoreductases and lyases are the most diverse classes in CO₂-substrate

mediated reactions. Oxidoreductases can utilize CO₂ as either an electron acceptor or donor in different redox reactions, whereas lyases are involved in both carboxylation and decarboxylation processes, enabling them to take part in many CO₂-related metabolic pathways across various organisms. Apparently, isomerases are not involved, since the nature of the CO₂ molecule has a fixed structure, lacking molecular complexity, with only one possible rearrangement of its molecules (one central carbon double-bonded to two oxygen molecules). It is important to note that, while CO₂ plays its own role as a substrate, other carbon species derived from CO₂ (most commonly bicarbonate ions) are often utilized instead of CO₂ directly, expanding the complexity of CO₂-related enzymatic reactions (Bierbaumer et al., 2023).

The given diversity of enzymes involved in CO₂-mediated reactions does not necessarily reflect their prevalence or frequency in nature. Nonetheless, this diversity offers valuable insights into the potential biochemical processes involving CO₂ across different biological systems. It should be acknowledged that databases like BRENDA reflect only our current knowledge, which is far from complete and constantly evolving as ongoing discoveries of microbial diversity and enzymes continue to expand our understanding.

In the research context of CCUS, several metalloenzymes may serve as ideal candidates for such applications (Deng et al., 2024; Villa et al., 2023). Highlighting the CO₂ Capture technologies, the zinc-containing carbonic anhydrase, a lyase-class enzyme, is highly reported due to its highly efficient and reversible reaction, achieving a turnover rate of 10⁶ s⁻¹ without requiring any cofactors (Shao et al., 2024).

In the context of CO₂ utilization, enzymes belonging to the oxidoreductase class, particularly formate dehydrogenases (FDH), carbon monoxide dehydrogenases (CODH), formylmethanofuran dehydrogenases (FMD) and nitrogenases, are among the most promising candidates. These oxidoreductases facilitate the direct reduction of CO₂ by catalyzing electron transfer reactions, requiring external electron donors. Specifically, they rely on energy-rich cofactors such as ferredoxins and nicotinamide adenine dinucleotides (NAD(P)H) to drive the reduction process. Applications of oxidoreduction enzymes can be expanded

when combined with electrochemical, photochemical, or other enzymatic systems that provide the necessary energy (electrons and/or protons) or broaden the range of CO₂-derived products.

1.5 Formic acid

Formic acid (from the Latin word formica, meaning “ant”), the acid counterpart of formate, is not only the simplest carboxylic acid but also ranks among the top 100 most important chemical compounds, with wide applications across various industrial sectors such as chemical, pharmaceutical, food, agricultural, rubber, livestock feed, and textile industries (Fig. 8) (Chen et al., 2020; Liu et al., 2015). In biomedical applications, formic acid has historically been used not extensively in clinical practice for the treatment of skin conditions such as warts and pediculosis (Bhat et al., 2001; DeFelice et al., 1989). However, it is now primarily valued for its ancillary roles in pharmaceutical processes rather than as a direct therapeutic agent.

At the laboratory scale, formic acid serves multiple roles in chemical synthesis, including as a reducing agent, building block, green solvent, and in analytical chemistry to enhance the solubility and recovery of analytes. As a green commodity, it is relatively nontoxic and noncorrosive, which enables easy handling. Furthermore, according to the European Chemicals Agency, formic acid is biodegradable in wastewater or seawater since it is not coupled with nitrates, phosphates, or sulfate ions.

A promising aspect of formic acid is its use as a green fuel or precursor for other high-value fuels, including methanol, bio-oils, and hydrogen (H₂). Remarkably, it serves as an efficient hydrogen storage material due to its high hydrogen content (4.4% by weight), ease of transportation, and ability to release hydrogen gas upon catalytic decomposition under mild conditions. Additionally, formic acid shows potential for use in carbon monoxide (CO) storage and as a direct hydrogen donor.

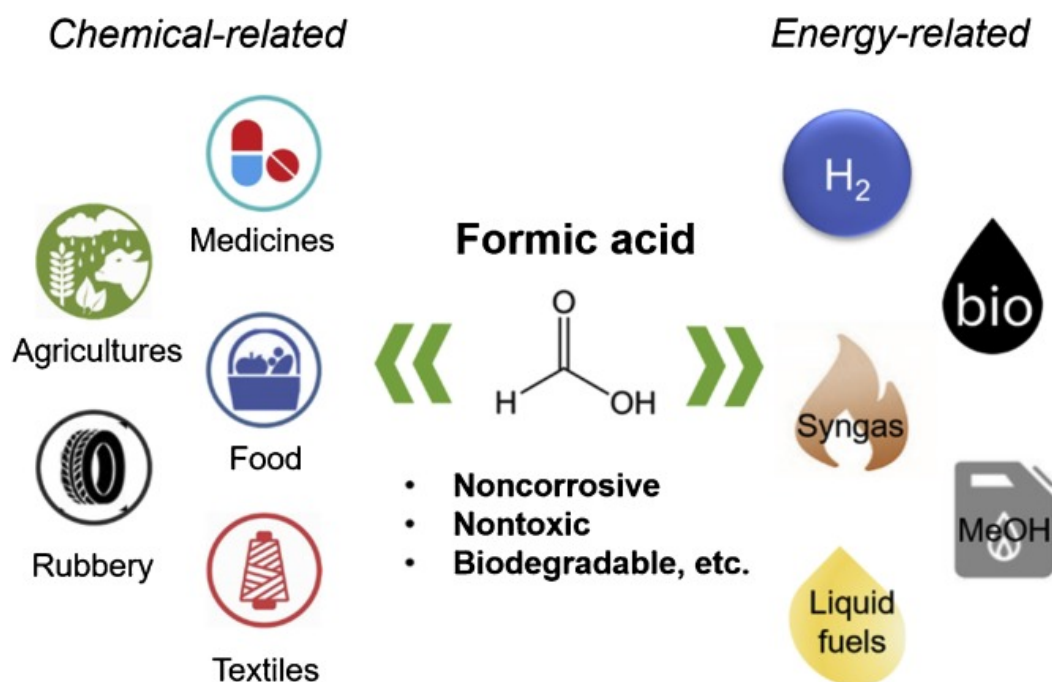
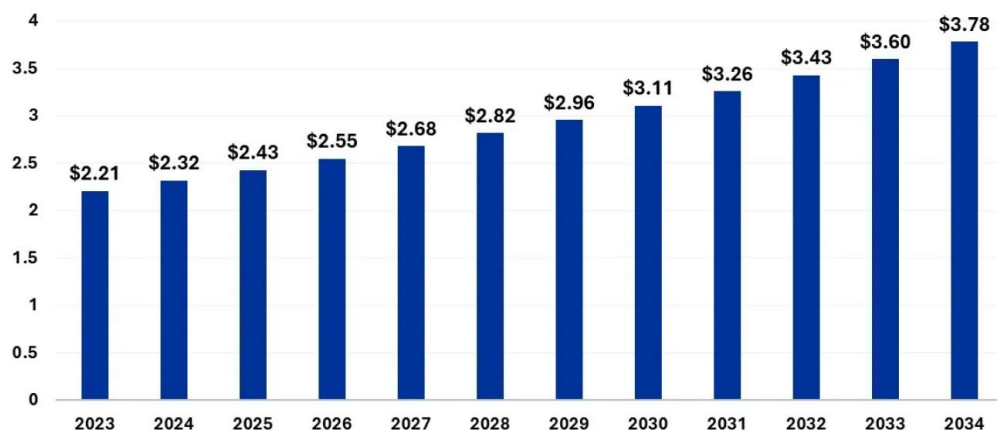


Figure 8 Formic acid applications in nowadays industrial sectors (Chen et al., 2020).

The global formic acid market is experiencing significant growth, driven by its versatile applications across various industries. In 2024, the market was valued at approximately 2.32 billion USD and is projected to reach USD 3.78 billion by 2032, reflecting an annual growth rate of 5% between 2024 and 2032 (Fig. 9) (Precedence Research, 2024). Currently, industrial production of formic acid relies on a fossil-based, two-step process in which methanol reacts with carbon monoxide to produce methyl formate, which is subsequently hydrolyzed to yield formic acid (Bulushev & Ross, 2018). However, to meet decarbonization goals, more sustainable technologies must be developed, utilizing renewable feedstocks such as biomass and CO_2 as formic acid precursors. This transition to renewable resources will promote low-carbon, sustainable development across modern industries.



Source: <https://www.precedenceresearch.com/formic-acid-market>

Figure 9 Estimated Formic acid market size from 2023 to 2034 (USD billion) (Precedence Research, 2024).

2. Enzymes

2.1 Carbonic Anhydrase

Back in 1933, the discovery of the enzyme Carbonic Anhydrase (CA, EC 4.2.1.1) marked a significant milestone in understanding CO₂ transport and acid-base balance in biological systems. It provided crucial insights into how the body efficiently eliminates CO₂ and regulates blood pH (Liljas & Laurberg, 2000; Meldrum & Roughton, 1933). As depicted Eq. 7, CAs accelerate the reversible hydration of CO₂ to carbonic acid (H₂CO₃), which spontaneously disassociates to bicarbonate (HCO₃⁻) and protons (H⁺) (Pierre, 2012). Remarkably, these biocatalysts achieve an exceptionally high conversion rate, reaching a maximum of 10⁶ s⁻¹ (Villa et al., 2023).



CAs are ubiquitous enzymes, present in both prokaryotes and eukaryotes, and have so far been categorized into eight families (α -, β -, γ -, δ -, ζ -, η -, θ -, and ι -CAs), each one carrying diverse physiological roles involving CO₂. Most CAs are monomeric proteins (Fig. 10A) with an average molecular weight of 30 to 50 kDa, depending on the enzyme class. All classified CAs, except for ι -CAs, are

metalloenzymes, with Zn(II) being the most common metal in their active sites. Other metals such as Cd(II), Fe(II), and Co(II) can also serve this role, highlighting their essential nature, as the corresponding apoenzymes (metal-free forms) are completely catalytically inactive.

The hydratase activity of CAs has been extensively studied, especially in vertebrates and mammals (α -CAs family). Given their critical roles in human physiology, the inhibition or activation of Human CAs has been a key focus of clinical and pharmacological research for decades. (Pinard et al., 2015). In addition to their well-established role in CO₂ hydration, naturally occurring α -CAs have demonstrated the ability to catalyze a range of other reactions *in vitro* (Supuran, 2016). These include the hydration of cyanate, cyanamide, and aldehydes, as well as the hydrolysis of carboxylic, sulfonic, phosphate, and thioesters, among others. Remarkably, through protein engineering, the repertoire of reactions catalyzed by CAs can be further expanded, unlocking new enzymatic properties such as reductase, oxidase, metathesis, and selenoesterase activities (Angeli et al., 2020). These advancements position CAs as promising tools for innovative applications in organic chemistry.

2.1.1 Mechanism

The hydration reactions catalyzed by carbonic anhydrases (CAs) are well-understood in α -CAs (Supuran, 2016). As previously mentioned, the presence of a metal ion in the enzyme's active site is crucial, with Zn²⁺ serving this role in α -CAs. The active site adopts a bipartite conformation: one half is hydrophobic, primarily composed of residues such as Val and Leu, to trap the substrate, while the other half is hydrophilic to bind CO₂ and release the polar components into the reaction environment. The catalysis takes place in a deep and wide cavity containing the metal at the bottom. The active site is typically in a basic form, characterized by a tetrahedral geometry where Zn²⁺ is coordinated with a water molecule (as OH⁻) and three key residues (Fig. 10B), which vary depending on the enzyme class. These residues include histidines, cysteines, or glutamines. Adjacent to the active site, additional amino acid residues such as Thr and Glu enhance the

nucleophilicity and the orientation of the bound water molecule, further facilitating the reaction.

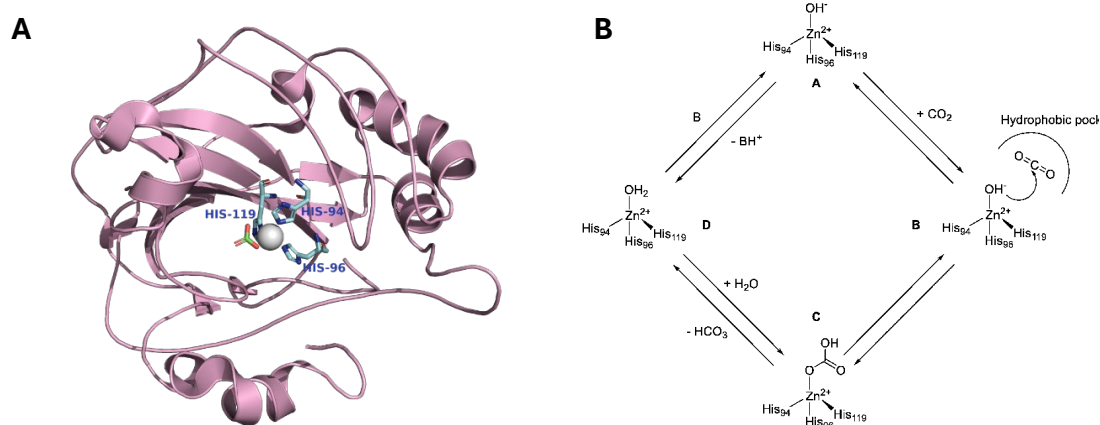


Figure 10 A. Three-dimensional structure of Human Carbonic Anhydrase II, an egg-shaped monomeric protein featuring a core of a ten-stranded antiparallel β -sheet surrounded by several helices and additional β -strands. The Zn^{2+} ion, represented as a gray sphere, is coordinated by a cluster of histidine residues, shown as sticks. Additionally, the bicarbonate molecule is displayed in stick representation (Protein Data Bank accession number 2VVB). B. A schematic overview of the catalytic mechanism of HCAII-mediated CO_2 hydration is provided.

The catalytic mechanism of α -, β -, and γ -carbonic anhydrases (CAs) proceeds in two main steps. In the first step, the zinc-bound water molecule acts as a nucleophile (neutral pH), attacking the CO_2 molecule bound within the hydrophobic pocket. This results in the formation of a bicarbonate-coordinated zinc complex. Subsequently, the bicarbonate is displaced by a new water molecule, regenerating Zn^{2+} -coordinated water. As bicarbonate is released into the solvent, the active center transitions to an acidic and catalytically inactive form. The second step involves the “proton shuttle,” which is the rate-limiting step of the catalytic cycle. This process transports the proton from the zinc-bound water molecule to the solvent outside the active center. The formation of Zn^{2+} -OH⁻ is essential to restore the active center to its basic form, allowing it to catalyze another CO_2 molecule. Notably, in the fastest CAs ($K_{cat} \sim 10^6 \text{ s}^{-1}$), the proton shuttle is accelerated by a cluster of histidines that coordinate the Zn^{2+} ion, and another one histidine residue located at the entrance of the active site. These features endow the enzyme with unique characteristics, enabling it to approach the aqueous diffusion limit of water ($10^8 \text{ to } 10^9 \text{ M}^{-1} \text{ s}^{-1}$) (Nelson, 2004).

Similarly to the hydration of CO_2 , mechanistic studies report that the hydrophobic pocket of these enzymes can accommodate larger ligands than CO_2

(esters, aldehydes) (Angeli et al., 2020). The hydration of CO_2 and the hydrolysis of esters share key mechanistic similarities, particularly in the formation of a tetrahedral intermediate via nucleophilic attack on a carbonyl group. Both reactions involve the addition of a nucleophile (hydroxide or water) to an electrophilic carbon center, stabilization of the oxyanionic intermediate, and subsequent proton transfer steps, as illustrated in Fig. 11. However, it is important to note that esterase activity is not present in all CA classes (e.g., δ -CA classes lack esterase activity), and these reactions are not the primary function of carbonic anhydrases. Consequently, ester hydrolysis does not proceed as rapidly as CO_2 hydration. Engineering efforts have successfully modified these enzymes to more efficiently catalyze ester substrates and improve their specificity for bulkier ligands, expanding their potential applications in biocatalysis.

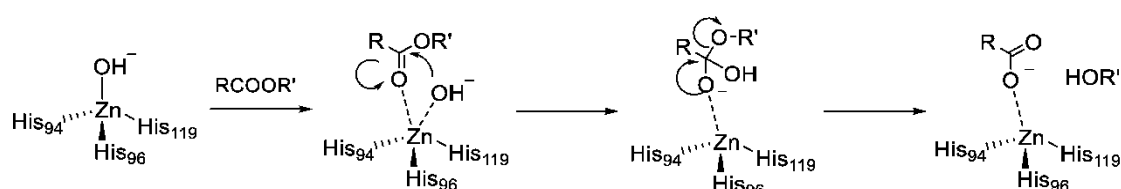


Figure 11 Suggested Mechanism of CA esterase activity (Angeli et al., 2020).

2.1.2 Harnessing CAs for Efficient and Thermostable Carbon Capture and Storage

CAs play a pivotal role in enhancing the efficiency of CCS technologies by accelerating the hydration of CO_2 and facilitating its conversion to bicarbonate or carbonate ions (Shao et al., 2024; Talekar et al., 2022; Villa et al., 2023). In chemical absorption, CA has proven effective in improving CO_2 uptake rates when combined with alkaline solvents such as monoethanolamine (MEA) or N-methyl diethanolamine (MDEA), offering increased efficiency and stability across varying pH and temperature ranges (Castro et al., 2022). In another method, chemical carbonation efficiently captures CO_2 by converting it into stable carbonate precipitates through its reaction with alkaline solutions like KOH or $\text{Ca}(\text{OH})_2$, with CA significantly accelerating the process. Since CO_2 uptake is the limiting step in chemical carbonation, the use of CAs enhances CO_2 uptake rates and improves reaction efficiency. Additionally, CA's utility extends to biomineralization, where

the enzyme enhances the formation of stable carbonate minerals under extreme conditions of high temperature, pressure, and alkalinity. To fully harness the potential of CA in sustainable CCS technologies, immobilization is crucial to protect the protein and enable reusability, while protein engineering further enhances its stability and functionality, ensuring improved efficiency, reduced energy demands, and greater viability for industrial-scale CO₂ sequestration.

Regarding to industrial applications, the widespread implementation of carbonic anhydrases (CAs) remains incomplete, highlighting the significance of utilizing thermostable variants (Di Fiore et al., 2015). The industrial sector presents considerable challenges and limitations for implementing biological entities in CCS, necessitating the use of highly stable biocatalysts capable of withstanding extreme conditions. These conditions include temperatures exceeding 80–100 °C, elevated pressure (to increase CO₂ solubilization) and alkaline pH levels, and the presence of high concentrations of salts, organic ions, and metals. Addressing these challenges requires the development of enzymes that maintain both stability and activity under such harsh conditions. Thus, to overcome these barriers three main approaches have been established for the retrieval of thermostable CAs: (i) identifying and isolating these enzymes from natural high-temperature environments, such as thermophilic bacteria and archaea, (ii) engineering existing mesophilic CAs to enhance their thermostability and (iii) employing bioinformatics-driven strategies, including metagenomic library screening and protein mining (Fisher et al., 2012; Rigkos et al., 2024). These strategies represent promising pathways for advancing the application of CAs in industrial CCS processes.

2.1.3 Activity assays of CAs

Assessing CA activity is crucial for understanding the enzyme's efficiency under specific conditions relevant to its application. These evaluating methods can be divided into three categories: i) manometric methods, ii) Electrometric or Wilbur-Anderson-related Assays and iii) colorimetric (4-nitrophenyl acetate assay) (Effendi & Ng, 2019; Pierre, 2012). As for the first category, manometric methods tend to be more complex, time-consuming, and require specialized

equipment (Karler & Woodbury, 1963). In contrast, the other two categories offer simpler setups, faster execution, and better suitability for high-throughput analysis. Specifically, electrometric or Wilbur-Anderson assays measure the hydratase activity of the enzyme, whereas 4-nitrophenyl acetate assays assess the esterase side-reaction of CA.

2.1.3.1 Electrometric or Wilbur-Anderson-related Assays

The electrometric or Wilbur Anderson (WA) assays were developed for the first time in 1948 (Wilbur & Anderson, 1948). The setup involves mixing a saturated CO₂ aqueous phase with a relatively low ionic strength buffer (usually 10–25 mM) containing the enzyme. WA assays require a pH meter equipped with a quick-response electrode to accurately measure the time required for the pH drop in the buffer solution, typically within the range of 8.3 to 6.3. Though, it should be noted that the starting and finishing pH points of this assay may vary across different publications.

CA's activity is measured in Wilbur-Anderson units, determined by the Eq. 8. Most importantly, WA assays are performed using ice-equilibrated solutions to slow down the enzymatic rate of CO₂ hydration, as CAs exhibit extremely high turnover numbers. Additionally, ice-cold temperatures maximize substrate availability and enhance the reproducibility of the method, as lower temperatures slow the equilibration of dissolved CO₂ with the air.

$$WAU = \frac{t_0 - t}{t} * \frac{d(f)}{C} \quad (\text{Eq. 8})$$

Equation 8 Wilbur Anderson Units (WAU) calculation formula: t₀ represents the time values of the non-enzymatically catalyzed reaction, t represents the time values of the enzymatically catalyzed reaction, d(f) is the dilution factor, and C is the enzyme concentration.

However, these electrometric WAU assays have some drawbacks: i) typical electrodes have a slow response at lower temperatures, ii) as a screening assay, they require large reaction volumes (> 5 mL), iii) proteins and other substances can adsorb to the electrode membrane, interfering with the measurements, iv) homogeneous mixing between the phases of CO₂-saturated water and buffer-enzyme can be challenging, and v) the results may not be replicable because the

pH log is not linear, and only a time event is recorded, which is eventually used in WA formula.

Alternative setups of WA assays can be performed using a stop-flow apparatus (Del Prete et al., 2020). In the stop-flow method the enzyme and the substrate are rapidly mixed in a flow system. This approach provides more accurate kinetic data by enabling real-time monitoring of the enzyme's activity and the calculation of steady-state kinetics of CAs (e.g. K_M , K_{cat}). Stop-flow setups are often used to calculate WA units, typically relying on colorimetric assays that measure the change in absorbance of an indicator (such as phenol red or bromothymol blue) within a known pH drop range. These assays begin and end at known absorbance values corresponding to pH changes. Remarkably, modified stop-flow assays that do not require a stop-flow apparatus and instead utilize a spectrometer have also been reported (Kim & Jo, 2022).

Lastly, in addition to the electrometric methods, a new, easy-to-perform and fast assay has been reported (Fuchs et al., 2021). This assay allows for measuring the turnover number of CAs hydratase activity with CO_2 under ambient conditions. In this method, a high-flow stream of gaseous CO_2 is introduced into a concentrated buffer (~0.1 M) containing the enzyme. The pH drop is recorded digitally by a fast-response electrode, and the pH drop-time course is plotted. The data are then evaluated through a series of calculations, and the results can be used to determine the initial activity of the enzyme, which in turn allows for the calculation of turnover numbers related to bicarbonate production.

2.1.3.2 Nitrophenyl acetate assay

The side esterase activity of CAs can be evaluated using the synthetic substrate 4-nitrophenyl acetate (pNPA), depicted at Fig. 12. This colorimetric assay relies on the enzyme's ability to hydrolyze pNPA into 4-nitrophenol (pNP) and acetic acid (Effendi & Ng, 2019; Kim & Jo, 2022). The yellow-colored reaction product, pNP, is detected spectrophotometrically by measuring the absorbance at 348 nm or at 400–410 nm. Enzyme activity is typically expressed in micromoles of pNP produced per minute under defined reaction conditions. Importantly, to

obtain accurate estimates of enzyme activity, the autohydrolysis rate of pNPA must be subtracted from the observed reaction rate.

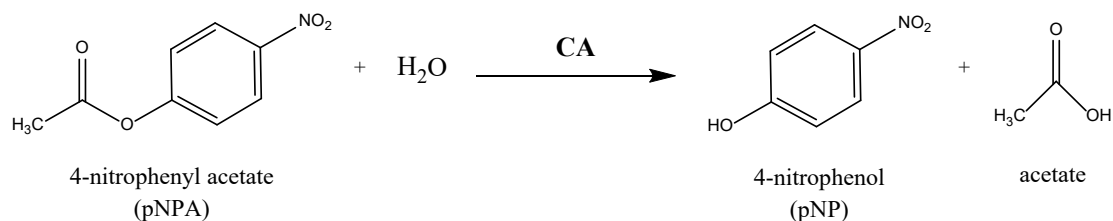


Figure 12 4-nitrophenyl acetate hydrolysis by Carbonic Anhydrase.

Compared to the Wilbur-Anderson (WA) assay, the pNPA assay offers greater controllability because the enzyme is less efficient at catalyzing this carboxylic ester reaction. This flexibility allows the assay to be performed at elevated temperatures (> 40 °C) under ambient pressure. The pNPA assay is simple, reliable, and replicable, though it cannot be applied universally, as certain CAs, particularly microbial ones, do not exhibit esterase activity. A notable advantage of this assay is that it requires no specialized equipment beyond a spectrophotometer and a water circulator, making it a routine method for assessing immobilized CA activity and conducting inhibition studies on native enzymes in the presence of heavy metal ions.

2.2 Formate Dehydrogenases

Formate dehydrogenases (FDHs) are a group of oxidoreductive enzymes primarily catalyzing the oxidation of formate to CO₂ (Amao, 2018). Instead of solely utilizing formate as the oxidation substrate (S_{ox}), FDHs employ a second substrate or redox partner as an electron acceptor, which is subsequently reduced (S_{red}). However, FDHs are also capable of reversibly reducing CO₂ to formate in a reaction that is not thermodynamically favored (redox potential E° = -420 mV) compared to the oxidation of formate (Maier et al., 2024).



FDHs play essential roles across all taxonomic kingdoms, being involved in multiple processes such as energy acquisition through the production of reducing equivalents from formate oxidation and C₁ metabolism. Accordingly, a wide

variety of FDHs with diverse structural compositions, active site architectures, and metabolic functions have been identified, reflecting their adaptability to different environmental conditions and metabolic requirements across various organisms.

FDHs are primarily categorized into two classes based on the presence or absence of metal ions in their active centers: (i) metal-dependent (W- or Mo-containing) and (ii) metal-independent (composed exclusively of amino acid residues in the active site). A secondary classification of FDHs is based on their redox partners, offering a more refined understanding of their functional diversity. FDHs employ various S_{red} including nicotinamide-type cofactors (NAD^+ or $NADP^+$), quinones, coenzyme F_{420} , cytochrome, NAD^+ -ferredoxin type as well as other cofactors [2Fe-2S], [4Fe-4S] clusters, FMN, FAD and heme. In this chapter, only NAD(P)-dependent FDHs (Eq. 10) will be discussed, particularly focusing on *Candida boidinii* FDH, which is the most well-characterized FDH to date.

NAD(P)-dependent FDHs



2.2.1 *Candida boidinii* Formate Dehydrogenase

FDH from the methylotrophic yeast *Candida boidinii* (CbFDH) is the most extensively researched and well-documented metal-independent FDH (Schirwitz et al., 2007). CbFDH was the first FDH to be heterologously expressed in *E.coli* cells and is currently a commercially available enzyme. Each CbFDH subunit consists of 364 amino residues forming a homodimer (~82 kDa), with two independent active sites (Fig. 13A). Each identical monomer consists of 15 α -helices and 13 β -strands integrating two distinctive domains: the NAD-binding domain and the catalytic domain. These two domains are connected by two helices and separated by a deep cleft that houses the active site. This cleft ensures that the substrates are positioned in proximity for the reaction.

Binding of the substrates induces a structural conformational change in the enzyme, shifting it from the apo (“open”) form, with a wide active-site cavity, to the holo (“closed”) form, the catalytically active state (Guo et al., 2016). In the

holo conformation, the active site is enclosed within a hydrophobic environment, which is critical for efficient catalysis. This closure of the channel and tunnel is essential to prevent water molecules from the surrounding solvent from entering and disrupting the hydride transfer reaction through hydrolysis.

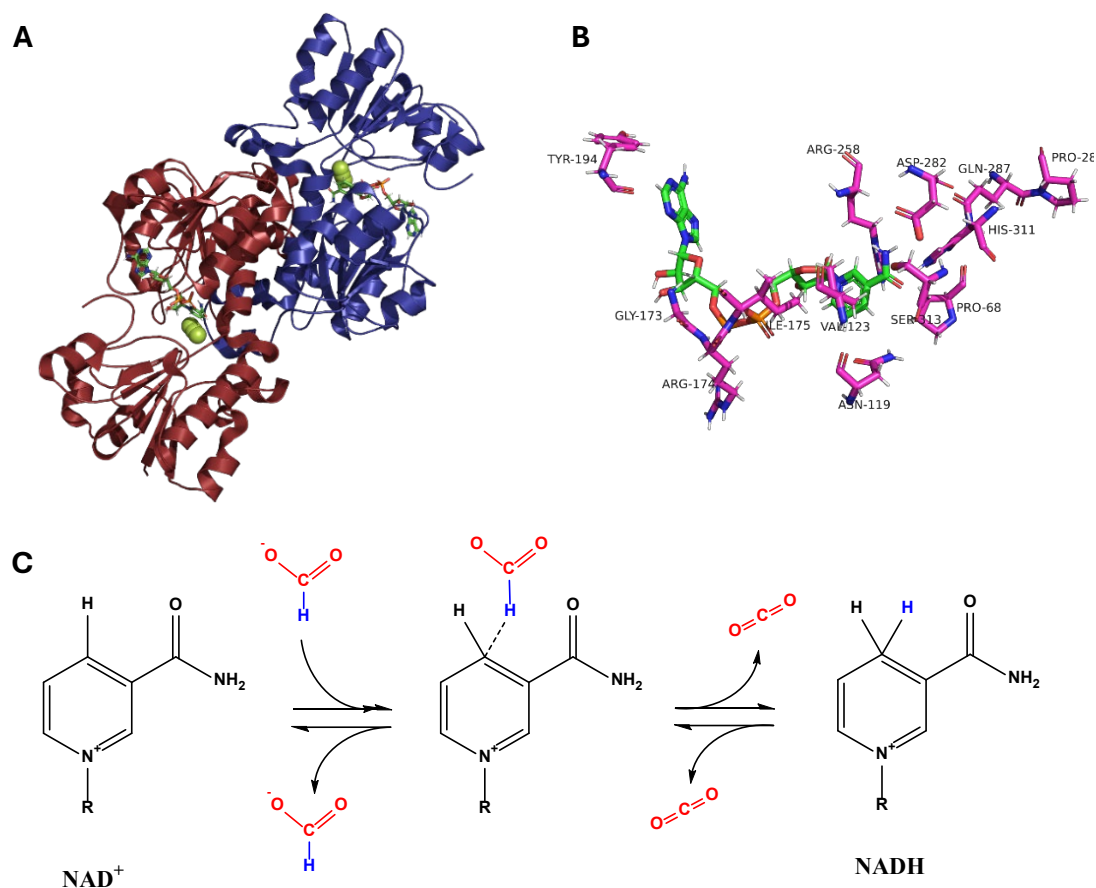


Figure 13 (A) Three-dimensional structure of the *Candida boidinii* formate dehydrogenase dimer, with each monomer shown in a different color, complexed with azide and NAD⁺ (PDB accession code: 5DN9). (B) Active site of metal-independent CbFDH, along with the presence of NAD cofactor. (C) Representation of formate oxidation and CO₂ reduction mechanisms of FDH.

2.2.2 Mechanism

2.2.2.1 Formate catalysis mechanism of metal-independent FDH

Studies of the active site of FDHs reveal several conserved amino acid residues that are crucial for the enzyme's catalytic function and structural stability (Fig. 13B). Among these, R258 and N119 are responsible for binding the formate molecule, while the nicotinamide ring of NAD⁺ is held in place through interactions with D282 and S313. Also, R174 plays a critical role in securing the phosphate linker of the NAD⁺ molecule. Additionally, insights on CbFDH NAD-binding domain revealed that the presence of K189 plays a crucial role at

exclusively binding NAD^+ cofactor instead of NAD(P)^+ . Lastly, residues Q287 and P288 support the function and orientation of H311, which acts as a proton acceptor (base) by donating its unshared electron pair, facilitating hydride transfer and stabilizing the transitional molecular arrangement (Labrou & Rigden, 2001).

The mechanism of formate oxidation in metal-independent FDHs involves the direct hydride transfer from a formate molecule to the oxidized nicotinamide group of NAD(P)^+ . At the enzyme's active site, both substrates, formate and NAD(P)^+ , bind in close proximity, causing NAD(P)^+ to adopt a bipolar conformation. This orientation increases the electrophilicity of NAD(P)^+ and facilitates an efficient direct hydride transfer from formate to NAD(P)^+ (Maia et al., 2021).

The mechanism is reported to involve two major events (Fig. 13C): i) the cleavage of the carbon–hydrogen bond of formate and ii) the nucleophilic attack on the C_4 of pyrimidine ring of NAD(P)^+ by the hydride ion from formate (Sato & Amao, 2023). Subsequently, a short-lived intermediate product is formed, leading to the final products, CO_2 and NAD(P)H , which are released from the active site into the solvent. After this process, the active site returns to its original state. Kinetic studies indicate that the rate-limiting step in this mechanism is the nucleophilic attack of the hydride ion from formate on the carbon at the 4-position of the nicotinamide group of NAD(P)^+ .

2.2.2.2 CO_2 catalysis mechanism of metal-independent FDH

The proposed mechanisms of CO_2 reduction by FDH involve the transfer of a hydride ion from NAD(P)H to either $\text{CO}_2(\text{aq})$ or HCO_3^- . As referred in section 1.3.1, the relative abundance of CO_2 species depends heavily on pH, making the HCO_3^- to CO_2 ratio a critical factor to consider. Given that the reaction occurs within a pH range of 6–9, where bicarbonate (HCO_3^-) is the predominant carbon species, the proposed mechanism primarily involves HCO_3^- . In this mechanism, a hydride ion from NAD(P)H interacts with the carbon atom of HCO_3^- , forming a short-lived intermediate. This intermediate contains a newly formed carbon-hydride bond and two negatively charged oxygen atoms. The buildup of negative charges leads to the separation of a hydroxide ion and the breakdown of the

intermediate into a formate ion and hydroxide ion (Fig. 14). These products then diffuse into the bulk solvent.

However, the mechanism described above is incomplete, as it pertains solely to activity in the presence of HCO_3^- . Contrarily, Sato and Amao (2020) demonstrated that the enzyme exclusively catalyzes CO_2 instead of HCO_3^- , highlighting the need to reconsider the proposed mechanistic pathway.

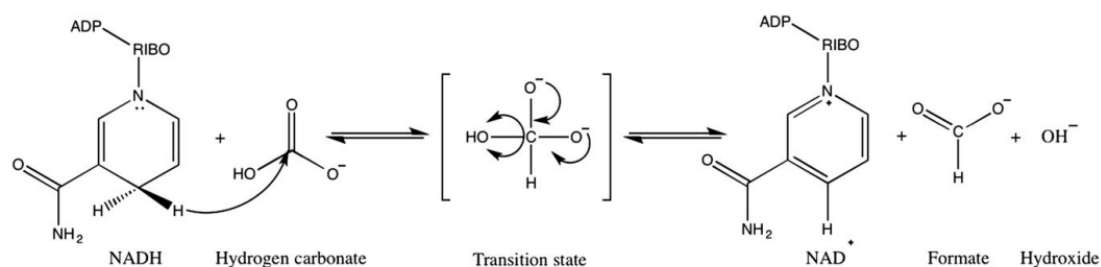


Figure 14 Proposed mechanism of HCO_3^- reduction into formate by non-metal containing FDH (Aslan et al., 2017).

3. Chemistry of CO_2 Catalysis

3.1 Thermodynamic Challenges in CO_2 Utilization

The chemical utilization of CO_2 presents a significant challenge, beyond the issues of its abundance and availability (Bierbaumer et al., 2023; Li et al., 2024). From a thermodynamic perspective, the carbon atom in CO_2 is in its highest oxidation state, with a standard Gibbs free energy of formation (ΔG°_f) of -394 kJ/mol (North, 2015). Consequently, any chemical modification or reduction of CO_2 requires a substantial energy input.

Fig. 15 illustrates the standard Gibbs free energy of formation (ΔG°_f) of various C_1 molecules, highlighting that CO_2 is the most thermodynamically stable species in this group. This stability makes the formation of CO_2 highly favorable. This also explains, in part, why CO_2 is often favored as a product in most enzymatic reactions, as reverse reactions (i.e., reduction of CO_2 to less oxidized C_1 molecules) are thermodynamically uphill.

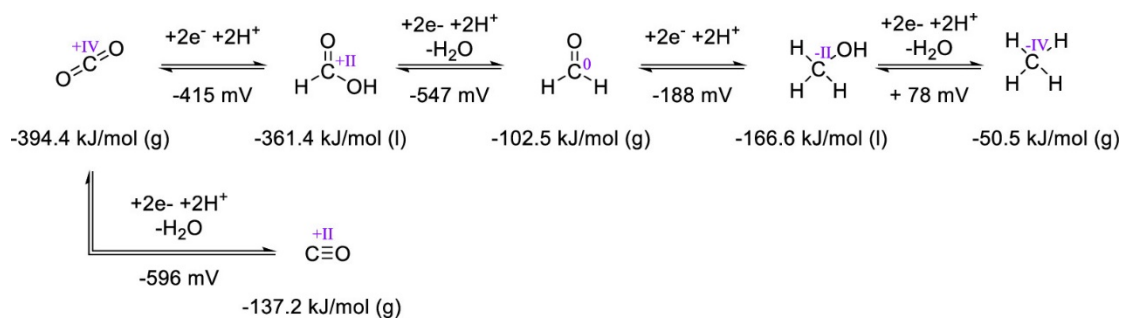


Figure 15 Standard Molar Gibbs Energy of Formation (ΔG°_f) and Experimental Reduction Potentials of Carbon Dioxide, Carbon Monoxide, Formic Acid, Formaldehyde, Methanol, and Methane, at 298.15 K expressed in kJ/mol (Oxidation States of Carbon Are Given As Roman Numerals) (Bierbaumer et al., 2023).

The state-of-the-art strategies for overcoming the energy barrier associated with CO_2 utilization, through both natural and synthetic approaches, have been described by Bierbaumer et al. (2023) and are summarized in Fig. 16. These approaches provide valuable methods to reduce energy requirements or shift reaction equilibria by integrating these reactions into synthetic exergonic pathways or enzyme cascades.

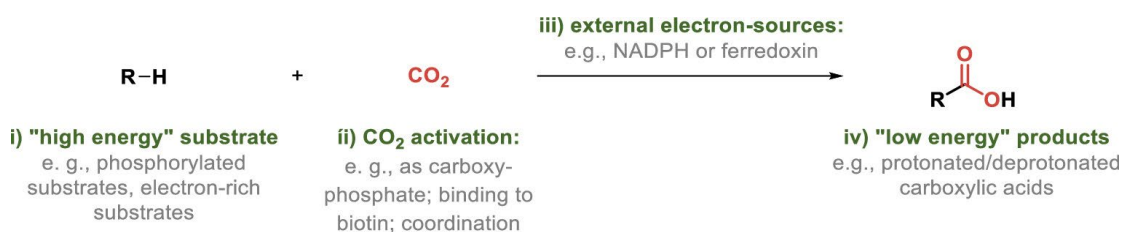


Figure 16 Approaches to reduce the required free energy in CO_2 conversion reactions (Bierbaumer et al., 2023).

3.2 Enzymatic Utilization of CO_2 into methanol

The utilization of enzymes as catalysts for converting CO_2 has gained considerable attention as an advanced biocatalysis topic. This approach features eco-friendly catalysts with mild operating conditions, high specificity and reduced by-product formation. For the first time in the early 1990s, conversion of CO_2 to methanol with the use of enzymes was attempted through an electrochemical approach, combining Formate Dehydrogenase (FDH), Methanol Dehydrogenase and electron mediators on electrode surfaces (Kuwabata et al., 1994). The feasibility of a solely enzyme-mediated cascade to catalytically reduce gaseous CO_2 into methanol was reported in 1999 (Obert & Dave, 1999). This pioneering research demonstrated a sequential 3-step one-pot reaction scheme using FDH,

Formaldehyde Dehydrogenase (FaldDH), and Alcohol Dehydrogenase (ADH) through encapsulation in sol-gel matrix.

Dehydrogenase-mediated methanol production requires the operation of three dehydrogenases in reverse, as opposed to their natural reactions (Fig. 17) (Hartanto et al., 2024; Shi et al., 2015). The most frequent occurring CO₂ cascade reactions involve enzymes originated from different organisms and such dehydrogenases are commercially available; FDH from methylotrophic yeast *Candida boidinii*, FaldDH from bacterium *Pseudomonas sp.* and ADH from the most common yeast, *Saccharomyces cerevisiae* (Villa et al., 2023). As referred, the final product of the 3-step pathway is methanol, although intermediate products, including formic acid and formaldehyde, are also generated, which are essential steps for the sequence of the reaction.

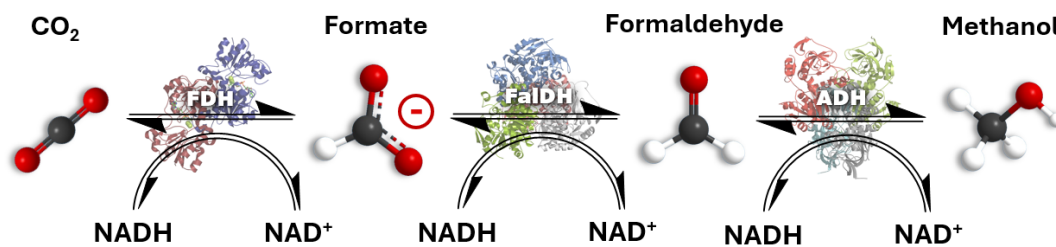


Figure 17 Synthetic Dehydrogenase-mediated cascade for sequential CO₂ into methanol.

The implementability of operating dehydrogenases in reverse is facilitated by high-energy input molecules, particularly nicotinamide adenine dinucleotide (NADH). This reverse operation requires significant energy input to overcome the thermodynamic barriers and drive the reaction in the non-spontaneous direction toward methanol. In this pathway, the production of 1 mole of methanol requires the consumption of 3 moles of NADH, which stoichiometrically corresponds to the transfer of 6 electrons onto the initial CO₂ substrate molecule. Since the cofactor is considered the limiting factor of the overall reaction, the following formula is used to calculate the reaction's efficiency:

$$Efficiency (\%) = \frac{3 \times mol MeOH}{1 \times mol NADH} \times 100 \quad (Eq. 11)$$

3.2 Challenges and Prospective Solutions

Dehydrogenase-mediated CO₂ reduction represents a highly promising approach for advancing biocatalysis in the context of CO₂ decarbonization. This method offers eco-friendly operating conditions, making it an attractive solution from an environmental perspective. However, several limitations hinder the efficiency of these bioconversions and the scalability of such enzymatic technologies for large-scale applications (Di Spiridione et al., 2022).

One of the most significant challenges in enzyme-mediated CO₂ reduction is the inconsistent reporting of critical experimental details in the scientific literature (Cazelles et al., 2013; Luo et al., 2015; Singh et al., 2018). Essential information, including the origin and quantities of the enzymes used, turnover numbers, and comprehensive analytical data, is frequently omitted. This lack of transparency complicates the ability to accurately compare studies or replicate experimental results, even at the laboratory scale. Addressing this issue through standardized reporting practices will be crucial for advancing the field and enabling the broader application of enzyme-based CO₂ reduction technologies.

3.2.1 Enzyme-Related Limitations Enzymatic Performance

While commercial dehydrogenase enzymes provide easy accessibility, they are unlikely to significantly optimize CO₂ reduction. These enzymes are expensive, available only in limited quantities, and exhibit low affinities for reverse substrates, accompanied by low efficiencies and poor stability. These limitations pose significant challenges for practical applications. Additionally, operating these enzymes in a one-pot reaction under uniform conditions is difficult, as their optimal operational parameters (e.g., pH, temperature, and cofactor requirements) often differ.

To address challenges related to enzyme stability and operational costs, enzyme immobilization is considered a versatile strategy. Immobilization facilitates enzyme recyclability, enhances stability, and simplifies downstream processing of CO₂-derived products. This approach also enables better integration of enzymes into scalable systems, addressing one of the critical barriers to industrial implementation.

To further reduce costs, heterologous expression provides a promising alternative. By enabling the production of enzymes in cost-effective microbial hosts, heterologous expression offers greater flexibility and control over enzyme characteristics. This includes the ability to engineer enzymes with improved activity, stability, and selectivity for reverse reactions.

In this context, the identification of potential enzymatic catalysts from extensive protein and enzyme databases is essential (Singh et al., 2018). *In silico* analysis of these candidates can help evaluate their suitability for reverse reactions. Computational approaches can also be leveraged to enhance catalytic efficiency and selectivity, modify cofactor specificity, and reduce the reliance on excess cofactors, which are often a major limitation in these reaction schemes.

Protein engineering, guided by structure-function analyses of enzymatic catalysts, is crucial in addressing these challenges (Calzadiaz-Ramirez & Meyer, 2022). Rational and directed evolution approaches can improve enzyme efficiency and stability under reaction conditions. These strategies, combined with computational tools, offer the potential to design enzymes tailored for specific reaction requirements, ultimately advancing the feasibility of CO₂ reduction systems.

3.2.2 Substrate Related Limitations

Due to the nature of the substrate, CO₂ has relatively poor solubility in aqueous solutions, with a solubility of approximately 0.034 mol L⁻¹ under ambient conditions. This characteristic represents a significant drawback, as limited substrate availability is considered one of the key factors driving the equilibrium away from the desired product, thereby negatively impacting overall reaction efficiency.

To tackle this limitation, boosting the availability of CO₂ emerges as a promising strategy to enhance catalytic efficiency. One potential solution involves using closed high-pressure systems, which can increase CO₂ solubility without being significantly influenced by relatively high temperatures, making them suitable for cascade reactions. Additionally, the implementation of materials with CO₂-adsorbing properties offers another promising avenue. These materials can

serve as supports for enzyme immobilization, improving the substrate concentration at the active site and the overall reaction efficiency.

Moreover, advanced materials specifically tailored for CO₂ adsorption such as nanoparticles, membranes, and other porous materials—can act as scaffolds for enzyme immobilization and encapsulation. These materials facilitate efficient CO₂ capture and enhance enzyme recyclability and simplify downstream processing of CO₂-derived products.

Facilitating faster capture and hydration of CO₂ in aqueous media is another highly promising approach. Incorporating the enzyme carbonic anhydrase (CA) into such systems has been shown to significantly accelerate these processes. Carbonic anhydrase promotes the rapid interconversion of CO₂ and bicarbonate, thereby increasing the availability of the substrate for enzymatic reactions. The enzyme CA has been reported to enhance the efficacy of product formation in various CO₂-related biocatalytic applications (section 2.1.2).

Beyond aqueous solutions, alternative CO₂-interacting media, such as ionic liquids and deep eutectic solvents, also hold significant potential for improving reaction efficiency (Antonopoulou et al., 2022; Zhao & Baker, 2023). These specialized solvents can provide unique physicochemical environments that enhance CO₂ solubility and reaction rates, further expanding the range of viable approaches for CO₂-based biocatalysis.

3.2.3 Cofactor Related Limitations

Achieving the high redox potential necessary to drive the reaction toward methanol production typically requires an excess of cofactors. However, cofactors such as NADH are both expensive and unstable under reaction conditions, and their stoichiometric use complicates the economic feasibility of these processes. Despite this limitation, external cofactor supplementation can still be employed to drive the reaction toward the desired products if cost considerations are not the primary concern. Alternatively, the use of artificial cofactors or the adoption of direct electron transfer mechanisms comprise more sustainable approaches.

Maintaining a high cofactor concentration is crucial for CO₂ reduction, as it directly influences the overall reaction efficiency. To address this, NADH regeneration can be achieved through various methods such as chemical, electrochemical, photochemical, enzymatic, etc., depicted at Fig. 18 (Wang et al., 2017).

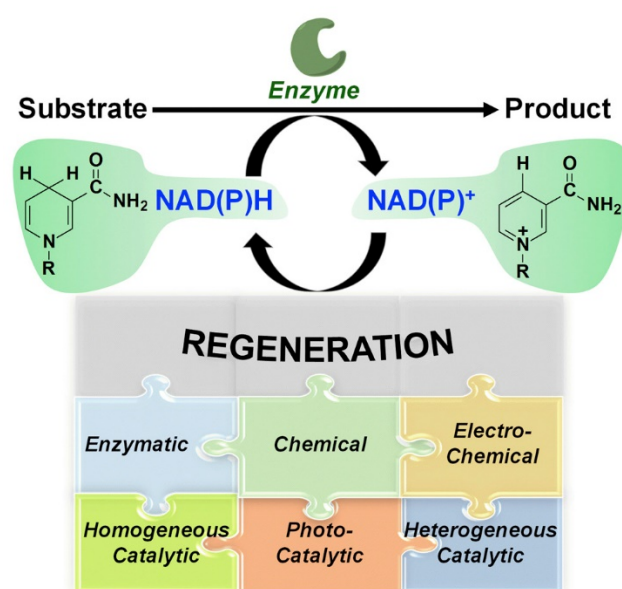


Figure 18 Summary of current available NAD(P)H Cofactor regeneration methods (Wang et al., 2017).

In enzymatic regeneration pathways, the ideal scenario involves the use of stable, cost-effective enzymes alongside sacrificial substrates that drive the regeneration reaction. It is also critical that intermediate products formed during cofactor regeneration, as well as the substrates used, do not interfere with the primary CO₂ reduction reaction.

A promising strategy to improve the efficiency and stability of these systems is the immobilization or encapsulation of the NADH cofactor (Ji et al., 2015; Ren et al., 2020). This approach allows for the integration of catalytic enzymes and a regenerating enzyme within a single system, providing flexibility in system design. Such immobilized systems have been reported to enhance cofactor stability, improve enzyme recyclability, and offer greater control over reaction conditions, thereby presenting a practical and scalable solution for CO₂ reduction.

4 Enzyme Immobilization

The term "enzyme immobilization" refers to the confinement or anchoring of an enzyme to an inert, insoluble material while retaining its catalytic activity (Es et al., 2015; Karl-Erich Jaeger, 2024). Typically, this process involves results in the formation of a heterogeneous system, where the catalytic activity of the immobilized enzyme is not significantly affected by mass transfer phenomena between the solid phase, where the biocatalyst is anchored, and the liquid phase of the reaction medium.

Enzyme immobilization offers several advantages rendering it a valuable strategy in biocatalytic applications for industrial processes (Pavlidis et al., 2014). Immobilized enzymes are more stable and resistant to changes in environmental conditions, exhibiting enhanced longevity and reusability. Immobilization also allows for the easy separation of enzymes from reaction mixtures, minimizing waste and making downstream processing more cost-effective. Another beneficial aspect of enzyme immobilization is the flexibility of the support, whose properties can enhance or modify the catalytic properties of the anchored enzyme. However, while enzyme immobilization might improve the scalability and productivity of biocatalytic reactions on a large scale, the presence of the solid support may result in reduced catalytic activity and stability of the native enzymes due to alterations in their tertiary structure.

The immobilization process can be achieved through various methods, depending on the way the enzyme is attached to a solid support. The most common techniques include adsorption, covalent bonding, cross-linking, and entrapment or encapsulation (Fig. 19). Each method has its unique mechanism and characteristics, offering specific advantages and disadvantages depending on the intended application and the environmental conditions in which the process takes place (Table 1).

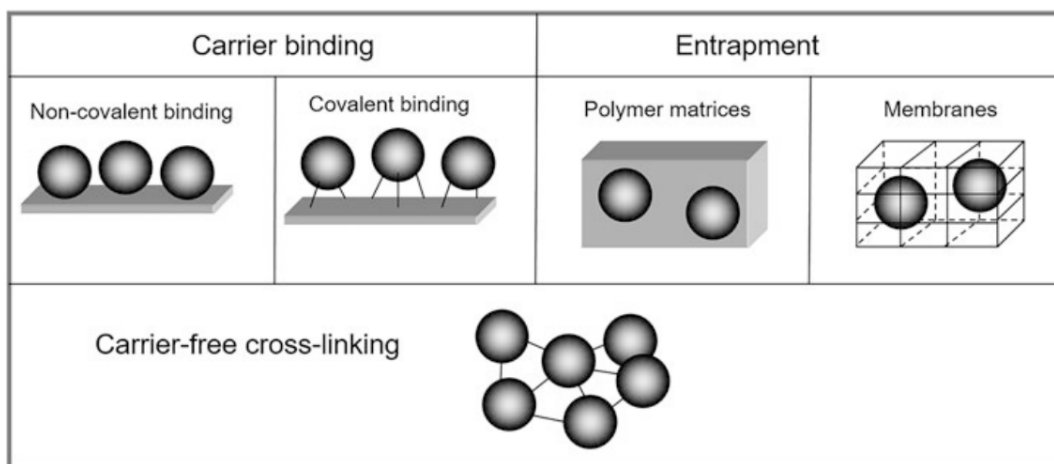


Figure 19 Schematic representation of the most frequently used methods for enzyme and cell immobilization. (Karl-Erich Jaeger, 2024)

Table 1 Summary of the Advantages and Disadvantages of Immobilization Techniques (Es et al., 2015).

Immobilization technique	Advantages	Disadvantages
Physical Adsorption	Simple and cheap High catalytic activity No conformational change of the biocatalyst No need to use reagents Reuse of expensive material	Low stability Possible loss of biomolecules Weak bonds might cause desorption of biocatalyst
Encapsulation and Entrapment	Protection of biocatalyst Allows the transport of low molecular weight compounds Enables continuous operation due to maintained cell density Facilitates cell separation and simplified downstream process	Limitations on mass transfer Low enzyme loading
Cross-linking	Allows controlled release of product Strong biocatalyst binding Prevents leakage Decreases desorption	Might cause alteration in active site Diffusion limitations Loss of enzyme activity
Covalent Binding	Increases the stability of biocatalyst Strong binding High heat stability Facilitates the enzyme contacts with its substrate Prevents elution of biocatalysts Flexibility in design of support material and method	Limited enzyme mobility causes decreased enzyme activity Less effective for immobilization of cells Support materials are not renewable

Adsorption and covalent bonding, the two methods described in this thesis, offer distinct approaches to enzyme immobilization. Adsorption involves the non-covalent attachment of enzymes to the support surface through dipole-

dipole and hydrophobic interactions, van der Waals forces, or hydrogen bonding. This method is a simple and cost-effective procedure; however, the relatively weak interactions can result in enzyme leaching under certain conditions. Contrariwise, covalent bonding forms strong, stable linkages between the enzyme and the support, enhancing the stability of the immobilized system. Nevertheless, this method restricts the free movement of enzyme molecules, which can reduce enzymatic activity. Despite this drawback, enzymes immobilized through covalent bonding can readily interact with substrates, as they are located on the surface of the support material.

Chapter Two: Materials and Methods

5. Materials

5.1 Commercial Enzymes

- Carbonic anhydrase from bovine erythrocytes (lyophilized powder, $\geq 2,000$ W-A units/mg protein) (C3934, Sigma-Aldrich)
- Formate dehydrogenase (*Candida boidinii*) (liquid, 300 Units at 25°C; ~ 600 Units at 37°C) (700004213, Neogen (Megazyme))
- Glutamate dehydrogenase from beef liver (lyophilized, pkg of 3000U) (10197734001, Roche)

5.2 Heterologous expressed Enzymes (*E.coli*)

- Carbonic anhydrase Lyophilized powders:
 - SyCA (*Sulfurihydrogenibium sp. YO3AOP1*)
 - BhCA (*Alkalihalobacillus halodurans*)
 - DvCA8.0 (*Desulfovibrio vulgaris*)
 - ApCA (*Aeribacillus pallidus*)
 - SazCA (*Sulfurihydrogenibium azorense*)

5.3 Nanoparticles

- Hierarchical Porous Carbons nanoparticles (HPCs)
- Aqueous olive leaf extract zinc oxide-iron oxide nanoparticles (ZnOFe)

5.4 Reagents

- 1-(3-Dimethylaminopropyl)-3-ethylcarbodiimide hydrochloride, 98+% (EDC, A10807, Alfa Aesar)
- 2,3,4,5,6-Pentafluorobenzyl bromide 99% (101052, Sigma-Aldrich)
- 4-Nitrophenol, spectrophotometric grade (pNP, 1048, Sigma-Aldrich)
- 4-Nitrophenyl acetate, esterase substrate (pNPA, N8130, Sigma-Aldrich)
- Acetonitrile, HPLC (Fisher)
- Acetyl acetone, >99% (P7754, Sigma)

- Bovine serum albumin (BSA) heat shock fraction, pH 7, ≥98% (A7906, Sigma-Aldrich)
- Calcium chloride dihydrate (*2H₂O) (21101, Fluka)
- Deionized Water (dH₂O)
- Dihyronicotinamide-adenine dinucleotide, disodium salt, NADH reduced ≥93% (1051, Gerbu Biotechnik GmbH)
- Double Distilled Water (ddH₂O)
- Ethyl acetate 99.8% (LAB-SCAN)
- Formic acid, 98-100% for analysis EMSURE® ACS Reagent, reag. Ph. Eur. (1.00264, Supelco Inc)
- GN-6 Metrical® MCE membrane disc filters (0.45 µm 47 mm S-Pack white gridded) (66191, Pall Corporation)
- HEPES, ≥99.5% (titration) (H3375, Sigma-Aldrich)
- L-Glutamic Acid *ReagentPlus*®, ≥99% (HPLC) (G1251, Sigma-Aldrich)
- N-Hydroxysuccinimide (NHS), 98% (130672, Sigma-Aldrich)
- Nylon Syringe Filter, Pore Size:0.22µm, Diameter:13mm (SFNY013022N, Membrane Solutions)
- Phenol red (research grade) (32095, SERVA)
- Pierce™ BCA Protein Assay Kit (23225, Thermo Scientific™)
- Potassium bromide (KBr), 99+%, for spectroscopy, IR grade (206391000, Thermo Scientific Chemicals)
- Sodium dihydrogen phosphate monohydrate for analysis EMSURE® ACS, Reag. Ph Eur (106346, Supelco)
- Sodium formate BioUltra, ≥99.0% (NT) (71539, Sigma-Aldrich)
- Sodium hydrogen carbonate Cell Culture grade (NaHCO₃) (A0384, AppliChem GmbH)
- Sodium phosphate dibasic dihydrate (Na₂HPO₄) puriss. p.a., reag. Ph. Eur., 98.5-101.0% (30435, Sigma)
- Sonax Anti-Fog windscreen spray (355241, Sonax GmbH)
- Tris-(hydroxymethyl)-aminomethane (Tris) (33742, Riedel)

- β -Nicotinamide adenine di-nucleotide, reduced disodium salt (β -NADH), $\geq 97\%$ (HPLC) (N8129, Sigma-Aldrich)
- β -Nicotinamide adenine dinucleotide hydrate (NAD^+), $\geq 99\%$ (N1511, Sigma-Aldrich)

6. Methods

6.1 Carbonic Anhydrase Assays

6.1.1 Preparation of CO_2 saturated H_2O

Initially, a glass serum bottle containing 50 mL of dd H_2O is placed in an ice-containing water bath to equilibrate to ice-cold temperature. Subsequently, the aqueous solution is purged with gaseous CO_2 through the tip of a needle at a uniform flow rate of 150 mL min^{-1} for at least 1 hour, as shown in Fig. 20. The pH of the solution is then measured, ensuring it drops below pH 4.0. The CO_2 bubbling is continued throughout the end of the Wilbur-Anderson assays.

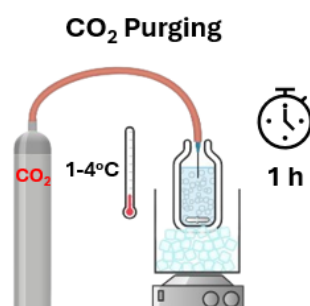


Figure 20 Preparation of CO_2 saturated H_2O Setup: CO_2 is bubbled through the glass serum bottle maintained at 1–4 °C.

6.1.2 Electrometric Wilbur Anderson Assay

CA's hydratase activity was evaluated by electrometric Wilbur-Anderson assay, as depicted in Fig. 21 (Wilbur & Anderson, 1948). The assays were performed with ice-cold equilibrated solutions (0-4 °C) in 13-mL glass tubes placed in an ice bath, utilizing a pH meter (Orion Star A111 Benchtop - Thermo Scientific). Initially, 3 mL of 0.02 M Tris-HCl buffer pH 8.3 (adjusted at 25°C) with the appropriate concentration of CA was equilibrated at ice cold temperature. The reaction was initiated by adding 2 mL of ice-cold CO_2 -saturated double-distilled water (dd H_2O), and the time taken for the pH to drop from 8.3 to 6.3 was recorded

using a stopwatch. All reactions were conducted under agitation to ensure thorough mixing of the buffer and the CO₂-saturated solutions. Eq. 8 formula was used for calculating the WA units. Reactions were carried out at least in triplicates.

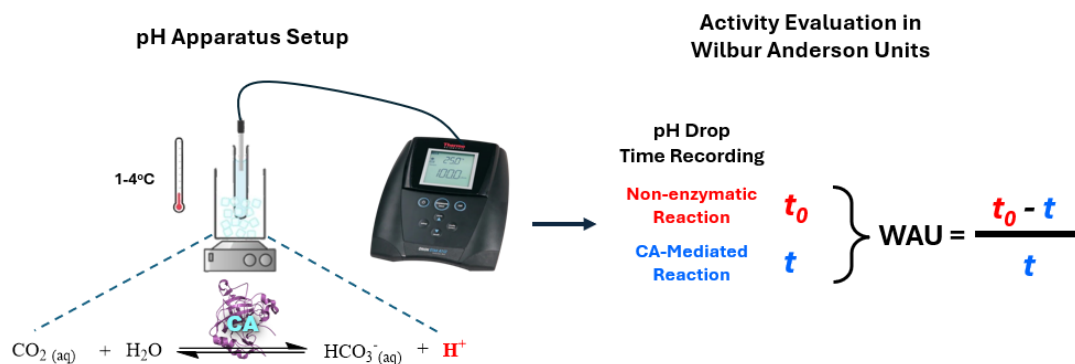


Figure 21 Schematic workflow of the electrometric Wilbur-Anderson Assay, illustrating the use of a pH meter and a stopwatch to record the time required for the pH drop. The hydratase activity of CA was evaluated using Wilbur-Anderson Units.

6.1.3 Colorimetric Wilbur Anderson Assay

CA's hydratase activity was measured by a colorimetric protocol introduced by Kim and Jo (2022). The assay was carried out at a spectrometer (Shimadzu UV-1601 UV-VIS) connected to a computer, set to measure the absorbance change at 570 nm, with a time interval of 0.1 seconds (Fig. 22). A water circulator connected to the system was set approximately to 1 °C throughout the experimental session. All solutions used were equilibrated at the lowest possible temperature inside ice.

For the assay, 600 µL of Tris-HCl 0.02 M buffer with 167 µM phenol red were placed inside a quartz cuvette. Subsequently, 10 µL of the enzymatic solution (dissolved at NaPi 0.05 M, pH 7.5) was added, followed by the addition of 400 µL of ice-cold CO₂-saturated deionized water to initiate the reaction. For blank solutions, 10 µL of phosphate buffer (0.05 mol L⁻¹, pH 7.5) were used. Data acquisition was initiated before the addition of the CO₂ substrate, and measurements stopped once the absorbance reached its minimum value. WAU were calculated based on the time required for the pH to drop from 7.5 to 6.5 according to the formula Eq. 8.

To establish reference points for phenol red absorption, 600 µL of buffer solution and 400 µL of deionized water were adjusted to pH 7.5 and 6.5,

respectively, and their absorbance was recorded. Absorbance of a 100 μM phenol red buffer solution at pH 7.5 was 1.3, while at pH 6.5 it was 0.25. Plastic cuvettes were treated twice with an antifogging agent (Sonax anti-fog windscreen spray, Sonax GmbH) before the reaction to prevent fogging caused by temperature differences from the external environment.

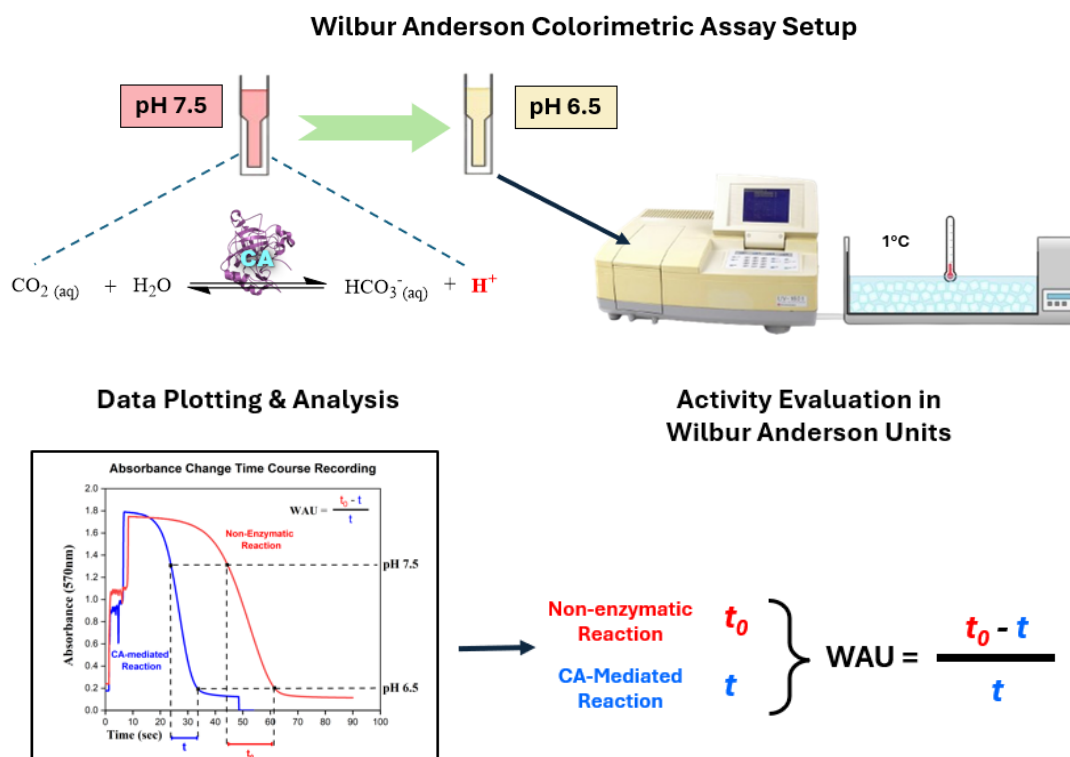


Figure 22 Schematic workflow of the colorimetric Wilbur-Anderson Assay, featuring the use of a spectrometer for measurement and data analysis to estimate the hydratase activity of CA.

6.1.4 Electrometric Assay pH-Stat

6.1.4.1 pH-stat Apparatus Setup

CA's hydratase activity was screened at room temperature using a modified electrometric assay (Fuchs et al., 2021; Steger et al., 2022). In this method, the pH drop was recorded using the electrode from a pH-stat apparatus (The AT-710 Automatic Potentiometric Titrator). Initially, 40 mL of freshly prepared Tris-HCl (0.1 M, pH 8.2) and 0.1 mL of enzyme solution (or buffer in case of blank) were placed inside a beaker, equilibrated at 25 °C and kept under constant agitation with a magnetic stirrer (Fig. 23). For the substrate, a high flow rate of gaseous CO_2 was required (0.5 bar), which was introduced into the enzyme's

solution through a tip of a needle. The recording of pH was initiated before the CO₂ supply into the medium. After equilibrating the CO₂ flow, the needle was submerged to the bottom of the beaker and the pH drop was recorded until it reached the minimum pH value of the buffer (approximately pH 6.5).

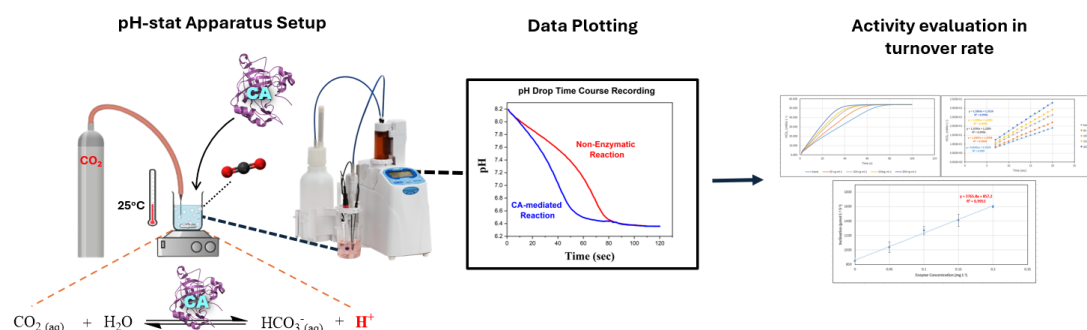


Figure 23 Schematic of the pH-stat apparatus setup and data analysis for estimating the turnover rate of CA. The figure illustrates the pH drop time-course recording for both CA-mediated and non-enzymatic reactions, followed by data plotting and analysis to determine the enzyme's activity.

6.1.4.2 Experimental Results Evaluation

The evaluation of the experimental results obtained from the pH-stat apparatus was based on a series of calculations to determine the activity of CA. In the first step, the concentration of protons [H⁺] (mol L⁻¹) in the reaction medium was calculated from the pH data using the pH formula:

$$\text{pH} = -\log_{10}[\text{H}^+] \Leftrightarrow [\text{H}^+] = 10^{(-\text{pH})} \quad (\text{Eq. 12})$$

The proton concentration, calculated from the pH data, was used to determine the bicarbonate concentration [HCO₃⁻] (mol L⁻¹) produced in the reaction medium. Bicarbonates were determined using the formula:

$$[\text{HCO}_3^-] = (-3.495 \times 10^{-10} + 0.056 \times [\text{H}^+] + [\text{H}^+]^2) / (7.943 \times 10^{-9} + [\text{H}^+]) \quad (\text{Eq. 13})$$

Subsequently, time-dependent graphs of bicarbonate concentration were plotted to illustrate the course of the reaction. Next, data from a short time interval of the reaction (typically the first 7-18 sec) were selected and plotted using linear regression, and their slope was calculated. The previously described steps were repeated to the blank samples, and the mean slope value ($n > 3$) of the blanks was subtracted from the slopes of the enzymatically catalyzed reactions. Finally, the

calculated enzymatic rates were expressed at $\mu\text{mol HCO}_3^- \text{ L}^{-1} \text{ s}^{-1}$ per milligram of CA protein.

6.1.5 Esterase activity

CA's esterase activity was determined through p-nitrophenyl acetate (pNPA) hydrolysis, where the increase in the absorbance at 405 nm, due to the release of p-nitrophenol (pNP), was recorded at 405 nm. Assays were performed inside a quartz cuvette with a final volume of the assay at 1 mL. The reaction was initiated by adding 50 μL pNPA solution of 60 mM (dissolved in acetonitrile) and the reaction buffer was Tris-HCl 50 mM pH 7.5. Autohydrolysis of pNPA was monitored and subtracted from the enzymatic catalyzed reaction.

6.1.5.1 Thermoactivity

The thermoactivity of commercial and thermostable CAs was evaluated using the pNPA assay, as described in section 6.1.5. Thermoactivity assays were performed in the range of 30 to 80 °C. Before initializing the reaction, quartz cuvettes containing both the buffer and the CA enzyme were equilibrated to the desired temperature. Subsequently, the reactions were initialized by adding pNPA to the mixture. All reactions were performed in triplicates.

6.1.6 CA-mediated CO₂ Mineralization Experiments

6.1.6.1 One-step CaCO₃ precipitation

The one-step CaCO₃ precipitation protocol is a modified version of a published method described by Kim et al. (2012). Initially, 30 mL of 0.2 M Tris-HCl buffer (pH 10.5) containing 0.1 M CaCl₂ and 0.5 mg of CA were placed in a Falcon tube. Precipitation of CaCO₃ was initiated by bubbling gaseous CO₂ through the solution at a uniform flow rate of 150 mL min⁻¹ for 1 minute. The Falcon tube was then capped and centrifuged (4000 rpm, 5 min) to retrieve the formed CaCO₃ precipitate. The supernatant was discarded, and the Falcon tube containing the precipitate was dried in an oven at 80 °C for at least 2 hours and then weighed. BSA was used as a negative control. The experiments were conducted in triplicates.

6.1.6.2 Two-step CaCO₃ precipitation

Initially, gaseous CO₂ was bubbled through a syringe tip at the bottom of a Falcon tube containing 20 mL of Tris-HCl buffer (0.05 M, pH 8.3), at a fixed flow rate of 150 mL min⁻¹ for 1 minute. Immediately after the bubbling step, 5 mL of 1.3 M Tris 5% CaCl₂·2H₂O solution was mixed with the hydrated CO₂ buffer to induce CaCO₃ precipitation. The resulting turbid mixture was either filtered immediately or incubated at 30 °C under agitation (150 rpm) for 2, 5 or 10 minutes. The CaCO₃ precipitates were retrieved through filtering *in vacuo* through 0.45 µm disc filters, dried at 80 °C for at least 2 hours and then weighed. The procedure described above was applied for bCA with final concentrations of 0.125, 0.250, and 0.5 µM of enzyme at the bubbling buffer (20 mL).

7.1 Dehydrogenase Assays

7.1.1 FDH Activity Assay and Kinetics

The activity of FDH was determined through the reaction of formate oxidation by monitoring the reduction of NAD⁺ to NADH spectrometrically (Cary 60 UV-Vis, Agilent). The reaction mixtures took place in a quartz cuvette containing 15 µg mL⁻¹ FDH (0.4 µM, calculated per enzymatically active monomer of 41,332 Da), 100 mM sodium formate, 1 mM NAD⁺ in NaPi buffer (0.05 M pH 7.5), in a total volume of 1 mL. The reactions were initiated by the addition of NAD⁺ and the production of NADH was recorded for 3 minutes with 5 seconds time interval. One unit is defined as the amount of enzyme necessary to reduce one µmol of NAD⁺ per minute. The rate of NADH production was calculated using its molar extinction coefficient at 340 nm, $\epsilon_{340\text{ nm}} = 6,220\text{ M}^{-1}\text{ cm}^{-1}$.

For investigating free FDH's kinetic profile, assays were performed using a spectrophotometer (Cary 60 UV-Vis, Agilent). The reactions took place in a quartz cuvette containing 15 µg/mL FDH (0.4 µM, calculated per enzymatically active monomer with a molecular weight of 41,332 Da) and varying concentrations of sodium formate and NAD⁺ in 0.05 M NaPi buffer (pH 7.5), with a final volume of 1 mL. For the kinetic profile against formate, sodium formate concentrations ranged from 1 to 120 mM, with a constant concentration of NAD⁺ at 1 mM. For the kinetic

profile against NAD⁺ kinetics, NAD⁺ concentrations ranged from 0.025 to 1 mM, with a constant sodium formate concentration of 100 mM. Reactions were performed at 30 °C, and NADH production was recorded over 3 minutes in duplicates. Michaelis-Menten nonlinear regression graphs and kinetic constants were calculated using Origin software.

7.1.2 FDH Thermoactivity and pH-activity

Free FDH was evaluated for its thermoactivity and pH-activity using formic acid oxidation, as previously described in the section 7.1.1.

To assess the thermoactivity of the free enzyme, reactions were performed at temperatures of 30, 40, 50, 60, and 70 °C. For pH-activity, 0.05 M buffers (NaPi and Tris-HCl) with pH values ranging from 6 to 9 were employed. In both cases, the optimum activity under the tested conditions was designated as 100%, and subsequent activities were expressed as percentages relative to this baseline value.

7.1.3 FDH thermal stability

The thermal stability of free FDH was evaluated by incubating the enzyme at 50 °C and 60 °C in a non-agitating thermoshaker. At specific time intervals, aliquots of the incubated enzyme solution were collected, transferred to Eppendorf tubes, and immediately placed on ice before performing the enzymatic assay. Residual activities were determined as described in section 7.1.1, with enzyme activity expressed as relative activity, setting the activity $t = 0$ to 100%. All assays were performed in duplicate.

7.1.4 Glutamate Dehydrogenase pH-activity

The pH-activity profile of GDH was determined spectrophotometrically (Cary 60 UV-Vis, Agilent) by monitoring the reduction of NAD⁺ to NADH at 340 nm, across pH values ranging from 6.0 to 9.0. The assays were performed in a quartz cuvette containing 55 $\mu\text{g mL}^{-1}$ GDH, 4 mM L-glutamic acid and 1 mM NAD⁺ in NaPi buffer (0.1 M), in a total volume of 1 mL. The reactions were initiated by the addition of NAD⁺ and the production of NADH was recorded for 3 minutes with 5 seconds time interval. One unit was defined as the amount of enzyme necessary

to reduce one μmol of NAD^+ per minute. The rate of NADH production was calculated using its molar extinction coefficient at 340 nm, $\epsilon_{340\text{nm}} = 6,220 \text{ M}^{-1} \text{ cm}^{-1}$. The optimum activity under the tested conditions was designated as 100%, and subsequent activities were expressed as percentages relative to this baseline value.

8 Enzyme Immobilization

8.1 Non-Covalent Immobilization of CA/FDH onto Hierarchical Porous Carbon Nanoparticles (HPCs)

Initially, HPCs were dispersed in 4 mL of NaPi Buffer (0.05 M, pH 7.5) in a 15-mL Falcon tube using an ultrasonic bath for 15 minutes. Subsequently, the enzyme solution was added to the nanoparticle solution, adjusting the total volume to 5 mL. The mixture was incubated at 30 °C with agitation at 180 rpm. Following this, the immobilization procedure was quenched by centrifugation at 4,000 rpm for 10 minutes (room temperature), and the supernatant was collected for determining the immobilization efficiency. The nanobiocatalyst was transferred to 1.5 mL Eppendorf tubes and washed twice with 1 mL of NaPi Buffer to remove any loosely bound enzyme (recovery of the nanobiocatalyst with 12,000 rpm for 5 minutes and 4°C during washing steps). The nanobiocatalyst was then dried *in vacuo* (SpeedVac DNA130 Vacuum Concentrator System, Thermo Scientific) at room temperature and stored at 4 °C until further use.

8.2 Hybrid zinc oxide–iron oxide ZnOFe(OLE) magnetic nanoparticles

8.2.1 Synthesis Of Hybrid Zinc oxide–Iron oxide magnetic nanoparticles

Hybrid zinc oxide–iron oxide (ZnOFe) magnetic nanoparticles were synthesized using *Olea europaea* leaf extract, which served as both a reducing and capping agent. The synthesis procedure was conducted in accordance with the method previously published by Fotiadou et al. (2021) and is briefly illustrated in Fig. 24.

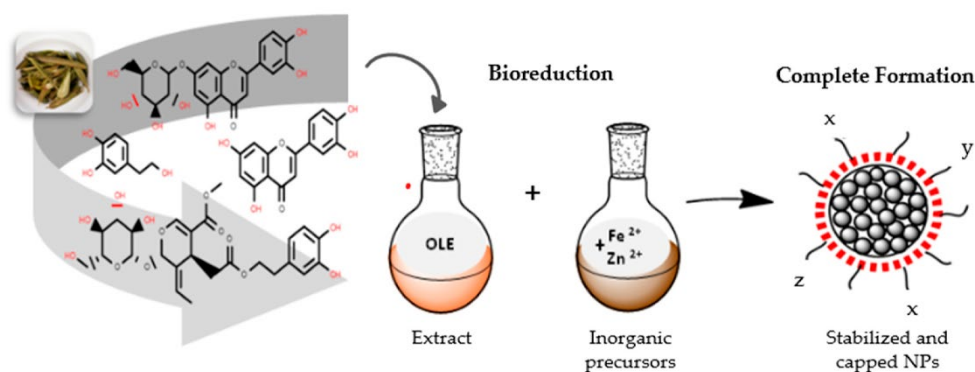


Figure 24 A schematic representation of ZnOFe biosynthesis using *Olea europaea* leaf extract (OLE) is shown. Phenols and flavonoids are the primary components of the aqueous OLE extract. This rich medium functions as a reducing and chelating agent during the biosynthesis of ZnOFe nanoparticles. Following the bioreduction of metal ions (Zn^{2+} ; Fe^{2+}) and the formation of nanoparticles, specific compounds from the phytoconstituent-rich extract, containing various terminal groups (X, Y, Z: CO, COC, COOH, OH, C–C), act as stabilizers or capping agents. These compounds coat the surface of the nanoparticles (represented by a red ring) to prevent agglomeration.

8.2.2 Immobilization of FDH onto ZnOFe (OLE) Nanoparticles

8.2.2.1 Non-Covalent Immobilization

Initially, 2 mg of ZnOFe nanoparticles were dispersed in 4 mL of NaPi Buffer (0.05 M, pH 7) in a 15-mL Falcon tube using an ultrasonic bath for 15 minutes. Subsequently, 0.5 mg of FDH was added to the nanoparticle solution, adjusting the total volume to 5 mL. The mixture was incubated at 30 °C under agitation (180 rpm) for 1 hour. Following this, the immobilization procedure was quenched by centrifugation at 4,000 rpm for 10 minutes (room temperature), and the supernatant was collected for determining the immobilization efficiency. The nanobiocatalyst was transferred to 1.5 mL Eppendorf tubes and washed twice with 1 mL of NaPi Buffer to remove any loosely bound enzyme (recovery of the nanobiocatalyst with 12,000 rpm for 5 minutes and 4 °C during washing steps). The nanobiocatalyst was then dried *in vacuo* (SpeedVac DNA130 Vacuum Concentrator System, Thermo Scientific) at room temperature and stored at 4 °C until further use.

8.2.2.2 Covalent Immobilization

Initially, 2 mg of ZnOFe nanoparticles were dispersed in 0.6 mL of HEPES buffer (0.05 M, pH 7) in a 2-mL Eppendorf tube using an ultrasonic bath for 15 minutes. Subsequently, into the dispersed nanoparticles, 0.48 mL of 10 mg mL⁻¹

EDC and 0.92 mL of 50 mg mL⁻¹ NHS were added, and the mixture was agitated at 800 rpm for 1 hour at 30 °C. The activated ZnOFe nanoparticles were retrieved with centrifugation (12,000 rpm, 4 °C for 5 minutes) and washed twice with HEPES buffer.

For the immobilization step, the activated nanoparticles were dispersed in HEPES buffer and 0.5 mg FDH was added to the mixture, adjusting the total volume to 2 mL. The mixture was agitated for 1 hour (750 rpm, 30 °C) inside a thermoblock. The immobilization process was quenched by centrifugation at 12,000 rpm and 4 °C for 5 minutes, and the supernatant was collected to determine the immobilization efficiency. The nanobiocatalyst was washed twice with HEPES buffer, with recovery achieved by centrifugation at 12,000 rpm and 4 °C for 5 minutes during each washing step. Finally, the nanobiocatalyst was dried *in vacuo* (SpeedVac DNA130 Vacuum Concentrator System, Thermo Scientific) at room temperature and stored at 4°C until further use.

8.3 Immobilization Efficiency of FDH Immobilization

The immobilization yield was evaluated using two different methods applied to the supernatant: i) measuring the protein content (w/v %), and ii) measuring the enzymatic activity (Units). These values were then compared to the initial protein content/activity of the enzyme solution before immobilization, as shown in Eq. 14.

$$\text{Immobilization Yield (\%)} = \left(1 - \frac{F}{I}\right) \times 100 \quad \text{Eq. 14}$$

Equation 14 Immobilization Yield Formula: F represents the total protein content (w/v %) or enzymatic activity (Units) in the supernatant after immobilization, while I represent the initial protein content (w/v %) or enzymatic activity (Units) before immobilization.

The residual protein content in the FDH solutions after immobilization was determined using a BCA Protein Assay Kit (Pierce™ BCA Protein Assay Kit, Thermo Scientific). Specifically, 25 µL of the supernatant was mixed with 200 µL of the BCA reagent (A & B stocks in a 50:1 ratio) in a 96-well plate and incubated at 37 °C for 30 minutes in the dark. After a 1-minute cool-down, the absorbance was measured at 562 nm using a plate reader. Blank samples, containing the buffer used in the immobilization procedure, were subtracted from the measurements.

The BCA calibration curve was established using known concentrations of bovine serum albumin (BSA).

The remaining enzymatic activity in the immobilization supernatant was determined by measuring the formate oxidation reaction, as previously described in section 7.1.1. The reaction was carried out in NaPi buffer (0.05 M, pH 7), and to enhance the sensitivity of the method, 100 μ L of the supernatant was used and the reaction temperature was set to 37 $^{\circ}$ C.

8.4 Activity Assays of Immobilized Enzymes

8.4.1 FDH@ZnOFe Activity Assay

Activity assays involving the immobilized FDH were performed in a modified procedure of the previously described activity assay in section 7.1.1. The reactions were conducted in 1.5 mL Eppendorf tubes containing the nanobiocatalyst (at a concentration of either 0.5 or 1 mg/mL), 100 mM sodium formate, and 1 mM NAD⁺ in 0.05 M NaPi buffer (pH 7.0), with a final reaction volume of 1 mL. The tubes were incubated in a thermoshaker at 30 $^{\circ}$ C under constant agitation (800 rpm). At specified time intervals (5 or 10 minutes), samples were centrifuged at 12,000 rpm for 1 minute, and the absorbance of a 200- μ L aliquot was measured spectrometrically at 340 nm using a plate reader (MULTISKAN SkyHigh, Thermo Scientific). Blank tests were performed using the equivalent amount of nanoparticles without enzyme.

8.4.2 FDH@ZnOFe Reusability

Both covalent and non-covalent FDH@ZnOFe nanobiocatalysts were evaluated for their reusability through the formic acid oxidation reaction. Reusability assays were conducted inside 1.5 mL Eppendorf tubes, containing 100 mM sodium formate, and 1 mM NAD⁺ in NaPi buffer (0.05 M, pH 7.0) with final reaction volume of 1 mL. For the non-covalently immobilized FDH@ZnOFe nanobiocatalyst, 1 mg/mL was used with a reaction time of 10 minutes. For the covalently immobilized FDH@ZnOFe nanobiocatalyst, 1 mg/mL was used with a reaction time of 5 minutes. Reactions were performed inside a thermoblock at 40 $^{\circ}$ C under constant agitation (800 rpm). After each catalytical cycle, the

nanobiocatalysts were retrieved with centrifugation (12,000 rpm for 1 minute, room temperature), and the absorbance of a 200 μL aliquot was recorded spectrometrically at 340 nm using a plate reader (MULTISKAN Skyhigh, Thermo Scientific). Prior to each reaction cycle, the nanobiocatalysts underwent a two-step wash with the reaction buffer and recovered with centrifugation (12,000 rpm for 2 minutes, 4 $^{\circ}\text{C}$). The activity of the first cycle was set as 100%, with subsequent activity measured as a percentage (%) relative to the initial one.

8.4.3 FDH@ZnOFe Thermoactivity and pH-activity

The covalently prepared FDH@ZnOFe nanobiocatalyst was evaluated for its thermoactivity and pH-activity using formic acid oxidation, as previously described in the section 8.4.1. For these experiments, 200 $\mu\text{g}/\text{mL}$ of the nanobiocatalyst was used.

To assess the thermoactivity of the nanobiocatalyst, reactions were performed at temperatures of 30, 40, 50, 60, and 70 $^{\circ}\text{C}$. For pH-activity, 0.05 M buffers (NaPi and Tris-HCl) with pH values ranging from 6 to 9 were employed. In both cases, the optimum activity under the tested conditions was designated as 100%, and subsequent activities were expressed as percentages relative to this baseline value.

8.4.4 FDH@ZnOFe Thermal stability

The thermal stability of the prepared covalently bound FDH@ZnOFe nanobiocatalyst was evaluated by incubating it at 60 $^{\circ}\text{C}$ in a non-agitating thermoshaker for up to 1 hour, with measurements taken at 15-minute intervals, in the absence of substrates. After incubation, the nanobiocatalyst was cooled in an ice bath, and the residual activities were assayed as described in the section 8.4.1. The activity was expressed as relative activity, setting the activity at $t=0$ min as 100%. All assays were performed in duplicate.

8.5 Fourier-transform infrared spectroscopy (FTIR)

The FTIR method was employed to confirm the immobilization of FDH onto the ZnOFe nanoparticles. The solid samples of the nanoparticles and the

nanobiocatalyst were ground thoroughly with KBr (>1% w/w, sample: KBr ratio) to achieve a homogenous blend, followed by pressurizing with a hand press to form 7 mm KBr pellets. For each prepared KBr pellet, a total of 32 scans were averaged, with fixed resolution at 4 cm⁻¹ within the wavenumber range of 4000-400 cm⁻¹ using a Jasco FT/IR 4700 infrared spectrometer (Jasco, Tokyo, Japan) equipped with a Peltier DLATGS detector. For characterization of the free FDH (available in liquid form), Attenuated Total Reflectance (ATR)-FTIR spectroscopy was utilized using the same settings and apparatus as previously described.

9 Enzymatic reduction of CO₂ to formic acid

9.1 pH stability of NADH Cofactor

The stability of the reduced cofactor NADH was evaluated by incubation under a range of pH conditions. Stability assays were performed in 5 mL septum-closed vials under anaerobic conditions utilizing 0.1 M NaPi buffer with pH values 6, 6.5, 7, 7.5 and 8. Initially, the buffers were pre-purged with nitrogen gas (N₂) at a fixed flow rate for 30 minutes to effectively remove dissolved air. A total of 5 mM of NADH was then dissolved in a final volume of 2 mL, and the headspace of each vial was purged with nitrogen gas for 1 minute to ensure saturation. Vials were then sealed with parafilm, followed by incubation at 30 °C under agitation. For sampling, aliquots were withdrawn anaerobically using a syringe at time points of 0, 2, 4, 6, and 24 hours. Then, the samples were diluted tenfold, and their absorbance was measured spectrometrically at 340 nm using a plate reader (MULTISKAN SkyHigh, Thermo Scientific). The results were expressed as residual stability, with the absorbance at 0 hours set as 100%.

9.2 FDH-mediated CO₂ Reduction to Formic Acid

FDH-mediated CO₂ reduction to formic acid was performed using either gaseous CO₂ or NaHCO₃ as the reaction substrates. Initially, 20 mL NaPi buffer (0.1 M, pH 7.0) was purged with N₂ to eliminate dissolved air. For reactions with gaseous CO₂, CO₂ was bubbled into the N₂-saturated buffer for 30 minutes, after which the buffer pH was readjusted to 7.0 with 2 M NaOH (Fig. 25). The final

reaction mixture consisted of nine parts CO₂-saturated buffer and one part N₂-saturated buffer.

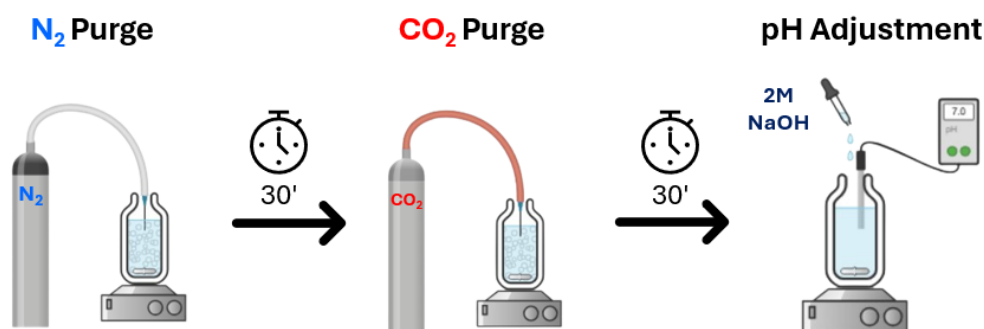


Figure 25 Bubbling steps with N₂ and CO₂, followed by pH adjustment prior to FDH-mediated CO₂ reduction.

For reactions with NaHCO₃ as the substrate, a 0.2 M NaHCO₃ solution was prepared using the N₂-saturated buffer and subsequently adjusted to pH 7.0 with 2 M HCl. Reactions were carried out with 0.1 M NaHCO₃, where half of the final reaction volume was sourced from the adjusted 0.2 M NaHCO₃ solution, and the remainder was made up with N₂-saturated buffer.

Regardless of the substrate choice, all reaction components were dispersed in the pH-adjusted buffer. Reactions with free enzymes were conducted in 5 mL glass vials, while those with immobilized FDH were carried out in Eppendorf tubes. Before initiating the reaction, the headspace of the reaction vessel was purged with N₂ gas for 1 minute to establish anaerobic conditions, after which the vessel was sealed with parafilm. The reactions were conducted at 30 °C under continuous agitation.

Samples were periodically withdrawn anaerobically using a syringe and filtered through 0.22 µm nylon syringe filters to determine the concentrations of formic acid and NADH (Fig. 26). Formic acid analysis required derivatization with the PFBBr reagent under alkaline conditions, followed by GC/MS analysis, as described in Section 10.1. In contrast, NADH was quantified directly by measuring its absorbance at 340 nm using a plate reader (MULTISKAN SkyHigh, Thermo Scientific).

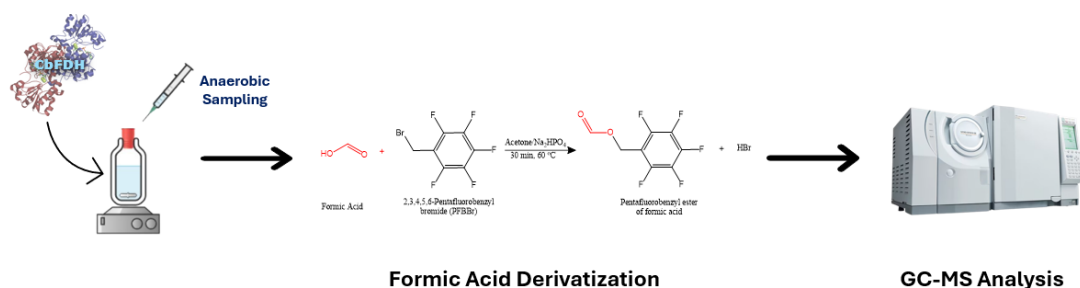


Figure 26 Anaerobic sampling of the reaction, followed by formic acid derivatization and GC-MS analysis.

FDH cascade reactions involving either CA, GDH, or both, along with the ratios and concentrations of these enzymes and the concentrations of the sacrificial substrate, will be described in the Results and Discussion section of this thesis.

The reaction's yield across different time stops was calculated with Eq. 15, through the comparison of the production of formic acid with the initial concentration of the cofactor (since CO₂ concentration is practically unknown in the reaction).

$$Efficiency (\%) = \frac{1 \times mol\ FA}{1 \times mol\ NADH} \times 100 \quad (Eq. 15)$$

Equation 17 Formic Acid (FA) Conversion Yield Equation based on the initial input of NADH cofactor in the reaction.

10 Analytical Methods

10.1 Formic Acid Quantification

10.1.1 Formic Acid Derivatization with 2,3,4,5,6-Pentafluorobenzyl bromide (PFBBr)

Formic acid quantification was evaluated through derivatization with PFBBr (Fig. 27) accordingly to a modified derivatization protocol (Lamarre et al., 2014). For derivatization, 50 µL aliquots of formic acid samples were placed in a 1.5 mL Eppendorf tube, followed by the addition of 20 µL of 0.25 M NaPi Buffer (pH 8) and 130 µL of 0.1 M PFBBr solution (dissolved in HPLC acetone). The samples were sealed with parafilm, vortexed for 1 minute and then heated at 60 °C inside a thermoblock for 30 minutes. After heating, the samples were allowed to cool at room temperature.

To extract the newly formed formic acid ester into an organic phase, 330 μL of ethyl acetate was added, followed by vortexing for 1 minute and centrifugation (13,000 rpm, 1 minute). The upper layer was retrieved, filtered through (0.22 μm nylon syringe filters), and placed into glass inserts before submission for GC-MS analysis. The process described above was used to generate a calibration curve using standard formic acid concentrations ranging from 25 to 250 $\mu\text{mol L}^{-1}$ in NaPi buffer (0.1 M, pH 7.0).

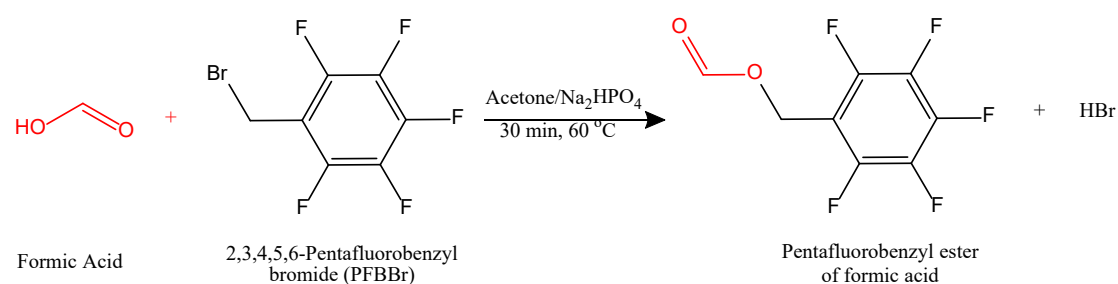


Figure 27 Derivatization Reaction of formic acid with PFBBr.

10.1.2 GC-MS analysis of PFBBr-formic acid ester

Derivatized formic acid, in the form of the PFBBr-formic acid ester, was analyzed using a GC-MS system (GCMS-QP2010 SE, Shimadzu, Tokyo, Japan) according to a modified protocol (Aguirre et al., 2023). Organic phased derived samples were injected with a volume of 1 μL using pulsed splitless mode into a MEGA-5 MS capillary column (30 m length \times 0.25 mm internal diameter \times 0.25 μm film thickness; MEGA, Legnano, Italy), consisting of 5% phenyl- and 95% methyl-polysiloxane. The system was operated in Electron Ionization (EI) mode at 70 eV and Selected Ion Monitoring (SIM) mode. The carrier gas was Helium with column flow at 1.2 mL min^{-1} , linear velocity at 40.1 cm sec^{-1} and pressure at 74.7 kPa. The injection port temperature was set at 250 $^\circ\text{C}$, ion source temperature at 200 $^\circ\text{C}$, and interface temperature at 200 $^\circ\text{C}$. The GC oven temperature program started with an initial hold at 65 $^\circ\text{C}$ for 1 min, followed by a gradient increase of 1.5 $^\circ\text{C}/\text{min}$ up to 80 $^\circ\text{C}$, and finally a gradient increase of 45 $^\circ\text{C}/\text{min}$ up to a final temperature of 250 $^\circ\text{C}$. Temperature was then returned to 65 $^\circ\text{C}$ for a new injection. The solvent cut time was set at 8.5 min. The PFBBr-formic acid ester product peak was eluted between 9 and 9.2 minutes. SIM mode parameters and m/z ion properties are presented in Table 2.

Table 2 SIM mode parameters and m/z ion properties used for quantification of derivatized formic acid.

<i>m/z</i>	Ion Property	Ratios (%) to <i>m/z</i> 226
226	Qualifier, Quantifier	100.00
227	Qualifier, Quantifier	10.11
197	Qualifier, Quantifier	12.42
19	Qualifier	-

Chapter Three: Results and Discussion

1 Carbonic Anhydrase Assays

1.1 Hydratase Activity of CAs

The hydratase activity of five thermophilic CAs, along with the commercial mesophilic bCA, was investigated using three different methods (Table 3). Typically, throughout the bibliography, CA's hydratase activity is routinely determined in Wilbur Anderson Units (WAU) either electrometrically or colometrically, though in our setups, a recently reported method was employed (pH-stat electrometric method), which determines the hydratase turnover number of CAs (Fuchs et al., 2021). A common aspect of the used methods for determining CAs' hydratase activity is the requirement for only a few hundred nanograms per milliliter of enzyme (since most CAs exhibit high turnover numbers), as well as the assay durations that do not exceed one to two minutes.

Table 3 Evaluation of CA enzyme hydratase activity in three different setups. The abbreviation WAU stands for Wilbur-Anderson Units, and the exponent notation is used for each applied method.

Enzyme	¹ WAU mg ⁻¹	² WAU mg ⁻¹	³ Turnover rate ($\mu\text{mol HCO}_3^{-1} \text{ s}^{-1} \text{ mg}^{-1}$)
ApCA	28 ± 3	32 ± 3	n.d.
BhCA	2318 ± 349	582 ± 31	357 ± 68
DvCA8.0	2051 ± 139	1218 ± 249	895 ± 38
SazCA	184 ± 43	128 ± 7	30 ± 6
SyCA	19299 ± 2299	15939 ± 823	5832 ± 316
bCA (Sigma, C3943)	10634 ± 954	51113 ± 2394	4824 ± 92

In terms of replicability, the colorimetric and pH-stat electrometric methods tend to be more reliable, as their results exhibit lower variance, and enzyme activity generally follows a dose-dependent increase with enzyme concentration (Kim & Jo, 2022). As reported in the literature, the electrometric

¹ Electrometric method (pH-meter setup)

² Colorimetric method (spectrometer setup)

³ Hydratase activity as turnover number, measured using a modified electrometric method with a pH-stat apparatus.

method, which is highly dependent on the logarithmic pH scale, presents limitations in accurately measuring activity at different enzyme concentrations. Additionally, a notable drawback in our setup is that the pH electrode used is not “designed” for measurements at icy cold temperatures, which often results in decalibration of the pH meter during prolonged assays conducted under such conditions.

It should be acknowledged that the sensitivity of each method varies, depending on the instrument used and the principles underlying the activity calculation. In our study, electrometric and colorimetric methods report activity in WAU, while the pH-stat method expresses activity in terms of turnover rate. A direct comparison of these methods should not be considered appropriate, as they employ entirely different experimental setups and parameter considerations for activity calculations, naturally leading to variations in reported activity units.

Furthermore, the CA activity results obtained in this study will not be compared to previously reported values in literature. A detailed enzymatic activity analysis is beyond the scope of this thesis, and the sensitivity and reproducibility of CA activity measurements remain a multifactorial challenge, highly dependent on the precision and sensitivity of the instrumentation used.

Among the thermophilic CAs, SyCA exhibits the highest hydratase activity, as consistently observed across all three methods. Following SyCA, DvCA8.0 and BhCA rank second and third, respectively. However, using the electrometric method, BhCA displays higher activity than DvCA8.0. Lastly, SazCA and ApCA occupy the fourth and fifth positions, respectively. Notably, ApCA activity could not be detected using the pH-stat method, even at enzyme concentrations as high as 2 µg/mL—the highest CA stock concentration ever used for this assay.

When comparing the thermophilic CAs to the mesophilic enzyme bCA, surprisingly, SyCA demonstrates greater hydratase activity in both the electrometric and pH-stat methods. Specifically, SyCA's activity is 1.8-fold higher than that of bCA in the electrometric method and 1.2-fold higher in the pH-stat method. However, bCA exhibits significantly higher activity in the colorimetric method, showing 3.2-fold greater activity than SyCA. Notably, bCA represents the highest hydratase activity ever recorded using our colorimetric setup.

The electrometric pH-stat method may be considered the most accurate assay for determining CA hydratase activity, as it was conducted at 25 °C, a temperature closer to practical CAs applications. Additionally, according to the original publisher of this assay, the method can be applied at slightly elevated temperatures, up to 40 °C, since CO₂ capture under ambient pressure conditions becomes impractical at higher temperatures due to minimal substrate availability (Steger et al., 2022). However, for the thermophilic enzymes, hydratase activity may be underestimated, as their optimal activity typically exceeds the mesophilic temperature range (20–45 °C), potentially leading to further enzyme activation at higher temperatures (Maffucci et al., 2020).

The need for a routinely applied method to determine CAs' primary activity at elevated temperatures remains a significant challenge. In the next section, the esterase activity of CAs is examined using p-nitrophenyl acetate (pNPA) as the reaction substrate, offering greater flexibility in assay conditions at highly elevated temperatures, thus leading to an estimation of the optimum working temperature of CAs.

1.2 Esterase Activity of CAs

The esterase activity of CAs was determined using pNPA as the reaction substrate, monitoring the production of p-nitrophenol (pNP) spectrophotometrically. Although this assay allows the characterization of CAs belonging to the α -family in commonly used activity units ($\mu\text{moles min}^{-1}$), it is not suitable for other CA families (Baliukynas et al., 2020). Thus, the esterase activity is a secondary reaction of these enzymes and does not reflect their primary hydratase function, which is widely used in the applications of these enzymes.

In our experimental setups, we assessed the esterase activity of five previously studied thermophilic CAs to determine their optimum working temperature at elevated temperatures. It is important to note that the autohydrolysis of pNPA increases with temperature; therefore, the autohydrolysis rate must always be subtracted from the activity measurements. Most importantly, the failure to account for pNPA autohydrolysis, even at mesophilic temperatures, leads to an overestimation of CA esterase activity.

The results of esterase activity assays using 3 mM pNPA as the initial substrate concentration, in the presence of Tris-HCl 0.05 M pH 7.5 buffer, are shown in Table 4. For most thermophilic enzymes, except BhCA, the optimum temperature is 70 °C, whereas for BhCA, it is 60 °C. For convenience in the values reading, the esterase activity of these enzymes was expressed as Units per gram of protein. Notably, these esterase units are approximately three orders of magnitude lower than that of the commercially available mesophilic bovine CA (bCA).

Table 4 Comparison of esterase activity of different thermophilic CAs at pH 7.5, in the presence of Tris buffer. The table lists various thermostable enzymes along with their optimal temperature (T_{opt}) in degrees Celsius and their catalytic activity in units of $\mu\text{moles min}^{-1} \text{g}^{-1}$ of protein.

Enzyme	T_{opt} (°C)	Units ($\mu\text{moles min}^{-1} \text{g}^{-1}$)
SyCA	70	409 ± 20.61
DvCA8.0	70	75.66 ± 3.85
BhCA	60	60.91 ± 0.00
SazCA	70	61.85 ± 0.00
ApCA	70	31.2 ± 1.66
bCA ¹	37	> 354 × 10 ³

Among the thermostable CAs, SyCA exhibited the highest esterase activity, followed by DvCA8.0, which displayed approximately 5.5-fold lower activity. SazCA and BhCA ranked third and fourth, respectively, with similar activity levels. When compared to hydratase of activity assays, the thermostable SyCA and DvCA8.0 consistently exhibited the highest and second-highest activities, respectively.

1.3 CA-mediated CO₂ Mineralization

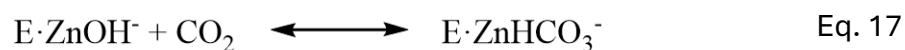
Biomining is a slow, exothermic natural process in which living organisms produce minerals, often leading to hardened or stiffened tissues

¹ In the last row of the table the esterase activity of the mesophile bCA is depicted, where the optimum temperature and the esterase activity⁽¹⁾ were obtained from a previously published paper (Demir et al., 2000).

(Weiner, 2003). This process involves silicates and, more commonly, divalent metals such as Ca^{2+} and Mg^{2+} , which interact with gaseous or dissolved CO_2 to form solid minerals.

The concentration of Ca^{2+} ions plays a crucial role in enhancing mineralization efficiency. In nature, the formation of bicarbonate is a rate-limiting step, occurring at a slow rate of $6.2 \times 10^{-3} \text{ s}^{-1}$ (Shao et al., 2024). However, certain factors can accelerate bicarbonate production. Mineralization processes are favored under alkaline conditions, where the equilibrium shifts toward carbonate formation, which then reacts with silicates and metals, leading to the precipitation of insoluble metal carbonates (Eq. 18).

CA-induced mineralization is a highly investigated research topic. As a mild-operating conditions promotor of CO_2 hydration, CAs dramatically accelerates the conversion of CO_2 to bicarbonate, described by Eq. 16 & Eq. 17, thus increasing overall mineralization efficiency. Furthermore, mineralization efficiency is dependent on various parameters of a system such as pH, salinity, temperature, and pressure. CAs present a promising approach to improve carbon capture rates due to their efficient catalytic hydration capabilities (Villa et al., 2023). However, for effective CO_2 capture in industrial environments, these enzymes must possess specific characteristics, including high catalytic activity, industrial conditions tolerance, stability, and reusability.



1.3.1 One-step CO_2 mineralization

A one-step CO_2 mineralization experiment was conducted to evaluate the feasibility of enhanced mineralization in the presence of five thermophilic CAs and one mesophilic-commercial bovine erythrocytes CA under ambient

temperature, pressure, and alkaline conditions. In this setup, a high-flow-rate gaseous CO₂ stream was introduced into a calcium-containing buffer to promote carbonate precipitation.

The mineralization results are presented in Fig. 28, with Fig. 28A showing the absolute values of CaCO₃ precipitate and Fig. 28B displaying the percentage increase in CaCO₃ precipitation compared to the blank solution.

During CO₂ purging, some non-enzymatic reactions occurred. However, as expected, the presence of CAs significantly accelerated CO₂ hydration, resulting in a more rapid turbidity increase compared to the blank solution immediately after introducing gaseous CO₂ into the alkaline buffer.

Among the tested enzymes, bCA exhibited the highest efficiency, reaching the upper limit of CaCO₃ production with no further accumulation. This superior performance can be attributed to its mesophilic nature, which likely allows optimal catalytic activity under the experimental conditions. Furthermore, bCA's exceptional efficiency aligns with its previously observed high enzymatic rate in hydratase assays, highlighting its potential for CO₂ mineralization applications under ambient conditions.

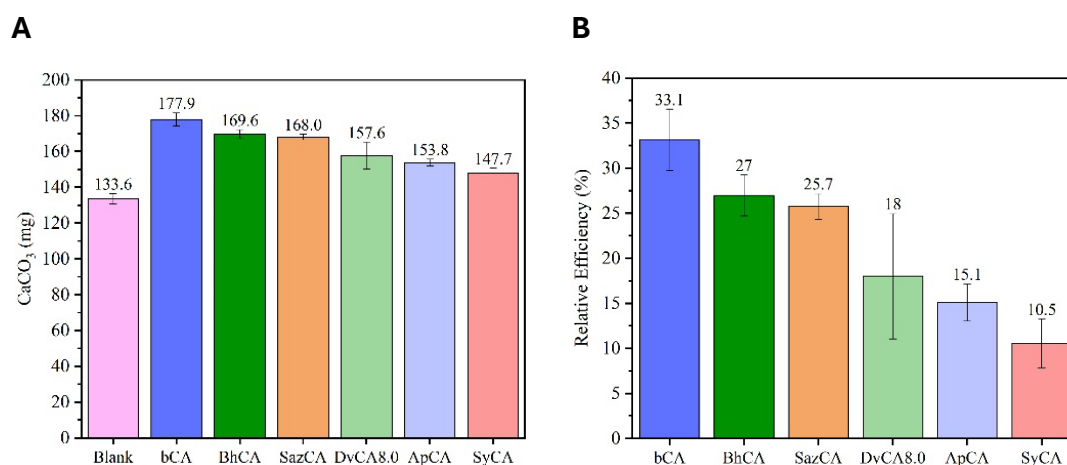


Figure 28 One-step CA-mediated CO₂ mineralization results. A. Precipitated CaCO₃ in absolute weight (mg), B Relative efficiency in CaCO₃ precipitates compared to blank sample.

Regarding the efficiency of the thermophilic CAs, BhCA and SazCA yielded the highest CaCO₃ precipitation, producing 27% and 25.7%, respectively, more precipitate than the blank reaction. DvCA8.0 and ApCA followed, ranking third and fourth, while SyCA exhibited the lowest CaCO₃ precipitation.

Surprisingly, despite SyCA displaying the highest hydratase activity among the tested CAs, it resulted in the lowest CaCO_3 precipitation, yielding less than half of what the other enzymes produced.

The key factors influencing these results are the dynamic interplay between enzymatic activity and stability under reaction conditions. The unexpectedly low CaCO_3 precipitation by SyCA suggests that under high alkalinity and gaseous flow rates, BhCA and SazCA are the most reaction-stable thermophilic CAs. However, it should be acknowledged that our experiments were conducted at the laboratory scale and standard conditions, and thus, the results may differ under industrial conditions. In particular, at higher temperatures, the thermophilic enzymes may exhibit increased efficiencies due to temperature-related activation.

1.3.2 Two-step CO_2 mineralization

The one-step CA-mediated CO_2 mineralization demonstrates the feasibility of CO_2 mineralization. However, when using immobilized enzymes, the process must be divided into two distinct steps to allow for the isolation and recovery of the immobilized catalyst before its reuse in another reaction cycle.

Initially, in the first step, the immobilized CA facilitates the capture of gaseous CO_2 into the aqueous phase. Following this, the biocatalyst is removed, washed, and prepared for reuse. In the second step, the captured CO_2 is introduced into an alkaline, metal-containing solution, where it reacts to form mineral precipitates. This stage is typically followed by an incubation phase to enhance mineral production and promote optimal crystallization. Lastly, precipitates are collected, dried, and weighed to compare the overall reaction efficiency.

In this study, two-step mineralization experiments were conducted using only free bCA to establish a control reaction setup. The two-step mineralization results are presented in Fig. 29A.

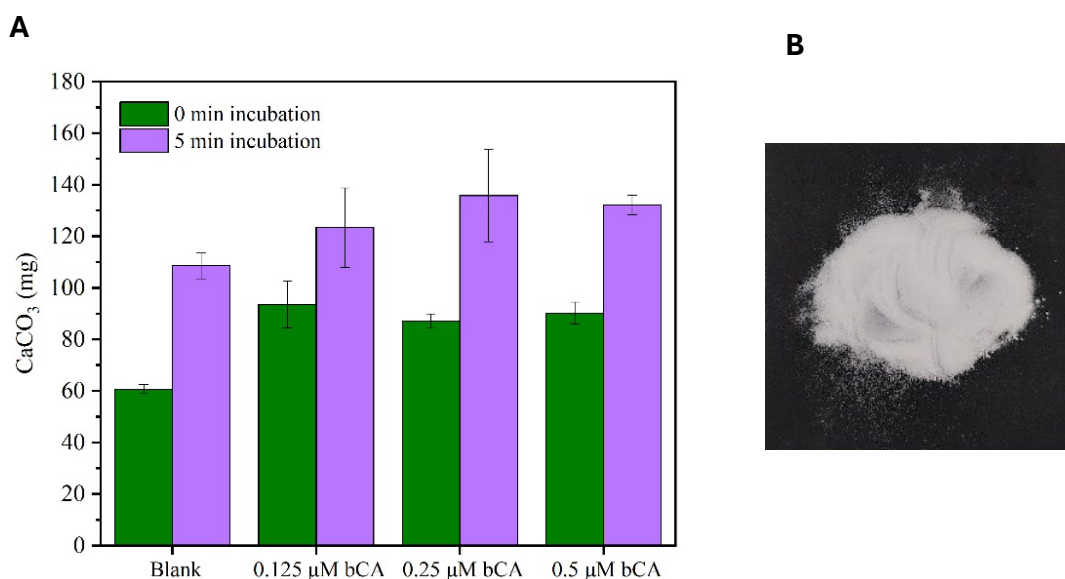


Figure 29 A. CA-mediated CO_2 mineralization results showing the absolute weight of CaCO_3 precipitates at two different incubation times (0 min and 5 min). B. Picture of the obtained and dried CaCO_3 powder.

In this experiment, the purging of the CA-containing solution with CO_2 was kept constant, and only the second step, after the introduction of the alkaline metal-containing solution, was investigated. In the second step, two different endpoints ($t = 0$ without incubation and $t = 5$ min with incubation at 30°C) were compared, either in the presence or in the absence of CA. It was essential to examine CaCO_3 precipitation at different time points because, as shown in Supplementary Fig. S2, after 10 minutes of incubation, CaCO_3 precipitation reaches equilibrium. At this point, the comparison between the presence and absence of the enzyme would show no significant difference in CaCO_3 precipitates.

The results of this method indicate that bCA significantly enhanced CaCO_3 formation at all the depicted bCA concentrations. Notably, the differences in CaCO_3 yield were more pronounced in the non-incubated samples. Specifically, without incubation, the CaCO_3 yield was approximately 1.5 times higher than in the blank reaction. However, after 5 minutes of incubation, the yield decreased compared to the non-incubated samples, showing an average increase of 1.3 times relative to the blank. Furthermore, this difference would be further reduced if 10 minutes of incubation were compared.

Regarding the enzyme concentration, it was observed that the maximum hydration rate was achieved even with the lowest used bCA concentration (0.125

μM). A dose-dependent relationship between enzyme concentration, hydration rate, and CaCO_3 yield would likely be observed at lower enzyme concentrations, although this was not the focus of this study.

The findings suggest that even in the absence of CA, the high-flow gaseous purging saturates the buffer solution with CO_2 , though the spontaneous hydration of CO_2 occurs at a slower rate compared to the presence of CA (Mirjafari et al., 2007). The high flow rate likely plays a crucial role in rapidly saturating the medium with CO_2 . Therefore, for future experimental setups, it is recommended to test lower flow rates to prolong the hydration process, allowing for a more controlled assessment of CA-mediated mineralization.

In conclusion, this study presents a framework for a two-step assessment of immobilized CA hydration activity. To effectively highlight CA-induced mineralization, shorter incubation times or lower gaseous CO_2 purging flow rates should be prioritized in future mineralization experiments.

Outline for Carbonic Anhydrase assays

In this thesis section, the hydratase and esterase activities of five thermophilic CAs were evaluated using multiple assay methods. Among the thermophilic CAs, SyCA consistently exhibited the highest hydratase and esterase activities, followed by DvCA8.0 and BhCA. Notably, SyCA outperformed the commercial mesophilic bCA in hydratase activity when measured using the electrometric and pH-stat methods, highlighting its potential for industrial applications. However, bCA exhibited significantly higher activity in the colorimetric assay, emphasizing the variability of results depending on the method used. The pH-stat electrometric method, conducted at 25 °C, was identified as the most accurate approach for hydratase activity determination, though it may underestimate the performance of thermophilic enzymes that function optimally at higher temperatures.

Furthermore, the esterase activity assays revealed that SyCA and DvCA8.0 also demonstrated the highest esterase activities, with optimal working temperatures at 70 °C. However, compared to the commercial bCA, their esterase efficiency was substantially lower. A critical challenge in CA's characterization remains the lack of “handy” activity measurement protocols at elevated temperatures, as current methods are primarily optimized for mesophilic enzymes. Future studies should focus on refining assay conditions to better reflect the optimal working temperatures of thermophilic CAs, which could enhance their applicability in industrial biocatalysis and CO₂ capture technologies.

Regarding the results of the one-step CO₂ mineralization, studies demonstrated that CA significantly enhances CO₂ hydration and thus the mineralization efficiency, with bCA exhibiting the highest efficiency, reaching the maximum CaCO₃ precipitation without further accumulation. Additionally, the thermophilic CAs, such as BhCA and SazCA, also showed increased CaCO₃ precipitation efficiency. However, SyCA, despite its high hydratase activity, resulted in the lowest CaCO₃ precipitation, possibly due to instability under high alkalinity and the adopted gaseous CO₂ flow rates.

Regarding the two-step mineralization experiments, it was revealed that CA increased CaCO_3 formation, with the highest yield observed in non-incubated samples. Interestingly, even at “low” concentrations ($0.125 \mu\text{M}$), bCA effectively enhanced CO_2 hydration, suggesting that higher concentrations may not be necessary for optimal mineralization. Additionally, high-flow CO_2 purging resulted in quick saturation of the solution; thus by reducing the flow rate could allow for more controlled hydration and mineralization in future experiments.

2 Enzyme Immobilization

2.1 Selection of Nanoparticles

In this section, a brief description is provided of the nanoparticles chosen for the enzyme immobilization of CA and FDH. Initially, Hierarchical Porous Carbons (HPCs) were considered the primary nanoparticles for CO₂ capture and reduction applications. HPCs are known for their high surface area, chemical stability, and diverse pore structures (Cai et al., 2022). Their selection was primarily based on their hierarchical porous architecture, as micropores and mesopores have been reported to enhance CO₂ adsorption (Zhang et al., 2020). The intricate interconnected pore network characteristic of HPCs permeates the entire material, facilitating superior communication between pores compared to other porous materials. The labyrinthine pore structure reduces gas mass transfer distances and minimizes resistance to CO₂ diffusion, resulting in enhanced adsorption kinetics. Furthermore, the high pore density significantly increases the specific surface area of the material, making HPCs a promising candidate for CO₂-catalyzing enzyme immobilization.

Additionally, in this thesis, hybrid zinc oxide-iron oxide (ZnOFe) nanoparticles were utilized as an enzyme immobilization support matrix. These nanoparticles are often synthesized using green methods, particularly via plant extracts rich in phenols and polyphenols, which aid in metal ion chelation. Specifically, ZnOFe nanoparticles in this study were synthesized using *Olea europaea* (olive leaf) aqueous extract as a reducing, chelating, and capping agent. Furthermore, ZnOFe nanoparticles exhibit magnetic properties, a spherical morphology, and a functionalized surface, enhancing their suitability for enzyme attachment through both physical adsorption and covalent bonding. Lastly, by providing a stable and reusable platform, ZnOFe nanoparticles have been previously reported to improve enzyme stability, activity, and recyclability, making them promising candidates for eco-friendly biocatalytic processes (Fotiadou et al., 2022; Fotiadou et al., 2021).

2.2 Thermophilic CAs Immobilization onto HPCs

The immobilization of five thermophilic CAs onto HPCs nanoparticles via physical adsorption was investigated. For these trials, various ratios of CA powders and HPCs were investigated, and the immobilization efficiency was calculated by measuring the residual protein content in the immobilization supernatant after the incubation phase. The results are shown in Table 5.

Table 5 Non-covalent immobilization efficiency of five thermophilic CAs onto HPCs nanoparticles. The mass of the CAs corresponds to the used lyophilized powder weight.

CA	CA:HPCs Ratio (mg)	Immobilization Yield (%)
SyCA	1:1	62.69 ± 0.86
	1:2	91.22 ± 0.51
	2:1	36.08 ± 1.31
BhCA	2:1	42.63 ± 2.75
	3:1	29.95 ± 5.27
	2:2	61.26 ± 0.95
DvCA8.0	3:2	95.99 ± 0.61
	4:2	84.47 ± 1.96
ApCA	1:2	90.92 ± 0.91
SazCA	1.5:2	97.03 ± 3.16

According to the measurement of the supernatant after immobilization, it was confirmed that all thermophilic CAs were successfully immobilized onto the HPCs. However, the observed immobilization yield variance between the different CAs is expected, as each enzyme has a unique amino acid sequence and, consequently, different tertiary structure and interaction sites with the nanoparticles.

To evaluate the activity of these immobilized nanobiocatalysts, the pNPA hydrolysis method was used. The assays were conducted at either 40 °C or 50 °C, with nanobiocatalyst concentrations of either 0.5 mg/mL or 1 mg/mL.

Notably, none of the nanobiocatalysts exhibited detectable esterase activity, even after 5 or 10 minutes of reaction time. While the blank assay samples

confirmed pNPA autohydrolysis, no further CA-related pNPA hydrolysis was observed in the supernatant of the reaction. Possibly, it can be assumed that this could be the result of the adsorption of the reaction product into the nanoparticle matrix. Other factors that might contribute to this are steric hindrances caused by enzyme confinement or potential structural disruption of the enzymes upon immobilization (Rodrigues et al., 2021). Additionally, since these enzymes are thermophilic, they may require higher assay temperatures, such as 60 °C or 70 °C, as these were previously identified as their optimal temperatures for esterase activity.

2.3 Thermophilic CAs immobilization onto ZnOFe

Considering the challenges associated with the immobilization of thermophilic CAs onto HPCs, the next part of this thesis investigated the non-covalent immobilization of the three highest active thermophilic CAs—SyCA, DvCA8.0, and BhCA—onto ZnOFe (OLE) nanoparticles. The experiments were conducted using a fixed CA protein-to-ZnOFe ratio of 1:2, with an immobilization time of 2 hours at 30 °C.

The results, presented in Table 6, confirm the successful immobilization of all three enzymes onto the ZnOFe nanoparticles. Among them, DvCA8.0 exhibited the highest immobilization efficiency, followed by SyCA, with BhCA showing the lowest efficiency. These findings highlight the varying affinities of the selected CAs for ZnOFe under the tested conditions.

Table 6 Non-covalent Immobilization efficiencies of thermophilic CA onto ZnOFe nanoparticles . Enzyme loading refers to the amount of protein loaded onto 1 mg of ZnOFe nanoparticles.

CA	CA:ZnOFe Ratio (mg)	Efficiency (%)	Enzyme Loading
SyCA	1:2	36.17 ± 7.96	0.18
DvCA8.0	1:2	68.29 ± 4.31	0.34
BhCA	1:2	24.72 ± 3.69	0.12

A key challenge in these immobilization studies is conducting activity assays at elevated temperatures. Higher temperatures accelerate the spontaneous hydrolysis of the pNPA ester, which is a critical factor to consider. Despite this, the pNPA hydrolysis assays were performed at 70 °C for SyCA and DvCA8.0 and at 60 °C for BhCA, as determined to be their optimal activity temperatures according to Supplementary Fig. S1.

The activity results, presented in Table 7, indicate that BhCA exhibited no detectable activity, even when nanobiocatalyst concentrations of 1–2 mg/mL were used. However, both SyCA and DvCA8.0 nanobiocatalysts demonstrated esterase activity, significantly exceeding the autohydrolysis control in the presence of nanoparticles alone. For SyCA, the immobilized enzyme's activity decreased approximately 20-fold compared to the free enzyme (0.418 U mg^{-1}), whereas for DvCA8.0, the activity was reduced 8-fold relative to its free form (0.076 U mg^{-1}).

Table 7 Activity Results of the immobilized thermophilic CAs at pNPA hydrolysis assay at their optimum temperature.

CA	CA:ZnOFe Ratio	Assay Temperature (°C)	Activity ($\mu\text{moles min}^{-1} \text{ mg}^{-1}$)
SyCA	1:2	70	0.0209 ± 0.0005
DvCA8.0	1:2	70	0.0095 ± 0.0015
BhCA	1:2	60	n.d.

The activity results suggest that the aforementioned nanobiocatalytic systems have the potential for CO₂ capture applications. However, in our setup, the applicability of these thermophilic enzymes is limited, as their optimal activity is observed above 60 °C, which makes CO₂ practically insoluble at ambient pressure (Steger et al., 2022). Therefore, for further experimentation, it is recommended to conduct the reaction in pressurized systems.

Based on the bibliography, the immobilization of thermophilic CAs is a highly developing topic, with SyCA and DvCA having been previously immobilized.

SyCA has been reported to be entrapped in polyacrylamide gel, retaining 29.8% of its activity after five consecutive cycles of CO₂ mineralization (Wahyu Effendi et al., 2021). Additionally, SyCA was immobilized onto polyacrylonitrile and polyethylene terephthalate nanofibers, resulting in enhanced stability and reusability of the immobilized nanobiocatalyst in CO₂ sequestration applications (Effendi et al., 2020). Lastly, two other publications have reported the immobilization of DvCA, either onto polyester beads or iron oxide magnetic nanoparticles, demonstrating remarkable tolerance of the immobilized enzyme compared to the free enzyme under industrial CO₂ capture conditions (Antonopoulou et al., 2025; Hooks & Rehm, 2015).

2.4 FDH Immobilization

2.4.1 FDH@HPCs nanobiocatalyst

FDH was immobilized onto HPCs nanoparticles through physical adsorption by incubating both components for 1 hour at 30 °C. Immobilization efficiency and enzyme loading onto HPCs were determined by measuring either the total protein content or the residual enzyme activity compared to the initial FDH activity.

According to the results in Table 8, all tested FDH:HPC ratios led to successful enzyme immobilization. It was observed that increasing the amount of FDH resulted in higher enzyme loading onto the nanoparticles. However, the highest immobilization yield was achieved at the lowest FDH:HPC ratio, while the highest enzyme loading was obtained when the highest enzyme concentration was used.

Table 8 Immobilization efficiencies of FDH onto HPCs using three different FDH:HPCs ratios (mg). Enzyme loading refers to the amount of protein loaded onto 1 mg of HPC nanoparticles.

FDH:HPCs Ratio	Efficiency¹ (%)	Enzyme Loading¹	Efficiency² (%)	Enzyme Loading²
0.5:1	67.11 ± 15.93	0.34	79.22 ± 0.12	0.40
1:1	44.30 ± 5.39	0.44	44.42 ± 0.03	0.44
2:1	32.92 ± 3.43	0.66	31.67 ± 0.02	0.63

To assess potential enzyme leakage after immobilization, the supernatants from the duplicate washing steps were analyzed using the aforementioned assays. No protein or enzymatic activity was detected, confirming that FDH remained confined within the HPCs. Furthermore, it is concluded that both the BCA assay and activity measurements were consistent with the FDH immobilization results.

The FDH@HPCs nanobiocatalysts were then tested for activity through formate oxidation assay, the native reaction of FDH. These assays were conducted using 0.1, 0.5, or 1 mg/mL of the nanobiocatalysts in an Eppendorf tube, incubated at 30 °C for 5, 10, or 30 minutes. Following centrifugation, the absorbance of the supernatant was measured at 340 nm using a plate reader and compared to a blank sample containing only HPCs. Regardless of the enzyme ratio or nanobiocatalyst concentration, no activity was observed, as the absorbance of the reaction supernatant was identical to that of the blank. This assay probably confirmed that NAD⁺ was not reduced to NADH, and formate was not oxidized to CO₂.

Since formate oxidation is the primary function of FDH, the lack of observed nanobiocatalyst activity presents a significant limitation. This inactivity suggests several possible scenarios (Boudrant et al., 2020; Rodrigues et al., 2021). One possibility is that the enzyme was immobilized in an unfavorable orientation,

¹ Immobilization yield determined using the BCA assay by measuring the total protein content in the supernatant after immobilization.

² Immobilization yield determined by comparing the enzyme activity before and after immobilization.

preventing substrate access to the active site. Alternatively, the anchoring process may have disrupted the enzyme's tertiary structure, rendering it nonfunctional. Despite successful immobilization, the nanobiocatalyst remains inactive, making it unsuitable for further applications. These findings highlight a key challenge in enzyme immobilization—not only ensuring enzyme attachment but also preserving its catalytic function.

Another potential reason for the lack of activity could be that substrates and products became trapped within the nanoparticle pores, preventing proper diffusion into the surrounding solution (Bolivar et al., 2022). Since FDH's primary role is formate oxidation, these results indicate that the immobilized enzyme does not exhibit enzymatic activity under the tested conditions.

However, in subchapter 3.6 of Chapter three, the FDH:HPC ratios of 0.5:1 and 1:1 were further tested in the CO₂ reduction assay to explore potential catalytic function in the reverse reaction of FDH.

2.4.2 FDH@ZnOFe nanobiocatalyst

The immobilization of FDH onto HPC nanoparticles, while successfully anchoring the enzyme, presented significant challenges in maintaining enzymatic activity. Therefore, as previously discussed, a new category of green nanoparticles, ZnOFe (OLE), was selected for further investigation. In this immobilization procedure, no optimization trials were conducted, and a fixed ratio of 0.5 mg FDH to 2 mg ZnOFe nanoparticles was used. Unlike the previous approach, two different immobilization methods were tested: non-covalent (physical adsorption) and covalent (carbodiimide-mediated immobilization).

The results of FDH@ZnOFe, presented in Table 9, confirming the successful immobilization of the enzyme onto the nanoparticles. Regarding the covalent method (EDC/NHS) was significantly more efficient, yielding approximately 2.6 times higher immobilization efficiency than physical adsorption according to the BCA assay and 2.1 times higher efficiency based on residual enzyme activity in the immobilization supernatant. Both methods of assessing immobilization efficiency were in agreement. Additionally, enzyme leaching from the nanobiocatalyst was not detected during the washing steps for

either immobilization method, further confirming the stability of the immobilized enzyme.

Table 9 Immobilization efficiencies of non-covalently and covalently immobilized FDH onto ZnOFe nanoparticles at 0.5:2 FDH:ZnOFe ratios (mg). Enzyme loading refers to the amount of protein loaded onto 1 mg of ZnOFe nanoparticles.

FDH:ZnOFe 0.5:2	Efficiency¹ (%)	Enzyme Loading¹	Efficiency² (%)	Enzyme Loading²
Non-covalent	30.56 ± 2.24	0.08	37.95 ± 2.96	0.09
Covalent (EDC/NHS)	82.81 ± 3.42	0.21	80.05 ± 3.30	0.20

2.4.3 Activity of FDH@ZnOFe Nanobiocatalysts

Both covalently and non-covalently immobilized FDH@ZnOFe nanobiocatalysts were tested through the formate oxidation assay. These assays were conducted using either 0.2 or 0.5 mg/mL of nanobiocatalyst at two different temperatures, either at 30 °C or 40 °C.

As presented in Table 10, both immobilization methods resulted in active nanobiocatalysts capable of performing the native activity of FDH. Notably, the covalent immobilization proved to be more “effective” in the enzyme’s confinement onto the nanoparticles. At 30 °C, the covalently immobilized FDH exhibited 8.4 times higher activity than the non-covalently immobilized counterpart. Similarly, at 40 °C, while the overall activity of both nanobiocatalysts increased as expected, the covalent method remained superior, showing approximately 8.6 times higher activity than the non-covalent one.

¹ Immobilization yield determined using the BCA assay by measuring the total protein content in the supernatant after immobilization

² Immobilization yield determined by comparing the enzyme activity before and after immobilization.

Table 10 Activity of FDH@ZnOFe nanobiocatalyst through the oxidation assay of formic acid in two different assay temperatures (30, 40 °C).

FDH:ZnOFe Ratio 0.5:1	Activity ($\mu\text{moles min}^{-1}\text{mg}^{-1}$ nanobiocatalyst)	
	30 °C	40 °C
Non-covalent ¹	0.0053 \pm 0.0003	0.0066 \pm 0.0001
Covalent ¹	0.0600 \pm 0.0023	0.0711 \pm 0.0015

Undoubtedly, regarding the activity of the free enzyme (1.94 U mg^{-1} at 30 °C), it can be observed that the immobilization onto nanoparticles led to a significant activity reduction. Specifically, FDH activity decreased by approximately 366-fold for the non-covalently immobilized FDH and 32-fold for the covalently immobilized FDH.

Given the higher immobilization yield of the covalent method, the increased FDH activity was anticipated. However, this is not always a direct correlation, as multiple factors influence enzyme confinement and functionality of an enzyme when attached on a nanoparticle's surface (Boudrant et al., 2020).

In the following subchapters, both covalently and non-covalently immobilized nanobiocatalysts were evaluated for reusability, analyzed through FTIR, and tested for CO₂ reduction. However, for further characterization of the nanobiocatalyst's biochemical properties related to formate oxidation, only the covalently immobilized FDH@ZnOFe was investigated.

2.4.4 Kinetic comparison of Free and Immobilized FDH (FDH@ZnOFe)

The kinetic analysis of FDH in the native enzyme's reaction, with sodium formate and NAD⁺ as substrates, was performed by fitting the experimental data to the non-linear Michaelis-Menten regression. The results (Table 11, Supplementary Fig. S3, S4) provide insights into the enzyme's affinity and catalytic efficiency toward each substrate.

¹ Reference to the Immobilization method.

The results of kinetic analysis of FDH suggest that the enzyme exhibits higher affinity for the NAD⁺ cofactor compared to formate ($K_M^{app}_{M/NAD^+} < K_M^{app}_{M/formate}$), which is in accordance with the existing bibliography (Guo et al., 2016). The affinity of FDH towards formate substrate is approximately 68 times higher than the affinity for the NAD⁺ cofactor. These observed apparent kinetic values may differ significantly from literature values, potential factors such as commercial enzyme source and assay conditions (Ansorge-Schumacher et al., 2006).

Table 11 Apparent Michaelis Menten kinetic constants (K_M^{app} , V_{max}^{app}) of free FDH and covalently immobilized FDH (FDH@ZnOFe).

FDH	K_M^{app} (mM)	V_{max}^{app} ($\mu\text{moles min}^{-1} \text{mg}^{-1}$)
Free-NAD ⁺	0.089 ± 0.007	2.087 ± 0.041
Free-Formate	6.139 ± 0.750	1.853 ± 0.051
FDH@ZnOFe- Formate	12.144 ± .130	0.066 ± 0.003

As for the V_{max}^{app} values, both for formate ($1.8526 \pm 0.05102 \mu\text{mol min}^{-1} \text{mg}^{-1}$) and NAD⁺ ($2.05864 \pm 0.04144 \mu\text{mol min}^{-1} \text{mg}^{-1}$) are expected to be the same, as they are derived from the same enzymatic reaction. The slight variation observed is likely due to the mathematical fitting of the Michaelis-Menten equation and typical experimental error.

As for the immobilized CbFDH, the Michaelis-Menten kinetics of covalently immobilized FDH (FDH@ZnOFe) were assessed using varying formate concentrations (Table 11, Supplementary Fig. S4). Michaelis-Menten kinetics were only assessed for the covalently immobilized FDH, since the non-covalently nanobiocatalyst was outperformed in terms of formic acid oxidation activity.

As expected for an immobilized nanobiocatalyst, the system's affinity for formate was significantly reduced, as indicated by the two-fold increase in $K_M^{app}_{M/formate}$. Additionally, the V_{max}^{app} of immobilized FDH was observed to be decreased by a factor of 28. These kinetic results suggest that the presence of ZnOFe nanoparticles restricted the enzyme's flexibility, potentially limiting

substrate accessibility and diffusion. This reduction in overall catalytic turnover and affinity to formate may be attributed to steric hindrance and the restricted diffusion of the substrate to the active site (Lin et al., 2020).

2.4.5 FDH@ZnOFe Reusability

Both covalently and non-covalently immobilized FDH@ZnOFe nanobiocatalysts were tested for their reusability using the formate oxidation (forward reaction). Although the nanobiocatalysts purpose was intended for CO₂ reduction, formate oxidation was chosen as the preferred assay to evaluate its reusability due to the higher enzymatic activity in the forward reaction of the enzyme and the advantage of rapid screening.

As shown in Fig. 30, both nanobiocatalysts demonstrate the reusability of immobilized FDH over ten consecutive cycles. Specifically, the non-covalently immobilized FDH retains approximately 70% of its activity after 10 cycles, while the covalently immobilized FDH retains about 50% of its initial activity. It is worth noting that although the non-covalently immobilized FDH appears more stable in terms of reusability, the covalently immobilized FDH exhibits higher overall activity. Therefore, when considering the overall efficiency of the system, the covalently immobilized FDH is the preferred choice.

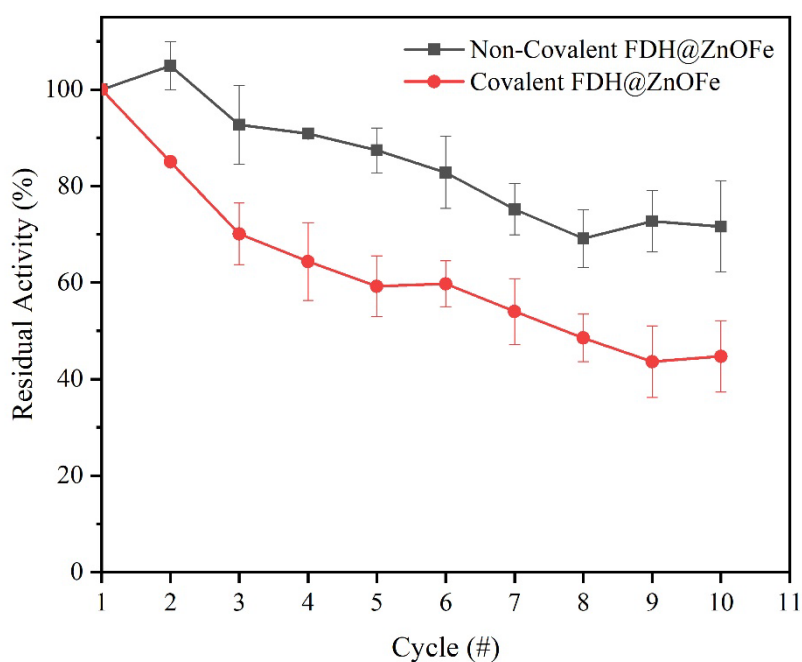


Figure 30 Non-covalently and Covalently immobilized FDH@ZnOFe Reusability Assay. Conditions: NaPi 0.05 M pH 7.0, 100 mM Sodium Formate, 1 mM NAD⁺, 40 °C, 650 rpm.

Previously conducted studies on FDH immobilized onto nickel-coordinated graphene oxide composites exhibited remarkable reusability capacity, retaining 63.8% of its initial activity after 8 consecutive cycles (Lin et al., 2018). Additionally, another study on *Candida methylca* FDH immobilized onto Immobead 150 supports, using three different functionalization methods for the solid particle surface, exhibited at least 38% retained activity of the immobilized FDH systems (Binay et al., 2016).

2.4.6 pH Activity and Thermoactivity of Covalently Immobilized FDH@ZnOFe

The covalently immobilized FDH@ZnOFe nanobiocatalyst was further characterized for its thermoactivity and pH activity. Results are depicted in Fig. 31A & 31B, which are compared with the free FDH.

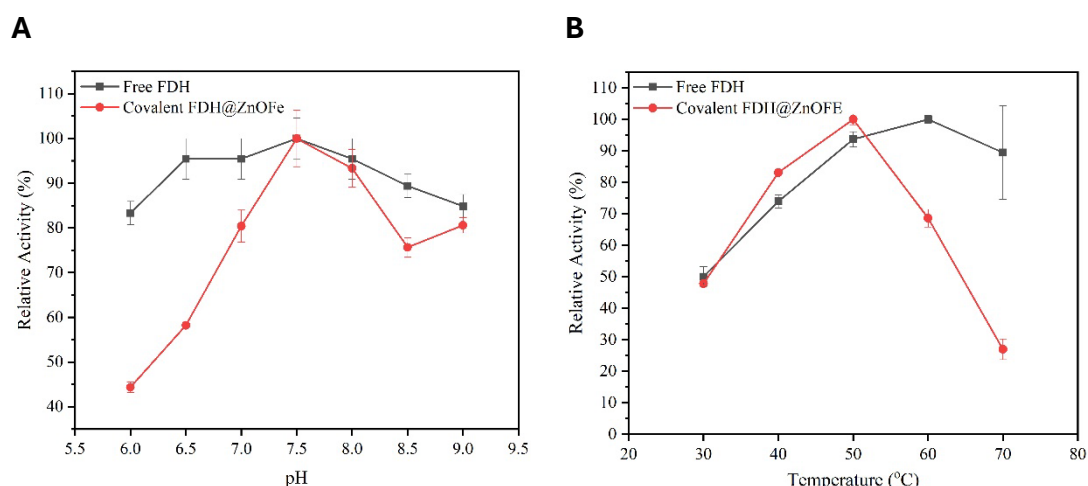


Figure 31 A. pH Activity assessment of Free and Covalently immobilized FDH@ZnOFe nanobiocatalyst at range of pH 6.0 to pH 9.0, B. Thermoactivity Assessment of Free and Covalently immobilized FDH@ZnOFe nanobiocatalyst at temperature range 30-70 °C.

Regarding the pH activity of the nanobiocatalyst, the immobilized enzyme has retained the optimum pH activity, which occurs at pH 7.5. However, the nanobiocatalyst did not exhibit higher relative activity when compared to the free enzymes. A significant drop in activity was observed at a neutral-acidic region of pH (pH 6.0-7.5), as well as a drop in activity in alkaline pH (pH 8.0-9.0). This effect of activity drop can be attributed to the interplay between the microenvironment change to the particular charge-effect microenvironment that the functionalized nanocarrier creates around the active core of the enzyme.

As for the thermoactivity of the immobilized FDH, both free and immobilized enzymes retain their maximal activity temperature at 50 °C. Though in higher temperatures, the activity of the immobilized enzymes drops dramatically at 60 and 70 °C. Possibly, the confinement of the enzyme onto the immobilization matrix induces structural strain on the enzyme, making it more susceptible to thermal denaturation.

2.4.7 Thermal Stability of FDH@ZnOFe at 60 °C

To further investigate the loss of FDH activity at 60 °C, the covalently immobilized nanobiocatalyst was assessed for its thermostability. As observed in Fig. 32, incubation of the nanobiocatalyst at 60 °C led to a significant loss of activity, even within the first 15 minutes. In comparison with the free enzyme, the activity drop was 1.5 times faster. More specifically, the nanobiocatalyst lost almost 90% of its relative activity after 15 minutes of incubation at 60 °C, and the deactivation continued over the next 30 minutes until it reached its lowest level.

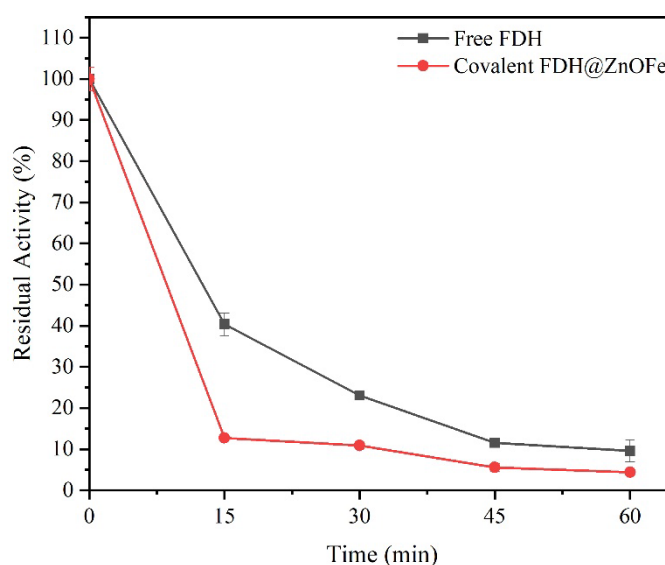


Figure 32 Thermostability assessment of Covalently Immobilized FDH onto ZnOFe nanorticles, at 60 oC in comparison with the free enzyme.

The findings of this study are in agreement with the loss of activity in thermoactivity assays, providing insights that the enzyme structure is not so rigid when immobilized onto the nanoparticle. This contributes to an less overall flexibility at higher temperatures. Though more thermostability studies with the immobilized enzyme should be conducted.

For future work and further evaluation of the nanobiocatalyst, considering thermostability studies at 50 °C, FDH retains 50% of its relative activity after 48 hours of consecutive incubation. Since the results from the thermoactivity of the free and immobilized enzyme come in agreement with the maximal activity of the enzyme, there is a possibility that FDH might exhibit higher stability at 50 °C, compared to the free enzyme.

2.4.8 FTIR of Free and Immobilized FDH

FTIR spectroscopy was performed to confirm the immobilization of FDH onto ZnO@Fe nanoparticles (Fig. 33). In the spectrum of ZnO@Fe nanoparticles, several peaks are observed between 600 and 1750 cm^{-1} . Peaks in the range of 1400–1500 cm^{-1} may correspond to C=C stretching from aromatic compounds present in the olive leaf extract. Additionally, peaks in the 600–700 cm^{-1} region correspond to Zn–O and Fe–O stretching vibrations, indicating metal oxide bonds. A broad peak near 3300 cm^{-1} is present in all samples, corresponding to intermolecular hydrogen bonding, which can be attributed to either O–H stretching from adsorbed water on the nanoparticle surface or phenolic group moieties from the olive leaf extract (Pagni, 2003).

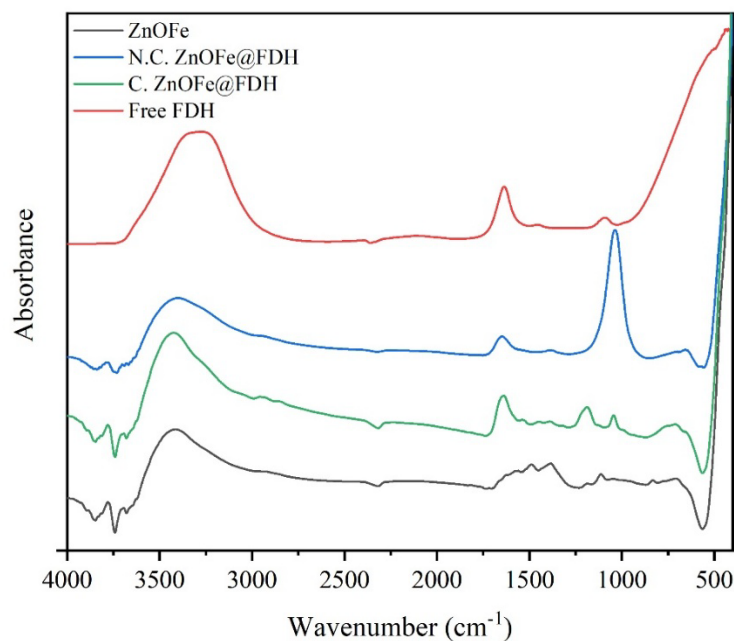


Figure 33 Fourier transform infrared (FTIR) for Free and Immobilized FDH@ZnOFe. The black line represents the ZnOFe nanoparticles, the blue line corresponds to non-covalently immobilized FDH, the green line depicts covalently immobilized FDH, and the red line shows the Attenuated Total Reflectance (ATR) spectrum of free FDH.

For the immobilized nanobiocatalysts, a prominent peak at 1650 cm^{-1} , corresponding to Amide I, is observed, confirming successful covalent immobilization. Amide I primarily arises from the C=O stretching vibrations of the protein backbone and is commonly used to assess secondary structural changes in proteins. More specifically, in the non-covalently immobilized nanobiocatalyst, both the Amide I (1650 cm^{-1}) and Amide II (1540 cm^{-1}) bands are present, further confirming FDH immobilization onto ZnO@Fe (Ji et al., 2020). Amide II originates from a combination of N-H bending and C-N stretching vibrations in proteins, indicating the presence of FDH (Deflores et al., 2009). Additionally, in the spectrum of covalently immobilized ZnO@Fe@FDH, a peak appears at 1190 cm^{-1} , which may correspond to C-O stretching from hydroxyl groups.

Lastly, in the spectrum of the free enzyme, the Amide I and Amide II peaks are clearly visible, along with an additional peak at 1080 cm^{-1} , which may be attributed to C-O stretching from amino acids containing C-O functional groups. This 1080 cm^{-1} peak is also present in the spectra of the immobilized nanobiocatalysts, though it appears slightly shifted and more intense in the case of non-covalent immobilization.

Outline for Enzyme Immobilization

The immobilization of thermophilic CAs onto HPCs and ZnOFe nanoparticles revealed significant variations in efficiency. While all CAs were successfully immobilized onto HPCs, their esterase activity remained undetectable, likely due to reaction product adsorption or limitations arising from the immobilization procedure, such as active site's steric hindrances, or enzyme's structural disruption. In contrast, ZnOFe-immobilized SyCA and DvCA8.0 exhibited esterase activity, though significantly reduced compared to their free forms, whereas BhCA remained inactive. These findings suggest that enzyme immobilization conditions must be carefully optimized, particularly regarding temperature, which plays a crucial role in both enzyme activity and substrate stability. Additionally, while these nanobiocatalysts show promise for CO₂ capture applications, their practical use may require pressurized systems to overcome the solubility limitations of CO₂ at high temperatures.

FDH was immobilized onto HPCs and ZnOFe nanoparticles using physical adsorption and covalent binding (EDC/NHS). While FDH@HPCs showed successful immobilization, no enzymatic activity was detected, similar to the immobilization of CAs onto HPCs. In contrast, FDH@ZnOFe nanobiocatalysts retained partially the activity of the free enzyme, with the covalent immobilization outperforming the activity of the non-covalent one. Additionally, kinetic analysis revealed a decrease in FDH's affinity for formate as well as decreased catalytic efficiency upon immobilization, likely due to steric hindrances at the enzyme's active site or diffusion limitations. Thermal and pH activity studies showed that the immobilized enzyme maintained optimal conditions but exhibited reduced stability at higher temperatures. Furthermore, the reusability tests of FDH@ZnOFe nanobiocatalysts demonstrated that the immobilized FDH provides a stable and reusable formate oxidation system for 10 consecutive catalytic cycles. Lastly, FTIR analysis confirmed successful enzyme attachment and structural changes, further supporting the successful immobilization of FDH.

3 CO₂ reduction to formic acid

3.1 pH activity of FDH AND GDH

The optimal pH activity of the dehydrogenases FDH and GDH was investigated through the forward reaction, by measuring NAD⁺ reduction to NADH with the concomitant oxidation of their primary substrates, either sodium formate or L-glutamate, respectively. According to Fig. 34, it is observed that FDH is a relatively pH-stable enzyme, since the enzyme's activity remains stable ($\geq 95\%$) within a pH range of 6.5 to 8. In contrast, GDH exhibits optimal activity at pH 8.5.

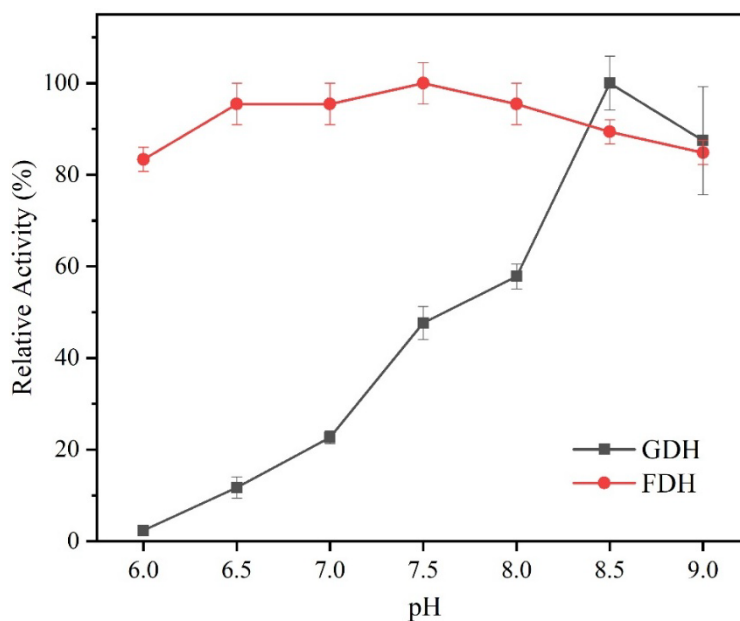


Figure 34 pH activity of the forward reactions of the Dehydrogenase, *Candida boidinii* FDH (red marker) and bovine liver GDH (black marker)

Regarding the applicability of the aforementioned enzymes in CO₂ reduction, the primary factor driving the reaction toward formic acid is the availability of CO₂ species. Although alkaline conditions appear to enhance GDH activity, they also lead to the accumulation of carbonate ions (CO₃²⁻) in the reaction medium. As already reported, FDH is not capable of catalytically reducing carbonates. Therefore, a more neutral or slightly acidic pH was preferred to increase the availability of bicarbonate and dissolved CO_{2(aq)} (Sato & Amao, 2020).

For this study, the reaction medium was maintained at pH 7.0 to balance CO_{2(aq)} - HCO₃⁻ availability and FDH's activity. With reference to GDH activity, as depicted in Fig. 34, GDH retains approximately 20% of its maximum activity at pH

7.0, which corresponds to approximately $0.17 \mu\text{mol min}^{-1} \text{mg}^{-1}$ (Supplementary Fig. S5).

From a general perspective, using an excess of regeneration enzyme activity and sacrificial substrate in a cofactor regeneration system is recommended to maximize efficiency and ensure consistent performance (Dascier et al., 2014). More importantly, considering the origin of the cofactor-regenerating biocatalyst, microbial enzymes are preferred due to their enhanced stability (De Jesus & Alkendi, 2022). In our study, we selected a commercially available eukaryotic (bovine) enzyme, which may present challenges for sustained conversion under reaction conditions.

3.2 Investigation of NADH stability

The stability of the NADH cofactor was investigated by incubating 5 mM of the NADH cofactor under reaction conditions (30 °C) in the presence of CO₂-saturated NaPi 0.1 M buffer. Saturation of the NaPi buffer with CO_{2(g)}, leads to the acidification of the solution due to loss of the regulatory capacity of the buffer; thus, prior to the addition of the cofactor, the buffer was adjusted back to the desired pH with the addition of 2 M NaOH solution. Additionally, to ensure an inert atmosphere, the vial was sealed with gaseous N₂ prior the enclosing, and samples were retrieved using a needle through the top septum.

As observed from Fig. 35, the spontaneous overtime NADH degradation occurs in every tested pH, highlighting the sensitive nature of the reduced cofactors under reaction conditions. Notably, our observations are in agreement with the existing bibliography, where it is stated that NADH is more stable at alkaline and neutral pH, compared to the slightly acidic ones (Knight et al., 1986).

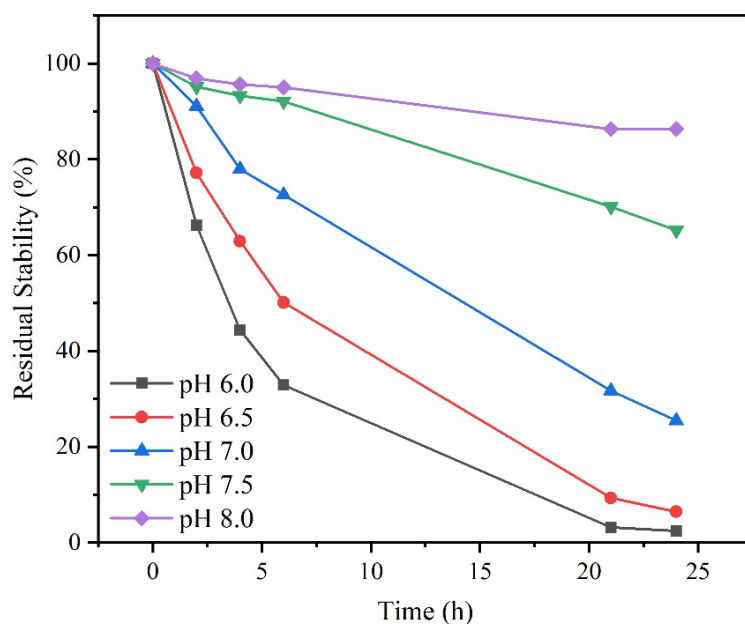


Figure 35 NADH cofactor stability assays in CO_2 -saturated 0.1 M sodium phosphate (NaPi) buffer at 30 °C under anaerobic conditions

From an assay monitoring perspective, the observed NADH degradation, especially at acidic pH values, directly affects the feasibility of spectrophotometric reaction monitoring over extended periods. The loss of the reaction's reducing equivalents due to cofactor instability can result in incomplete reactions or unreliable kinetic measurements, possibly leading to an overestimation of reaction kinetics. Consequently, the spectrophotometric recording of NADH is considered unsuitable for monitoring prolonged experimental setups unless the reaction occurs “rapidly”.

Moreover, the instability of NADH not only limits reaction monitoring but may also influence the overall reaction equilibrium. As NADH degrades, the equilibrium could shift, potentially favoring the reverse reaction and regenerating the substrate rather than driving product formation (Maier et al., 2024). This highlights the necessity of optimizing reaction conditions as stable pH conditions (formic acid generation might contribute to acidic pH), cofactor regeneration systems, or the employment of alternative electron donors to maintain reaction efficiency and minimize undesired shifts in equilibrium (Di Spiridione et al., 2022).

3.3 FDH-mediated reduction of CO₂ to formic acid

The enzymatic reduction of CO₂ with free *Candida boidinii* FDH (Fig. 36) was performed under inert atmosphere (N₂ saturated) in the presence of CO₂-saturated 0.1 M NaPi at 30 °C. It should be noted that the buffer solution was readjusted to pH 7 using 2 M NaOH prior to the addition of the enzyme and the cofactor. Bubbling gaseous CO₂ into the enzymatic solution was avoided to prevent; a. Enzyme deactivation at gas-liquid interfaces, which can cause aggregation and foam formation (Wang & Woodley, 2022), b. Unstable pH conditions, as CO₂ dissolution into the buffer solution over time, would lead to a loss of buffer regulatory capacity. Additionally, as previously mentioned, conducting this assay at an acidic pH would accelerate the degradation of the NADH cofactor, resulting in diminished enzymatic activity.

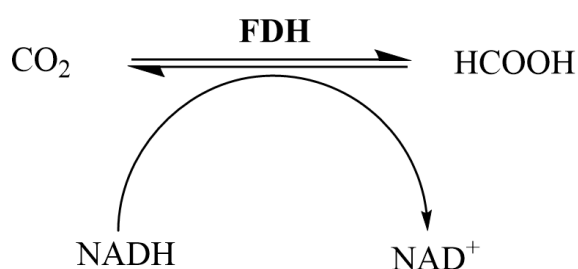


Figure 36 FDH-mediated CO₂ reduction to formic acid by with the concomitant oxidation of NADH to NAD⁺.

Regarding the substrate loading of the buffer, purging was performed under ambient conditions, which may have limited CO₂ solubility. In general, lower temperatures (ice-cold) are preferred to maximize CO₂ solubility (Mirjafari et al., 2007). However, there is a trade-off between substrate solubility and enzyme activity, as *Candida boidinii* is a mesophilic yeast. Therefore, temperatures between room temperature and 40 °C under ambient conditions appear to be the most optimal. Additionally, the solution should be adjusted close to the assay temperature to minimize fluctuations in the final pH, especially since the pH meters are calibrated at room temperature.

Working with CO₂ or other carbonate species as substrates in aqueous solutions remains a significant challenge since, unlike other substrates, there is no quick and direct method to measure their concentration in multi-solute setups.

According to the CO₂ species equilibrium under our pH conditions, there is a dynamic interplay between bicarbonate ions, which represent approximately 80%, and CO₂(aq), which accounts for the remaining ~20% (Fig. 3). Additionally, although the maximum solubility of CO₂ in pure water is approximately 33 mM, the ionic strength of our assay and the presence of solutes may reduce its solubility compared to this theoretical value due to the "salting-out" effect.

Regarding experimental handling, it should also be acknowledged that readjusting the solution to pH 7.0 can lead to partial loss of the CO₂ substrate due to its equilibrium with the atmosphere, especially under agitation during base titration with the pH meter. These factors may negatively impact overall system activity and contribute to significant variability between reaction batches. Therefore, a high number of independent experimental replicates is recommended (which, in our case, was not performed). To minimize CO₂ loss, it is advised to promptly load all reagents into the reaction vessel.

The selection of a "highly" concentrated buffer (0.1 M) was made to prevent slight acidification of the pH under reaction conditions, which could result from the production of formic acid. Additionally, pH 7.0 was chosen for three key reasons: a. cofactor degradation occurs at a slower rate compared to more acidic conditions; b. FDH retains at least 90% of its optimal activity (at least for its native activity); and c CO_{2(aq)} - HCO₃⁻ availability, either of which may serve as a substrate for the desired CO₂ reduction. To provide insights into the affinity of FDH for CO₂, it is worth noting that the Michaelis–Menten constant (K_M CO₂) for CO₂ in wild-type FDH from *Pseudomonas oxalaticus* has been reported to range between 30 and 50 mM. Additionally, the initial velocity of CO₂ reduction is approximately 30 times lower than that of the formate oxidation reaction (Ruschig et al., 1976).

Initially, in our experimental setups, in terms of CO₂ reduction by FDH, a comparison of different NADH concentrations was conducted (Fig. 37A and 37B). The estimation of the overall reaction yield across different time stops was calculated with Eq. 17, through the comparison of the production of formic acid with the initial concentration of the cofactor (since CO₂ concentration is practically unknown in the reaction). The theoretical yield of 1 mol of formic acid production requires 1:1 stoichiometry with 1 mol of NADH.

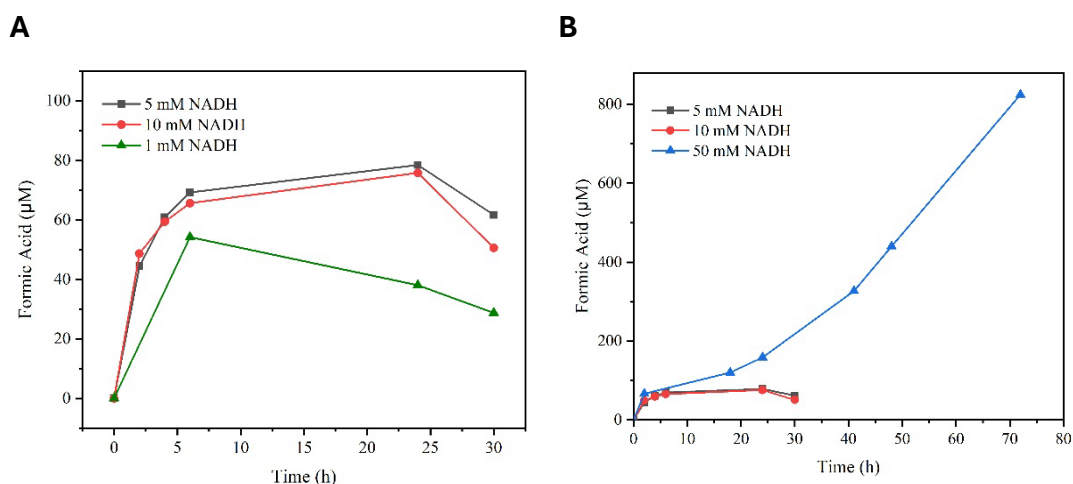


Figure 37 Comparison between different NADH cofactor concentrations of CO₂ reduction by *Candida boidinii* FDH. Reaction Conditions: 1 mg/mL FDH (~24.2 µM), CO₂-saturated NaPi Buffer 0.1 M pH 7.0, NADH, 110 rpm.

In our experiments, varying NADH concentrations influenced both the yield and stability of formic acid production. Specifically, with NADH concentrations of 5 mM and 10 mM, the reactions proceeded for up to 24 hours, yielding approximately 1.6% and 0.8% formic acid, respectively. Notably, at a lower NADH concentration of 1 mM, the highest formic acid yield of 5.4% was observed at 6 hours. However, after 24 hours of reaction time across all tested NADH concentrations, formic acid concentrations declined.

Rather than accumulating in the medium, formic acid concentrations decreased due to the thermodynamically favored oxidation of formate, a phenomenon commonly reported in the literature for reversible reactions (Aguirre et al., 2023; Sapountzaki et al., 2023; Zhang, Vasiliu, et al., 2021). Since CO₂ reduction by FDH is not the naturally occurring reaction for the wild-type enzyme, the accumulation of oxidized NAD⁺, likely due to time-dependent degradation rather than reduced cofactor consumption, leads to the oxidation of the produced formate.

To address the issue of “early” reaction reversibility, another trial was conducted using an excess of cofactor by supplementing the reaction with 50 mM NADH. In this case, formic acid production continued even after 72 hours of total reaction time, yielding approximately 1.25% conversion. This trial highlights the importance of maintaining a consistently high concentration of reducing equivalents for sustained reaction progression. Additionally, this assay is an index

for; a. FDH stability under reaction conditions for at least 72 continuous hours, b. CO₂ or bicarbonate species presence into the reaction medium.

Notably, these initial trials indicate that a high NADH concentration is crucial for efficient reversible CO₂ reduction. However, even at 50 mM NADH, the total reaction yield remains below 10% of the NADH input. The overall process remains cost-prohibitive due to the high expense of both the commercial enzyme and the cofactor. Nevertheless, since 1 mM NADH demonstrated the highest efficiency in these trials, the next sub-chapter will introduce the results of a cofactor regeneration system incorporating bovine liver glutamate dehydrogenase (GDH).

Our low formic acid yield aligns with findings in the existing literature on CO₂ reduction using commercially available cbFDH (Aguirre et al., 2023; Singh et al., 2018). Studies suggest that the primary factor limiting activity is the biocatalyst itself, which exhibits a low affinity for bicarbonate and CO₂, thereby reducing the overall catalytic efficiency of such bioconversion processes (Di Spiridione et al., 2022; Maier et al., 2024).

From an optimization standpoint, cbFDH has been shown to achieve higher conversion yields when paired with artificial cofactors in electrochemical systems, highlighting its potential for process upscaling (Fera et al., 2025; Zhang, Vasiliu, et al., 2021). Additionally, bacterial FDHs are generally favored for CO₂ reduction due to their superior efficiency compared to their eukaryotic counterparts (Choe et al., 2014). Finally, efforts to enhance enzyme selectivity for CO₂ over formate have led to the *in silico* engineering of two cbFDH mutants, resulting in a 1.75-fold increase in k_{cat}/K_M values compared to the wild-type enzyme (Shi et al., 2023).

3.4 Cofactor Regeneration in the presence of Glutamate Dehydrogenase

Implementing Glutamate Dehydrogenase (GDH) as an NADH regeneration system was considered to enhance the overall presence of the reduced cofactor in the system (Fig. 38). This approach could potentially prolong reaction times, thereby delaying the reversibility of the CO₂ reaction and achieving higher conversion yields with lower cofactor concentration in shorter reaction times.

Ideally, such systems could minimize overall reaction costs by initially supplementing the system with the oxidized cofactor NAD^+ .

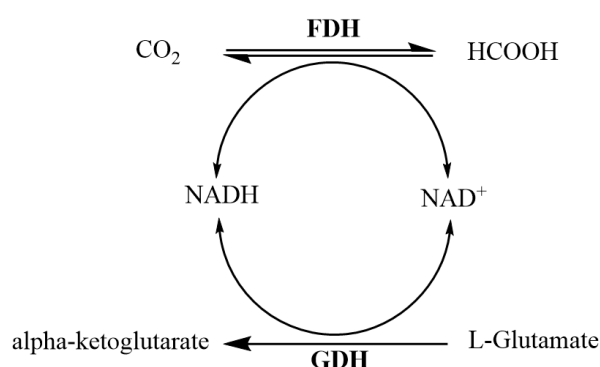


Figure 38 FDH-mediated reduction of CO_2 to formic acid with the addition of GDH cofactor regeneration system.

In our trials, the concentration of FDH was maintained at 1 mg/mL to ensure that cofactor regeneration was the sole variable. Herein, 1 mg/mL or 3 mg/mL GDH and 10 mM L-glutamate were added into the reaction vessel just before the addition of FDH. Considering that L-glutamate is in excess, we would expect similar reaction yields, with sub-millimolar concentrations of NADH, as observed in the 5 and 10 mM NADH reactions during the initial hours of the reaction.

The results of formic acid yields starting with 1 mM NADH in the presence of GDH are shown in Fig. 39A. It is observed that the addition of GDH does not affect the overall system's efficiency, resulting in conversion rates of 5% during the first 6 hours. Furthermore, tripling the GDH concentration leads to the same yields. The reversibility of the reaction is observed in all FDH-GDH setups after overnight incubation, implying that GDH is not effectively regenerating the reducing equivalents.

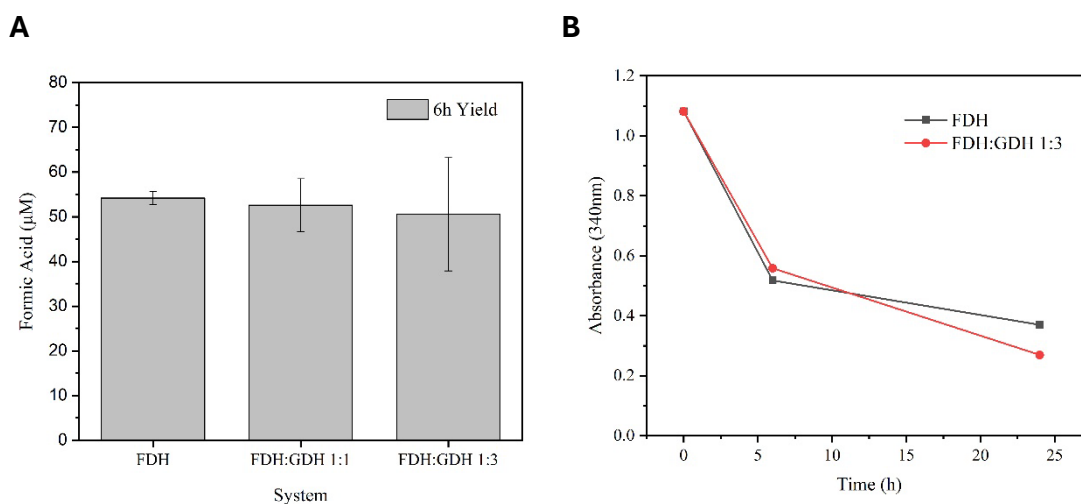


Figure 39 A. Comparison of Formic Acid Yields: FDH Alone vs. Combined FDH and GDH Systems After 6 Hours B. Monitoring NADH Levels: FDH vs. FDH:GDH System at a 1:3 Ratio. Reaction conditions: 1 mg/ml FDH (~24.2 µM), GDH, 1 mM NADH, 10 mM L-Glutamate, CO₂ saturated NaPi 0.1 M pH 7.0, 30 °C 110 rpm.

To investigate the issue of NADH regeneration further, the concentration of the overall systems NADH was monitored at 340 nm (Fig. 39B). This allowed the selective tracking of NADH without interference from other solutes (since the other solutes don't absorb at this wavelength). As observed at Fig. 39B, NADH consumption/degradation in both systems followed a similar trend in absorbance drop, indicating that GDH was not active under the reaction conditions. This inactivity may be due to insufficient GDH concentration to facilitate NADH recycling or the enzyme's sensitivity resulting from its eukaryotic origin.

3.5 Comparison between bubbled CO₂ or NaHCO₃

Bubbled CO₂ and commercially available NaHCO₃ were probed as a source of substrate in FDH-mediated CO₂ reduction. Fig. 40 presents a comparison between using bubbled CO₂ and NaHCO₃ with FDH and a 50 mM NADH cofactor concentration. Both assays were performed at pH 7.0; however, in the case of NaHCO₃, the buffer was readjusted using 2 M HCl. Using an external NaHCO₃ stock is more cost-effective and requires less handling during substrate stock preparation, as it eliminates the need for the 30-minute saturation process. Even though the maximum concentration of dissolved CO₂ in water is 34 mM, a higher concentration of NaHCO₃ stock can be prepared. However, this does not imply that CO₂ solubility in water is increased.

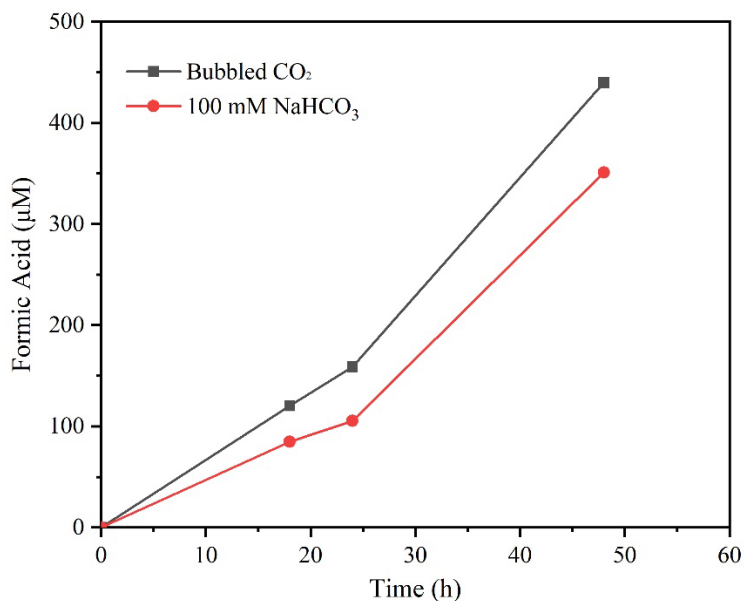


Figure 40 CO₂ reduction to Formic Acid by FDH time course with different sources of CO₂; CO₂(g) and NaHCO₃. Reaction conditions: 1 mg/ml FDH (~24.2 µM), 50 mM NADH, NaPi 0.1 M pH 7.0, 30 °C.

Regarding the reaction time course, the reaction profiles appear similar, with CO₂ yields of approximately 0.9% for bubbled CO₂ and ~0.7% for 100 mM NaHCO₃, resulting in a negligible difference. This experimental setup demonstrates that both methods of substrate acquisition can be effectively used for CO₂ reduction assays.

3.6 CO₂ reduction with Immobilized FDH

In this section, we discuss the results of CO₂ reduction into formic acid using immobilized FDH nanobiocatalysts. Two types of nanobiocatalysts were employed: FDH@HPCs and FDH@ZnOFe. For FDH@HPCs, CO₂(g) was selected as the reaction substrate due to the unique property of HPCs, which can absorb gases within their porous structure. In contrast, for FDH@ZnOFe, 100 mM NaHCO₃ was used as the substrate to simplify and accelerate buffer preparation. In all cases, since NADH availability is the limiting factor, each reaction was supplemented with 50 mM NADH to drive the reaction irreversibly.

For FDH@HPCs, two different nanobiocatalyst ratios were tested: 0.5:1 and 1:1 (FDH:HPCs). As mentioned in the previous section, the FDH@HPCs nanobiocatalysts did not exhibit dehydrogenase activity, despite the successful adsorption of the protein onto the nanoparticles. Surprisingly, both tested ratios

led to the production of formic acid, with concentrations not exceeding 100 μM over a total reaction time of 4 hours (data not shown). However, fluctuations in formic acid concentrations were observed, likely due to the porous structure of the nanoparticles, which may contribute to the adsorption of reaction substrates and/or products.

An attempt was made to replicate the experiment using the FDH@HPCs nanobiocatalyst with a doubled concentration of nanobiocatalyst (1.4 mg/mL). However, in this case, formic acid was not detected. This issue is likely due to the porous nature of the nanoparticles, which may adsorb both the substrate and the product, making it challenging to achieve reproducibility and scale up the assay. The only viable solution to this challenge is ensuring consistent replicability of the assay using lower concentrations of the nanobiocatalyst, thereby minimizing product adsorption.

Additionally, both non-covalently and covalently immobilized FDH@ZnOFe nanobiocatalysts were tested for CO_2 reduction. The reaction vessels contained 4 mg/mL FDH@ZnOFe nanobiocatalysts, 100 mM NaHCO_3 , and 50 mM NADH. However, neither of these nanobiocatalysts yielded any detectable formic acid when sampled at 6 and 24 hours. Although a slight increase in the derivatized product was observed after 24 hours, its concentration was below our calibration threshold ($< 25 \mu\text{M}$), making it difficult to determine whether this was a true signal or noise.

Numerous publications have demonstrated that immobilizing CO_2 -catalyzing enzymes coupled with cofactor regeneration systems enhances product formation. For instance, encapsulating FDH into Fe_3O_4 /ZIF-8 composites optimized the formic acid yield 3.4-fold compared to free FDH with the use of NaHCO_3 as reaction substrate (Aguirre et al., 2023). A study using FDH, FaldDH, and ADH immobilized on magnetite nanoparticles significantly boosted methanol yield, achieving 64-fold more yield of free enzymes under CO_2 pressure (Marques et al., 2018). Additionally, CA, FDH, and GDH in HKUST-1 framework layered structures significantly enhanced formic acid production, yielding over 13.1 times more than free enzymes with bubbled CO_2 (Li et al., 2019). Encapsulation of FDH,

FalDH, and ADH in ZIF-8 increased methanol concentration from 0.061 to 0.320 mM (5-fold) in three hours (Zhang, Li, et al., 2021).

These examples highlight how solid carriers improve the productivity of sequential cascade hydrogenation in CO₂ reduction mediated by dehydrogenases. The fixation of enzymes enhances their reaction stability, while the carrier material improves CO₂ adsorption, increasing substrate availability and facilitating more efficient catalysis (Ahmad Rizal Lim et al., 2021; Antonopoulou et al., 2022).

Outline for FDH-mediated CO₂ reduction

The final part of this thesis focused on exploring the potential of reversing the native FDH reaction by supplementing excess reducing equivalents to drive CO₂ reduction to formic acid. Based on our experimental results, a pH of 7.0 appears to be the optimal medium for sustained CO₂ conversion, likely due to the high availability of HCO₃⁻ and the enhanced stability of NADH. However, as previously discussed in the literature, FDH exhibits low affinity for CO₂, resulting in limited catalytic efficiency. The highest NADH concentration used (50 mM) extended formic acid production for 72 hours, but the yield remained significantly low (~1.25 %).

Another critical challenge in CO₂ biocatalysis is the reversibility of the reaction, which leads to the conversion of produced formic acid back to CO₂ as the oxidized NAD⁺ cofactor accumulates in the medium. To tackle this challenge, an attempt was made to employ a GDH-mediated cofactor regeneration system; however, no improvement in formic acid concentration or NADH regeneration was observed, likely due to the instability of GDH under the reaction conditions.

Regarding the immobilized nanobiocatalysts, FDH immobilization into HPCs appeared successful based on the immobilization yields. However, adsorption issues due to the nanoparticle pores hindered effective monitoring of the reaction. As for the FDH@ZnOFe nanobiocatalysts, no CO₂ reduction activity was observed, indicating that the quantities used were insufficient for effective CO₂ reduction.

Supplementary

Enzyme Protein Content

Dehydrogenases

Supplementary Table S1 Protein content of commercially available dehydrogenases.

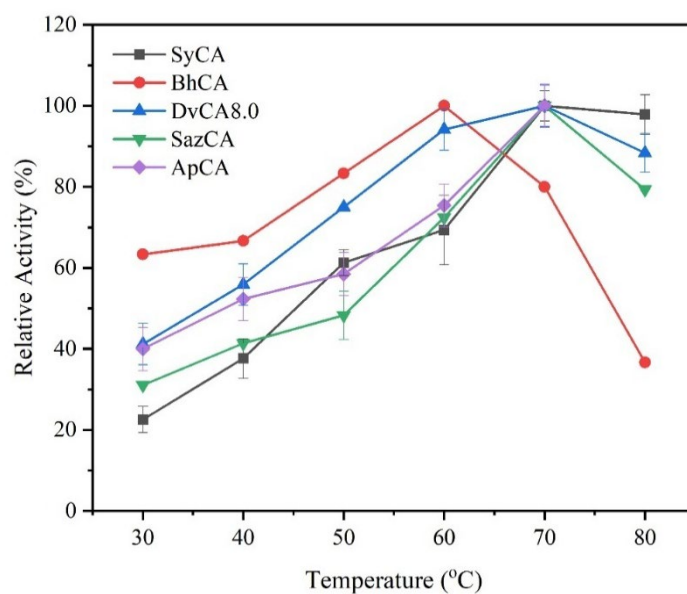
Dehydrogenase	Organism	Protein Content
FDH	<i>Candida boidinii</i>	52.3 ± 4.4 µg/µL
GDH	<i>beef liver</i>	55.83 ± 5.71 % w/w

Carbonic Anhydrases

Supplementary Table S2 Protein content of heterologously expressed CAs and commercially available bovine carbonic anhydrase(*).

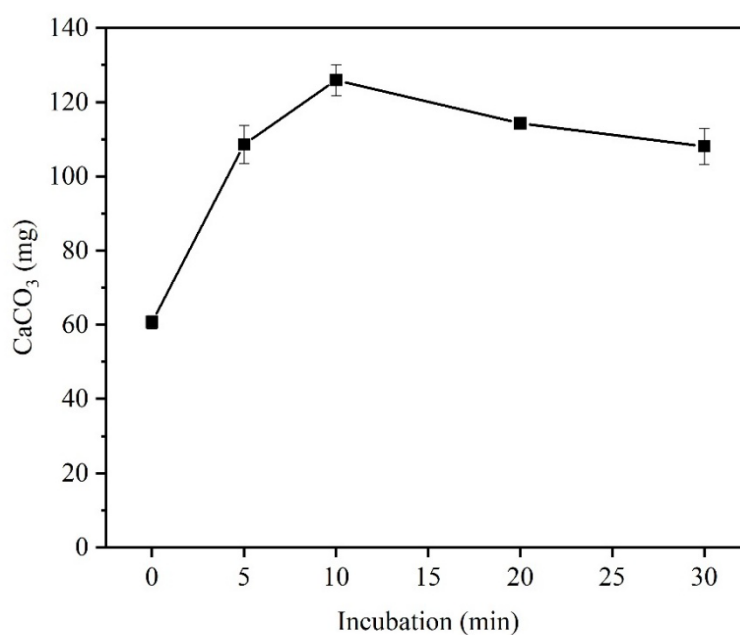
Carbonic Anhydrase	Organism	Protein Content (% w/w powder)
SyCA	<i>Sulfurihydrogenibium sp. YO3AOP1</i>	68.4 ± 1.7
ApCA	<i>Aeribacillus pallidus</i>	80.1 ± 7.3
DvCA8.0	<i>Desulfovibrio vulgaris</i>	34.6 ± 2.1
BhCA	<i>Alkalihalobacillus halodurans</i>	55.5 ± 1.3
SazCA	<i>Sulfurihydrogenibium azorense</i>	36.1 ± 1.8
BCA (≥2,000 WAU/mg protein)*	<i>Bos taurus</i> (Bovine) erythrocytes	78.2 ± 8.0

Thermoactivity of CAs



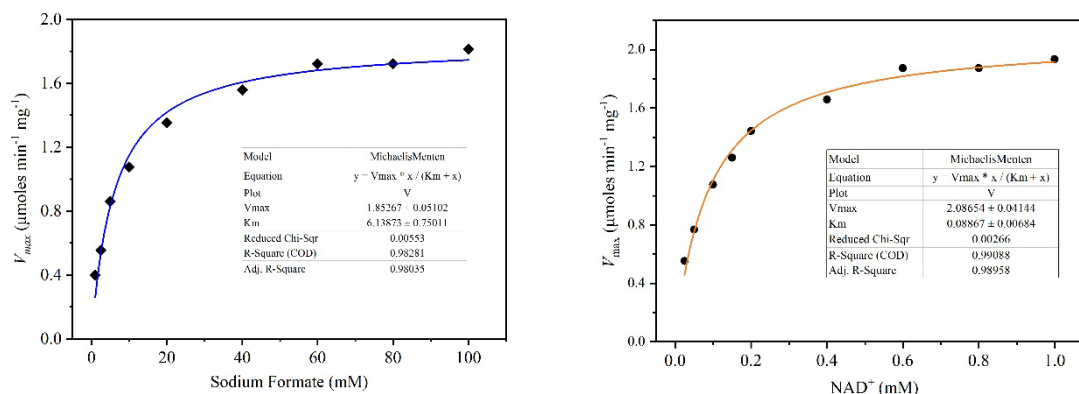
Supplementary Figure S1 Thermoactivity profile of five thermophilic CAs' esterase assay using 3 mM pNPA as substrate.

Non-CA-mediated CaCO₃ precipitation



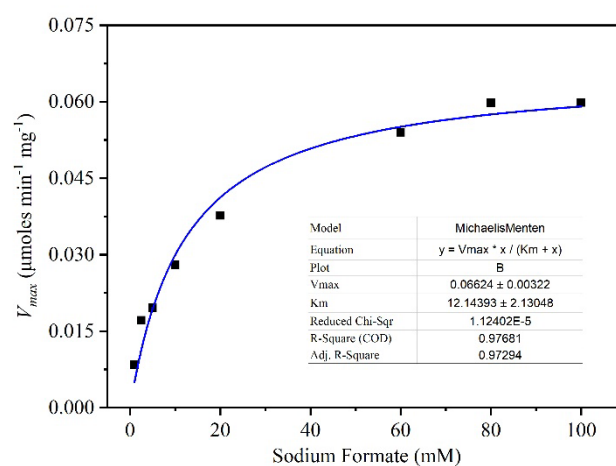
Supplementary Figure S2 Non-CA-mediated CaCO₃ precipitates yield after different times of sample incubation at 30 °C.

Free FDH Michaelis Menten Kinetics



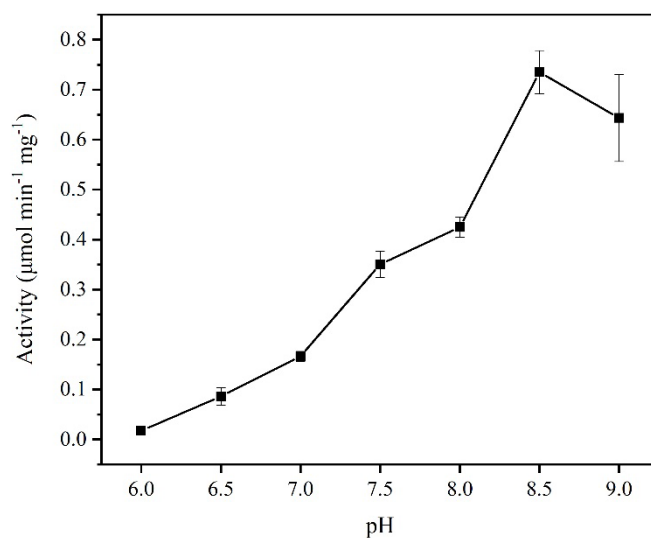
Supplementary Figure S3 Michaelis-Menten kinetics of CbFDH with Sodium Formate (left) and NAD⁺ (right) as substrates. The enzyme kinetics were analyzed by fitting the data to the Michaelis-Menten equation, by OriginPro software.

Covalently immobilized FDH@ZnOFe Michaelis Menten Kinetics



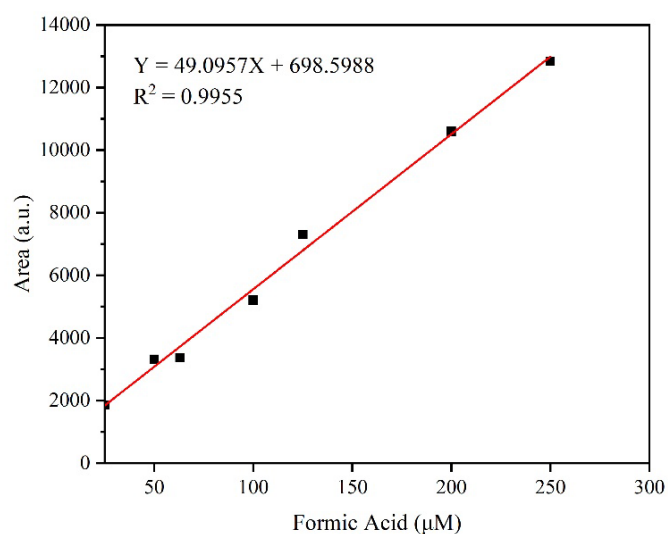
Supplementary Figure S4 Michaelis-Menten kinetics of CbFDH with Sodium Formate as substrate. The enzyme kinetics were analyzed by fitting the data to the Michaelis-Menten equation, by OriginPro software.

GDH pH Activity Profile



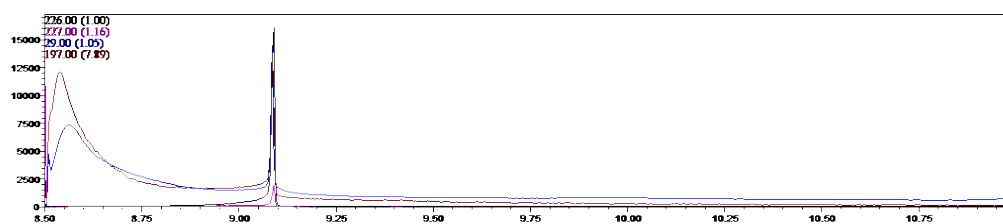
Supplementary Figure S5 pH-activity through oxidation of L-Glutamate (4 mM) to α -ketoglutarate in the presence of NAD⁺ (1 mM) at 30°C. Buffer used: pH 6.0-8.0 NaPi 0.1 M, pH 8.5-9.0 Tris-HCl 0.1 M.

Derivatized PFBBR-Formic Acid Ester Calibration Line (GC-MS)



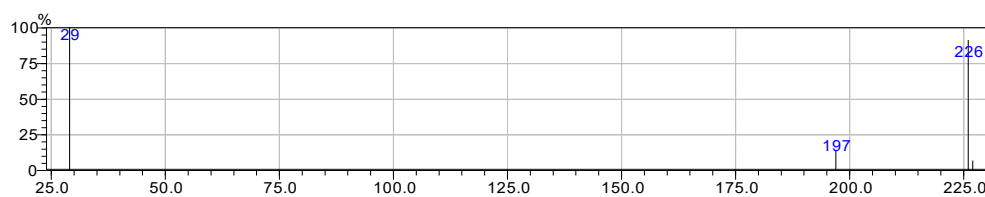
Supplementary Figure S6 Formic Acid Calibration Line after Derivatization with PFBBR.

GC-MS Chromatogram of derivatized Formic Acid-PFBBR Ester



Supplementary Figure S7 GC-MS Chromatogram of derivatized Formic Acid-PFBBR Ester (Retention Time ~9.15 min). Underivatized PFBBR (m/z iron values of 29 & 197) is also displayed with retention time at ~8.6 min.

Total Ion Chromatogram of Formic Acid-PFBBr Ester



Supplementary Figure S8 Total Ion Chromatogram (TIC) from GC-MS analysis of Formic Acid-PFBBr Ester. The displayed m/z ion values from this chromatogram were used to filter the SIM mode from the MS.

Bibliography

- Aguirre, M. E., Ramirez, C. L., & Di Iorio, Y. (2023). Stable and Reusable Fe(3) O(4) /ZIF-8 Composite for Encapsulation of FDH Enzyme under Mild Conditions Applicable to CO(2) Reduction. *Chemistry*, 29(47), e202301113. <https://doi.org/10.1002/chem.202301113>
- Ahmad Rizal Lim, F. N., Marpani, F., Anak Dilol, V. E., Mohamad Pauzi, S., Othman, N. H., Alias, N. H., Nik Him, N. R., Luo, J., & Abd Rahman, N. (2021). A Review on the Design and Performance of Enzyme-Aided Catalysis of Carbon Dioxide in Membrane, Electrochemical Cell and Photocatalytic Reactors. *Membranes (Basel)*, 12(1). <https://doi.org/10.3390/membranes12010028>
- Amao, Y. (2018). Formate dehydrogenase for CO₂ utilization and its application. *Journal of CO₂ Utilization*, 26, 623-641. <https://doi.org/10.1016/j.jcou.2018.06.022>
- Angeli, A., Carta, F., & Supuran, C. T. (2020). Carbonic Anhydrases: Versatile and Useful Biocatalysts in Chemistry and Biochemistry. *Catalysts*, 10(9). <https://doi.org/10.3390/catal10091008>
- Ansorge-Schumacher, M. B., Slusarczyk, H., Schumers, J., & Hirtz, D. (2006). Directed evolution of formate dehydrogenase from *Candida boidinii* for improved stability during entrapment in polyacrylamide. *FEBS J*, 273(17), 3938-3945. <https://doi.org/10.1111/j.1742-4658.2006.05395.x>
- Antonopoulou, I., de Oliveira Maciel, A., Di Giacomo, M., Russo, M. E., Rova, U., Christakopoulos, P., Salatino, P., & Marzocchella, A. (2025). Accelerated carbonate weathering by immobilized recombinant carbonic anhydrase. *Journal of CO₂ Utilization*, 94. <https://doi.org/10.1016/j.jcou.2025.103050>
- Antonopoulou, I., Rova, U., & Christakopoulos, P. (2022). CO(2) to Methanol: A Highly Efficient Enzyme Cascade. *Methods Mol Biol*, 2487, 317-344. https://doi.org/10.1007/978-1-0716-2269-8_19
- Aslan, A. S., Valjakka, J., Ruupunen, J., Yildirim, D., Turner, N. J., Turunen, O., & Binay, B. (2017). *Chaetomium thermophilum* formate dehydrogenase has high activity in the reduction of hydrogen carbonate (HCO₃⁻) to formate. *Protein Eng Des Sel*, 30(1), 47-55. <https://doi.org/10.1093/protein/gzw062>
- Baliukynas, M., Veteikyte, A., Kairys, V., & Matijosyte, I. (2020). The hydrolysis of indoxyl acetate: A versatile reaction to assay carbonic anhydrase activity by high-throughput screening. *Enzyme Microb Technol*, 139, 109584. <https://doi.org/10.1016/j.enzymictec.2020.109584>
- Bhat, R. M., Vidya, K., & Kamath, G. (2001). Topical formic acid puncture technique for the treatment of common warts. *Int J Dermatol*, 40(6), 415-419. <https://doi.org/10.1046/j.1365-4362.2001.01242.x>
- Bierbaumer, S., Nattermann, M., Schulz, L., Zschoche, R., Erb, T. J., Winkler, C. K., Tinzl, M., & Glueck, S. M. (2023). Enzymatic Conversion of CO(2): From Natural to Artificial Utilization. *Chem Rev*, 123(9), 5702-5754. <https://doi.org/10.1021/acs.chemrev.2c00581>
- Binay, B., Alagoz, D., Yildirim, D., Celik, A., & Tukul, S. S. (2016). Highly stable and reusable immobilized formate dehydrogenases: Promising biocatalysts

- for in situ regeneration of NADH. *Beilstein J Org Chem*, 12, 271-277.
<https://doi.org/10.3762/bjoc.12.29>
- Bolivar, J. M., Woodley, J. M., & Fernandez-Lafuente, R. (2022). Is enzyme immobilization a mature discipline? Some critical considerations to capitalize on the benefits of immobilization. *Chem Soc Rev*, 51(15), 6251-6290. <https://doi.org/10.1039/d2cs00083k>
- Boudrant, J., Woodley, J. M., & Fernandez-Lafuente, R. (2020). Parameters necessary to define an immobilized enzyme preparation. *Process Biochemistry*, 90, 66-80. <https://doi.org/10.1016/j.procbio.2019.11.026>
- Bulushev, D. A., & Ross, J. R. H. (2018). Towards Sustainable Production of Formic Acid. *ChemSusChem*, 11(5), 821-836.
<https://doi.org/10.1002/cssc.201702075>
- Butler, J. N. (2019). *Carbon Dioxide Equilibria and their Applications*.
<https://doi.org/10.1201/9781315138770>
- Cai, L. F., Zhan, J. M., Liang, J., Yang, L., & Yin, J. (2022). Structural control of a novel hierarchical porous carbon material and its adsorption properties. *Sci Rep*, 12(1), 3118. <https://doi.org/10.1038/s41598-022-06781-9>
- Calzadiaz-Ramirez, L., & Meyer, A. S. (2022). Formate dehydrogenases for CO₂ utilization. *Curr Opin Biotechnol*, 73, 95-100.
<https://doi.org/10.1016/j.copbio.2021.07.011>
- Cassia, R., Nocioni, M., Correa-Aragunde, N., & Lamattina, L. (2018). Climate Change and the Impact of Greenhouse Gases: CO₂ and NO, Friends and Foes of Plant Oxidative Stress. *Front Plant Sci*, 9, 273.
<https://doi.org/10.3389/fpls.2018.00273>
- Castro, A. M. d., Neves, L. A., Corvo, M. C., Cabrita, E. J., & Crespo, J. G. (2022). Effect of carbonic anhydrase on CO₂ absorption promoted by choline hydroxide using supported liquid membranes. *Separation and Purification Technology*, 280. <https://doi.org/10.1016/j.seppur.2021.119921>
- Cazelles, R., Drone, J., Fajula, F., Ersen, O., Moldovan, S., & Galarneau, A. (2013). Reduction of CO₂ to methanol by a polyenzymatic system encapsulated in phospholipids-silica nanocapsules. *New Journal of Chemistry*, 37(11).
<https://doi.org/10.1039/c3nj00688c>
- Chang, A., Jeske, L., Ulbrich, S., Hofmann, J., Koblitz, J., Schomburg, I., Neumann-Schaal, M., Jahn, D., & Schomburg, D. (2021). BRENDA, the ELIXIR core data resource in 2021: new developments and updates. *Nucleic Acids Res*, 49(D1), D498-D508.
<https://doi.org/10.1093/nar/gkaa1025>
- Chen, X., Liu, Y., & Wu, J. (2020). Sustainable production of formic acid from biomass and carbon dioxide. *Molecular Catalysis*, 483.
<https://doi.org/10.1016/j.mcat.2019.110716>
- Choe, H., Joo, J. C., Cho, D. H., Kim, M. H., Lee, S. H., Jung, K. D., & Kim, Y. H. (2014). Efficient CO₂-reducing activity of NAD-dependent formate dehydrogenase from *Thiobacillus* sp. KNK65MA for formate production from CO₂ gas. *PLoS One*, 9(7), e103111.
<https://doi.org/10.1371/journal.pone.0103111>
- Commons, W. (2024). Page name: File:Carbon dioxide 3D ball.png. Wikimedia Commons. Retrieved December from

https://commons.wikimedia.org/w/index.php?title=File:Carbon_dioxide_3D_ball.png&oldid=848288258

- Dascier, D., Kambourakis, S., Hua, L., Rozzell, J. D., & Stewart, J. D. (2014). Influence of Cofactor Regeneration Strategies on Preparative-Scale, Asymmetric Carbonyl Reductions by Engineered *Escherichia coli*. *Org Process Res Dev*, 18(6), 793-800. <https://doi.org/10.1021/op400312n>
- De Jesus, R., & Alkendi, R. (2022). A minireview on the bioremediative potential of microbial enzymes as solution to emerging microplastic pollution. *Front Microbiol*, 13, 1066133. <https://doi.org/10.3389/fmicb.2022.1066133>
- De Luna, P., Hahn, C., Higgins, D., Jaffer, S. A., Jaramillo, T. F., & Sargent, E. H. (2019). What would it take for renewably powered electrosynthesis to displace petrochemical processes? *Science*, 364(6438). <https://doi.org/10.1126/science.aav3506>
- DeFelice, J., Rumsfield, J., Bernstein, J. E., & Roshal, J. Y. (1989). Clinical evaluation of an after-pediculicide nit removal system. *Int J Dermatol*, 28(7), 468-470. <https://doi.org/10.1111/j.1365-4362.1989.tb02511.x>
- Deflores, L. P., Ganim, Z., Nicodemus, R. A., & Tokmakoff, A. (2009). Amide I'-II' 2D IR spectroscopy provides enhanced protein secondary structural sensitivity. *J Am Chem Soc*, 131(9), 3385-3391. <https://doi.org/10.1021/ja8094922>
- Del Prete, S., De Luca, V., Nocentini, A., Scaloni, A., Mastrolorenzo, M. D., Supuran, C. T., & Capasso, C. (2020). Anion Inhibition Studies of the Beta-Carbonic Anhydrase from *Escherichia coli*. *Molecules*, 25(11). <https://doi.org/10.3390/molecules25112564>
- Demir, Y., Demir, N., Nadaroglu, H., & Bakan, E. (2000). Purification and characterization of carbonic anhydrase from bovine erythrocyte plasma membrane. *Prep Biochem Biotechnol*, 30(1), 49-59. <https://doi.org/10.1080/10826060008544944>
- Deng, Y., Wang, J. X., Ghosh, B., & Lu, Y. (2024). Enzymatic CO₂ reduction catalyzed by natural and artificial Metalloenzymes. *J Inorg Biochem*, 259, 112669. <https://doi.org/10.1016/j.jinorgbio.2024.112669>
- Di Fiore, A., Alterio, V., Monti, S. M., De Simone, G., & D'Ambrosio, K. (2015). Thermostable Carbonic Anhydrases in Biotechnological Applications. *Int J Mol Sci*, 16(7), 15456-15480. <https://doi.org/10.3390/ijms160715456>
- Di Spiridione, C., Aresta, M., & Dibenedetto, A. (2022). Improving the Enzymatic Cascade of Reactions for the Reduction of CO₂ to CH₃OH in Water: From Enzymes Immobilization Strategies to Cofactor Regeneration and Cofactor Suppression. *Molecules*, 27(15). <https://doi.org/10.3390/molecules27154913>
- Effendi, S. S. W., Chiu, C. Y., Chang, Y. K., & Ng, I. S. (2020). Crosslinked on novel nanofibers with thermophilic carbonic anhydrase for carbon dioxide sequestration. *Int J Biol Macromol*, 152, 930-938. <https://doi.org/10.1016/j.ijbiomac.2019.11.234>
- Effendi, S. S. W., & Ng, I. S. (2019). The prospective and potential of carbonic anhydrase for carbon dioxide sequestration: A critical review. *Process Biochemistry*, 87, 55-65. <https://doi.org/10.1016/j.procbio.2019.08.018>

- Es, I., Vieira, J. D., & Amaral, A. C. (2015). Principles, techniques, and applications of biocatalyst immobilization for industrial application. *Appl Microbiol Biotechnol*, 99(5), 2065-2082. <https://doi.org/10.1007/s00253-015-6390-y>
- Fera, M.-C., Jayakumar, K., Bueno, D. G., Abad, J. M., De Lacey, A. L., & Pita, M. (2025). Bioelectrocatalytic CO₂ reduction to formate by *Candida boidinii* formate dehydrogenase overcoming NADH dependence with tailored amino-viologen redox polymers. *Journal of CO₂ Utilization*, 93. <https://doi.org/10.1016/j.jcou.2025.103041>
- Fisher, Z., Boone, C. D., Biswas, S. M., Venkatakrishnan, B., Aggarwal, M., Tu, C., Agbandje-McKenna, M., Silverman, D., & McKenna, R. (2012). Kinetic and structural characterization of thermostabilized mutants of human carbonic anhydrase II. *Protein Eng Des Sel*, 25(7), 347-355. <https://doi.org/10.1093/protein/gzs027>
- Fotiadou, R., Bellou, M. G., Spyrou, K., Yan, F., Rudolf, P., Gournis, D., & Stamatis, H. (2022). Effect of deep eutectic solvents on the biocatalytic properties of β -glucosidase@ZnOFe nano-biocatalyst. *Sustainable Chemistry and Pharmacy*, 30. <https://doi.org/10.1016/j.scp.2022.100886>
- Fotiadou, R., Chatzikonstantinou, A. V., Hammami, M. A., Chalmpes, N., Moschovas, D., Spyrou, K., Polydera, A. C., Avgeropoulos, A., Gournis, D., & Stamatis, H. (2021). Green Synthesized Magnetic Nanoparticles as Effective Nanosupport for the Immobilization of Lipase: Application for the Synthesis of Lipophenols. *Nanomaterials (Basel)*, 11(2). <https://doi.org/10.3390/nano11020458>
- Fuchs, W., Steger, F., Reich, J., Ribitsch, D., Rittmann, S. K. M. R., & Bochmann, G. (2021). A Simple and Straightforward Method for Activity Measurement of Carbonic Anhydrases. *Catalysts*, 11(7). <https://doi.org/10.3390/catal11070819>
- Guo, Q., Gakhar, L., Wickersham, K., Francis, K., Vardi-Kilshain, A., Major, D. T., Cheatum, C. M., & Kohen, A. (2016). Structural and Kinetic Studies of Formate Dehydrogenase from *Candida boidinii*. *Biochemistry*, 55(19), 2760-2771. <https://doi.org/10.1021/acs.biochem.6b00181>
- Hartanto, Y., Cocon, K. D., & Luis, P. (2024). Enzymatic carbon capture and conversion technology. In *Advances and Technology Development in Greenhouse Gases: Emission, Capture and Conversion* (pp. 181-202). <https://doi.org/10.1016/b978-0-443-19233-3.00013-4>
- Haynes, W. M. (2014). *CRC Handbook of Chemistry and Physics*. <https://doi.org/10.1201/b17118>
- Hepburn, C., Adlen, E., Beddington, J., Carter, E. A., Fuss, S., Mac Dowell, N., Minx, J. C., Smith, P., & Williams, C. K. (2019). The technological and economic prospects for CO₂ utilization and removal. *Nature*, 575(7781), 87-97. <https://doi.org/10.1038/s41586-019-1681-6>
- Hooks, D. O., & Rehm, B. H. (2015). Surface display of highly-stable *Desulfovibrio vulgaris* carbonic anhydrase on polyester beads for CO₂ capture. *Biotechnol Lett*, 37(7), 1415-1420. <https://doi.org/10.1007/s10529-015-1803-7>

- IEA. (2024). *CO2 Emissions in 2023*. IEA. <https://www.iea.org/reports/co2-emissions-in-2023>
- Jeske, L., Placzek, S., Schomburg, I., Chang, A., & Schomburg, D. (2019). BRENDA in 2019: a European ELIXIR core data resource. *Nucleic Acids Res*, 47(D1), D542-D549. <https://doi.org/10.1093/nar/gky1048>
- Ji, X., Su, Z., Wang, P., Ma, G., & Zhang, S. (2015). Tethering of nicotinamide adenine dinucleotide inside hollow nanofibers for high-yield synthesis of methanol from carbon dioxide catalyzed by coencapsulated multienzymes. *ACS Nano*, 9(4), 4600-4610. <https://doi.org/10.1021/acsnano.5b01278>
- Ji, Y., Yang, X., Ji, Z., Zhu, L., Ma, N., Chen, D., Jia, X., Tang, J., & Cao, Y. (2020). DFT-Calculated IR Spectrum Amide I, II, and III Band Contributions of N-Methylacetamide Fine Components. *ACS Omega*, 5(15), 8572-8578. <https://doi.org/10.1021/acsomega.9b04421>
- Jones, M. W., Peters, G. P., Gasser, T., Andrew, R. M., Schwingshackl, C., Gutschow, J., Houghton, R. A., Friedlingstein, P., Pongratz, J., & Le Quere, C. (2023). National contributions to climate change due to historical emissions of carbon dioxide, methane, and nitrous oxide since 1850. *Sci Data*, 10(1), 155. <https://doi.org/10.1038/s41597-023-02041-1>
- Kang, D., Yoo, Y., & Park, J. (2020). Accelerated chemical conversion of metal cations dissolved in seawater-based reject brine solution for desalination and CO2 utilization. *Desalination*, 473. <https://doi.org/10.1016/j.desal.2019.114147>
- Karl-Erich Jaeger, A. L., Christoph Syldatk. (2024). *Introduction to Enzyme Technology*. <https://doi.org/10.1007/978-3-031-42999-6>
- Karler, R., & Woodbury, D. M. (1963). Modified Manometric Method for Determination of Carbonic Anhydrase in Tissues. *Anal Biochem*, 6, 381-392. [https://doi.org/10.1016/0003-2697\(63\)90091-5](https://doi.org/10.1016/0003-2697(63)90091-5)
- Kim, I. G., Jo, B. H., Kang, D. G., Kim, C. S., Choi, Y. S., & Cha, H. J. (2012). Biomineralization-based conversion of carbon dioxide to calcium carbonate using recombinant carbonic anhydrase. *Chemosphere*, 87(10), 1091-1096. <https://doi.org/10.1016/j.chemosphere.2012.02.003>
- Kim, J. H., & Jo, B. H. (2022). A Colorimetric CO2 Hydration Assay for Facile, Accurate, and Precise Determination of Carbonic Anhydrase Activity. *Catalysts*, 12(11). <https://doi.org/10.3390/catal12111391>
- Knight, J. A., Wu, L. H., & Wu, J. T. (1986). Stability of NADPH: effect of various factors on the kinetics of degradation. *Clinical Chemistry*, 32(2), 314-319. <https://doi.org/10.1093/clinchem/32.2.314>
- Knoche, W. (1980). Chemical Reactions of CO2 in Water. In *Biophysics and Physiology of Carbon Dioxide* (pp. 3-11). https://doi.org/10.1007/978-3-642-67572-0_1
- Kobayashi, K., & Firoozabadi, A. (2023). Branching in molecular structure enhancement of solubility in CO(2). *PNAS Nexus*, 2(11), pgad393. <https://doi.org/10.1093/pnasnexus/pgad393>
- Konig, M., Vaes, J., Klemm, E., & Pant, D. (2019). Solvents and Supporting Electrolytes in the Electrocatalytic Reduction of CO(2). *iScience*, 19, 135-160. <https://doi.org/10.1016/j.isci.2019.07.014>

- Kuwabata, S., Tsuda, R., & Yoneyama, H. (1994). Electrochemical conversion of carbon dioxide to methanol with the assistance of formate dehydrogenase and methanol dehydrogenase as biocatalysts. *Journal of the American Chemical Society*, 116(12), 5437-5443.
<https://doi.org/10.1021/ja00091a056>
- Labrou, N. E., & Rigden, D. J. (2001). Active-site characterization of *Candida boidinii* formate dehydrogenase. *Biochem J*, 354(Pt 2), 455-463.
<https://doi.org/10.1042/0264-6021:3540455>
- Lee, H., Calvin, K., Dasgupta, D., Krinner, G., Mukherji, A., Thorne, P. W., Trisos, C., Romero, J., Aldunce, P., Barret, K., Blanco, G., Cheung, W. W. L., Connors, S. L., Denton, F., Diongue-Niang, A., Dodman, D., Garschagen, M., Geden, O., Hayward, B.,...Park, Y. (2023). IPCC, 2023: Climate Change 2023: Synthesis Report, Summary for Policymakers. Contribution of Working Groups I, II and III to the Sixth Assessment Report of the Intergovernmental Panel on Climate Change [Core Writing Team, H. Lee and J. Romero (eds.)]. IPCC, Geneva, Switzerland. 1-34.
<https://doi.org/10.59327/ipcc/ar6-9789291691647.001>
- Li, A., Cao, X., Fu, R., Guo, S., & Fei, Q. (2024). Biocatalysis of CO₂ and CH₄: Key enzymes and challenges. *Biotechnol Adv*, 72, 108347.
<https://doi.org/10.1016/j.biotechadv.2024.108347>
- Li, Y., Wen, L., Tan, T., & Lv, Y. (2019). Sequential Co-immobilization of Enzymes in Metal-Organic Frameworks for Efficient Biocatalytic Conversion of Adsorbed CO₂ to Formate. *Front Bioeng Biotechnol*, 7, 394.
<https://doi.org/10.3389/fbioe.2019.00394>
- Liljas, A., & Laurberg, M. (2000). A wheel invented three times. The molecular structures of the three carbonic anhydrases. *EMBO Rep*, 1(1), 16-17.
<https://doi.org/10.1093/embo-reports/kvd016>
- Lin, P., Zhang, Y., Ren, H., Wang, Y., Wang, S., & Fang, B. (2018). Assembly of graphene oxide-formate dehydrogenase composites by nickel-coordination with enhanced stability and reusability. *Eng Life Sci*, 18(5), 326-333. <https://doi.org/10.1002/elsc.201700137>
- Lin, P., Zhang, Y., Yao, G., Huo, H., Ren, H., Wang, Y., Wang, S., & Fang, B. (2020). Immobilization of formate dehydrogenase on polyethylenimine-grafted graphene oxide with kinetics and stability study. *Eng Life Sci*, 20(3-4), 104-111. <https://doi.org/10.1002/elsc.201900134>
- Liu, X., Li, S., Liu, Y., & Cao, Y. (2015). Formic acid: A versatile renewable reagent for green and sustainable chemical synthesis. *Chinese Journal of Catalysis*, 36(9), 1461-1475. [https://doi.org/10.1016/s1872-2067\(15\)60861-0](https://doi.org/10.1016/s1872-2067(15)60861-0)
- Luo, J., Meyer, A. S., Mateiu, R. V., & Pinelo, M. (2015). Cascade catalysis in membranes with enzyme immobilization for multi-enzymatic conversion of CO₂ to methanol. *N Biotechnol*, 32(3), 319-327.
<https://doi.org/10.1016/j.nbt.2015.02.006>
- Maffucci, I., Laage, D., Sterpone, F., & Stirnemann, G. (2020). Thermal Adaptation of Enzymes: Impacts of Conformational Shifts on Catalytic Activation Energy and Optimum Temperature. *Chemistry*, 26(44), 10045-10056.
<https://doi.org/10.1002/chem.202001973>

- Maia, L. B., Moura, I., & Moura, J. J. G. (2021). Carbon Dioxide Utilisation—The Formate Route. In *Enzymes for Solving Humankind's Problems* (pp. 29-81). https://doi.org/10.1007/978-3-030-58315-6_2
- Maier, A., Mguni, L. M., Ngo, A. C. R., & Tischler, D. (2024). Formate Dehydrogenase: Recent Developments for NADH and NADPH Recycling in Biocatalysis. *ChemCatChem*, 16(21). <https://doi.org/10.1002/cctc.202401021>
- Mao, S., Zhang, D., Li, Y., & Liu, N. (2013). An improved model for calculating CO₂ solubility in aqueous NaCl solutions and the application to CO₂-H₂O-NaCl fluid inclusions. *Chemical Geology*, 347, 43-58. <https://doi.org/10.1016/j.chemgeo.2013.03.010>
- Marcus, Y. (2018). Solubility Parameter of Carbon Dioxide-An Enigma. *ACS Omega*, 3(1), 524-528. <https://doi.org/10.1021/acsomega.7b01665>
- Marques, C. G. C. N., Andrade, L. H., & Toma, H. E. (2018). Carbon dioxide/methanol conversion cycle based on cascade enzymatic reactions supported on superparamagnetic nanoparticles. *An Acad Bras Cienc*, 90(1 Suppl 1), 593-606. <https://doi.org/10.1590/0001-3765201720170330>
- Meldrum, N. U., & Roughton, F. J. (1933). Carbonic anhydrase. Its preparation and properties. *J Physiol*, 80(2), 113-142. <https://doi.org/10.1113/jphysiol.1933.sp003077>
- Mirjafari, P., Asghari, K., & Mahinpey, N. (2007). Investigating the Application of Enzyme Carbonic Anhydrase for CO₂ Sequestration Purposes. *Industrial & Engineering Chemistry Research*, 46(3), 921-926. <https://doi.org/10.1021/ie060287u>
- Mortezaei, K., Amirlatifi, A., Ghazanfari, E., & Vahedifard, F. (2021). Potential CO₂ leakage from geological storage sites: advances and challenges. *Environmental Geotechnics*, 8(1), 3-27. <https://doi.org/10.1680/jenge.18.00041>
- Nelson, D. L. a. C., M.M. (2004). *Lehninger Principles of Biochemistry* (4th Edition ed.). W. H. Freeman.
- NOOA. (2024). *2023 was the world's warmest year on record, by far*. National Oceanic and Atmospheric Administration. <https://www.noaa.gov/news/2023-was-worlds-warmest-year-on-record-by-far>
- North, M. (2015). What is CO₂? Thermodynamics, Basic Reactions and Physical Chemistry. In *Carbon Dioxide Utilisation* (pp. 3-17). <https://doi.org/10.1016/b978-0-444-62746-9.00001-3>
- Obert, R., & Dave, B. C. (1999). Enzymatic Conversion of Carbon Dioxide to Methanol: Enhanced Methanol Production in Silica Sol-Gel Matrices. *Journal of the American Chemical Society*, 121(51), 12192-12193. <https://doi.org/10.1021/ja991899r>
- Pagni, R. M. (2003). Techniques in Organic Chemistry: Miniscale, Standard Taper Microscale, and Williamson Microscale (Mohrig, Jerry R.; Hammond, Christina Noring; Schatz, Paul F.; Morrill, Terence C.). *Journal of Chemical Education*, 80(4). <https://doi.org/10.1021/ed080p388>

- Pavlidis, I. V., Patila, M., Polydera, A. C., Gournis, D., & Stamatis, H. (2014). Immobilization of Enzymes and other Biomolecules on Graphene. In *Functionalization of Graphene* (pp. 139-172). <https://doi.org/10.1002/9783527672790.ch5>
- Pierre, A. C. (2012). Enzymatic Carbon Dioxide Capture. *ISRN Chemical Engineering*, 2012, 1-22. <https://doi.org/10.5402/2012/753687>
- Pinard, M. A., Mahon, B., & McKenna, R. (2015). Probing the surface of human carbonic anhydrase for clues towards the design of isoform specific inhibitors. *Biomed Res Int*, 2015, 453543. <https://doi.org/10.1155/2015/453543>
- R., L. (2024). *Climate Change: Atmospheric Carbon Dioxide*, NOAA Climate.gov. Retrieved December 2024 from <https://www.climate.gov/news-features/understanding-climate/climate-change-atmospheric-carbon-dioxide>
- Ren, S., Wang, Z., Bilal, M., Feng, Y., Jiang, Y., Jia, S., & Cui, J. (2020). Co-immobilization multienzyme nanoreactor with co-factor regeneration for conversion of CO₂. *Int J Biol Macromol*, 155, 110-118. <https://doi.org/10.1016/j.ijbiomac.2020.03.177>
- Research, P. (2024). *Formic Acid Market Size, Share, and Trends 2024 to 2034*. Retrieved December from <https://www.precedenceresearch.com/formic-acid-market>
- Rigkos, K., Filis, G., Antonopoulou, I., de Oliveira Maciel, A., Saridis, P., Zarafeta, D., & Skretas, G. (2024). Biomimetic CO₂ Capture Unlocked through Enzyme Mining: Discovery of a Highly Thermo- and Alkali-Stable Carbonic Anhydrase. *Environ Sci Technol*, 58(40), 17732-17742. <https://doi.org/10.1021/acs.est.4c04291>
- Rodrigues, R. C., Berenguer-Murcia, A., Carballares, D., Morellon-Sterling, R., & Fernandez-Lafuente, R. (2021). Stabilization of enzymes via immobilization: Multipoint covalent attachment and other stabilization strategies. *Biotechnol Adv*, 52, 107821. <https://doi.org/10.1016/j.biotechadv.2021.107821>
- Ruschig, U., Muller, U., Willnow, P., & Hopner, T. (1976). CO₂ reduction to formate by NADH catalysed by formate dehydrogenase from *Pseudomonas oxalaticus*. *Eur J Biochem*, 70(2), 325-330. <https://doi.org/10.1111/j.1432-1033.1976.tb11021.x>
- Sapountzaki, E., Rova, U., Christakopoulos, P., & Antonopoulou, I. (2023). Renewable Hydrogen Production and Storage Via Enzymatic Interconversion of CO₂ and Formate with Electrochemical Cofactor Regeneration. *ChemSusChem*, 16(17), e202202312. <https://doi.org/10.1002/cssc.202202312>
- Sato, R., & Amao, Y. (2020). Can formate dehydrogenase from *Candida boidinii* catalytically reduce carbon dioxide, bicarbonate, or carbonate to formate? *New Journal of Chemistry*, 44(28), 11922-11926. <https://doi.org/10.1039/d0nj01183e>
- Sato, R., & Amao, Y. (2023). Studies on the catalytic mechanism of formate dehydrogenase from *Candida boidinii* using isotope-labelled substrate

- and co-enzyme. *Catalysis Today*, 411-412.
<https://doi.org/10.1016/j.cattod.2022.06.011>
- Schirwitz, K., Schmidt, A., & Lamzin, V. S. (2007). High-resolution structures of formate dehydrogenase from *Candida boidinii*. *Protein Sci*, 16(6), 1146-1156. <https://doi.org/10.1110/ps.062741707>
- Schulz, K. G., Riebesell, U., Rost, B., Thoms, S., & Zeebe, R. E. (2006). Determination of the rate constants for the carbon dioxide to bicarbonate inter-conversion in pH-buffered seawater systems. *Marine Chemistry*, 100(1-2), 53-65. <https://doi.org/10.1016/j.marchem.2005.11.001>
- Shao, P., Ye, J., Shen, Y., Zhang, S., & Zhao, J. (2024). Recent advancements in carbonic anhydrase for CO₂ capture: A mini review. *Gas Science and Engineering*, 123. <https://doi.org/10.1016/j.gjsce.2024.205237>
- Shi, H. L., Yuan, S. W., Xi, X. Q., Xie, Y. L., Yue, C., Zhang, Y. J., Yao, L. G., Xue, C., & Tang, C. D. (2023). Engineering of formate dehydrogenase for improving conversion potential of carbon dioxide to formate. *World J Microbiol Biotechnol*, 39(12), 352. <https://doi.org/10.1007/s11274-023-03739-5>
- Shi, J., Jiang, Y., Jiang, Z., Wang, X., Wang, X., Zhang, S., Han, P., & Yang, C. (2015). Enzymatic conversion of carbon dioxide. *Chem Soc Rev*, 44(17), 5981-6000. <https://doi.org/10.1039/c5cs00182j>
- Singh, R. K., Singh, R., Sivakumar, D., Kondaveeti, S., Kim, T., Li, J., Sung, B. H., Cho, B.-K., Kim, D. R., Kim, S. C., Kalia, V. C., Zhang, Y.-H. P. J., Zhao, H., Kang, Y. C., & Lee, J.-K. (2018). Insights into Cell-Free Conversion of CO₂ to Chemicals by a Multienzyme Cascade Reaction. *ACS Catalysis*, 8(12), 11085-11093. <https://doi.org/10.1021/acscatal.8b02646>
- Steel, L., Liu, Q., Mackay, E., & Maroto-Valer, M. M. (2016). CO₂ solubility measurements in brine under reservoir conditions: A comparison of experimental and geochemical modeling methods. *Greenhouse Gases: Science and Technology*, 6(2), 197-217. <https://doi.org/10.1002/ghg.1590>
- Steger, F., Reich, J., Fuchs, W., Rittmann, S. K. R., Gubitza, G. M., Ribitsch, D., & Bochmann, G. (2022). Comparison of Carbonic Anhydrases for CO₂ Sequestration. *Int J Mol Sci*, 23(2). <https://doi.org/10.3390/ijms23020957>
- Supuran, C. T. (2016). Structure and function of carbonic anhydrases. *Biochem J*, 473(14), 2023-2032. <https://doi.org/10.1042/BCJ20160115>
- Talekar, S., Jo, B. H., Dordick, J. S., & Kim, J. (2022). Carbonic anhydrase for CO₂ capture, conversion and utilization. *Curr Opin Biotechnol*, 74, 230-240. <https://doi.org/10.1016/j.copbio.2021.12.003>
- Villa, R., Nieto, S., Donaire, A., & Lozano, P. (2023). Direct Biocatalytic Processes for CO₂ Capture as a Green Tool to Produce Value-Added Chemicals. *Molecules*, 28(14). <https://doi.org/10.3390/molecules28145520>
- Wahyu Effendi, S. S., Tan, S. I., Ting, W. W., & Ng, I. S. (2021). Enhanced recombinant Sulfurihydrogenibium yellowstonense carbonic anhydrase activity and thermostability by chaperone GroEL for carbon dioxide biomineralization. *Chemosphere*, 271, 128461. <https://doi.org/10.1016/j.chemosphere.2020.128461>
- Wang, J., & Woodley, J. M. (2022). In Situ Cofactor Regeneration Using NAD(P)H Oxidase: Enzyme Stability in a Bubble Column. *ChemCatChem*, 14(15). <https://doi.org/10.1002/cctc.202200255>

- Wang, X., Saba, T., Yiu, H. H. P., Howe, R. F., Anderson, J. A., & Shi, J. (2017). Cofactor NAD(P)H Regeneration Inspired by Heterogeneous Pathways. *Chem*, 2(5), 621-654. <https://doi.org/10.1016/j.chempr.2017.04.009>
- Weiner, S. (2003). An Overview of Biomineralization Processes and the Problem of the Vital Effect. *Reviews in Mineralogy and Geochemistry*, 54(1), 1-29. <https://doi.org/10.2113/0540001>
- Wilbur, K. M., & Anderson, N. G. (1948). Electrometric and Colorimetric Determination of Carbonic Anhydrase. *Journal of Biological Chemistry*, 176(1), 147-154. [https://doi.org/10.1016/s0021-9258\(18\)51011-5](https://doi.org/10.1016/s0021-9258(18)51011-5)
- Zhang, W., Bao, Y., & Bao, A. (2020). Preparation of nitrogen-doped hierarchical porous carbon materials by a template-free method and application to CO₂ capture. *Journal of Environmental Chemical Engineering*, 8(3). <https://doi.org/10.1016/j.jece.2020.103732>
- Zhang, Y., Ji, X., Xie, Y., & Lu, X. (2016). Screening of conventional ionic liquids for carbon dioxide capture and separation. *Applied Energy*, 162, 1160-1170. <https://doi.org/10.1016/j.apenergy.2015.03.071>
- Zhang, Z., Li, J., Ji, M., Liu, Y., Wang, N., Zhang, X., Zhang, S., & Ji, X. (2021). Encapsulation of multiple enzymes in a metal-organic framework with enhanced electro-enzymatic reduction of CO₂ to methanol. *Green Chemistry*, 23(6), 2362-2371. <https://doi.org/10.1039/d1gc00241d>
- Zhang, Z., Vasiliu, T., Li, F., Laaksonen, A., Mocci, F., & Ji, X. (2021). Electrochemically driven efficient enzymatic conversion of CO₂ to formic acid with artificial cofactors. *Journal of CO₂ Utilization*, 52. <https://doi.org/10.1016/j.jcou.2021.101679>
- Zhao, H., & Baker, G. A. (2023). Functionalized Ionic Liquids for CO₂ Capture under Ambient Pressure. *Green Chem Lett Rev*, 16(1). <https://doi.org/10.1080/17518253.2022.2149280>